ΕΛΛΗΝΙΚΗ
ΕΠΙΣΤΗΜΟΝΙΚΗ
ΕΤΑΙΡΕΙΑ
ΕΔΑΦΟΜΗΧΑΝΙΚΗΣ
& ΓΕΩΤΕΧΝΙΚΗΣ
ΜΗΧΑΝΙΚΗΣ

Τα Νέα της Ε Ε Ε Ε Γ Μ

101

Αρ. 101 – ΑΠΡΙΛΙΟΣ 2017

Ζητούνται Συνεκδότες για το περιοδικό

Γράφαμε στο προηγούμενο επετειακό τεύχος του ηλεκτρονικού περιοδικού μας ότι "*έχουμε την εντύπωση ότι η ελληνική, αλλά και η διεθνής γεωτεχνική κοινότητα, έχει εκφρασθή πολύ θετικά για το περιοδικό*". Και πράγματι η αναγνώριση από την διεθνή γεωτεχνική κοινότητα ήρθε αμέσως ("*I like your bulletin, which is also relevant to other members of ISSMGE*", Charles Ng, President ISSMGE) και στο επόμενο τεύχος του ISSMGE Bulletin Οκτωβρίου 2017 θα παρατεθούν 22 σελίδες από το επετειακό τεύχος.

Παρ' όλα αυτά η ολοκλήρωση και κυκλοφορία των τευχών γίνεται όλο και με μεγαλύτερη καθυστέρηση. Το ανά τις οθόνες σας 101ο Τεύχος του περιοδικού Απριλίου 2017 κυκλοφορεί τον Οκτώβριο. Δυστυχώς οι επαγγελματικές υποχρεώσεις του Εκδότη και η λόγω αυτών υποχρεωτική απουσία του από την Ελλάδα για μεγάλα χρονικά διαστήματα, δεν επιτρέπουν, πλέον, την έγκαιρη ανά μήνα σύνταξη του περιοδικού, παρά το ότι η ενδιαφέρουσα για τους συναδέλφους ύλη αυξάνεται καθημερινά. Έχουμε ήδη συγκεντρώσει ύλη για τα επόμενα τεύχη Μαΐου, Ιουνίου, Ιουλίου, Αυγούστου, Σεπτεμβρίου και Οκτωβρίου αλλά δεν υπάρχουν διαθέσιμα "χέρια" για να την αξιοποιήσουν.

Για τον λόγο αυτό, προσκαλούμε όλους τους συναδέλφους, που μπορούν και ενδιαφέρονται να συμμετάσχουν στην έκδοση του περιοδικού να επικοινωνήσουν με τον Εκδότη. Απαιτούμενο προσόν η πολύ καλή γνώση Microsoft Office.

Π Ε Ρ Ι Ε Χ Ο Μ Ε Ν Α

ΑΡΘΡΑ

Παρουσίαση άρθρων, στην συγγραφή των οποίων μετείχαν Έλληνες, στο XVI European Conference on Soil Mechanics and Geotechnical Engineering, Edinburgh, 13-17 September 2015 (κατ' αλφαβητική σειρά, στα ελληνικά, του ονόματος του πρώτου συγγραφέα).

The Role of Distributed Sensing in Understanding the Engineering Performance of Geotechnical Structures

Le rôle des systèmes de mesure distribuée par fibre optique dans l'analyse de la performance des ouvrages géotechniques

K.Soga, V. Kwan, L. Pelecanos, Y. Rui, T. Schwamb, H. Seo and M. Wilcock

Keynote Paper

ABSTRACT Engineering design limits are often based on strain and/or stress developing in the structure. For structures interacting with soil (e.g. underground infrastructure such as foundations, tunnels or pipelines), the ground loads are distributed spatially (i.e. not point loads) and hence the state of the structure will be better understood if the complete in situ strain regime (or displacement profile) is known. An innovative distributed fibre optic strain measurement system allows having thousands of "strain gauges" along a single cable connected to structures, embedded in soil or grouted into boreholes. Because of the simple and quick installation technique, distributed optical fibre sensing can be as practical as the other conventional measurements. This paper describes four case studies that utilised distributed strain sensing to understand the engineering performance of piles, thermal piles, diaphragm walls and concrete tunnel linings, in which fibre optic cables were either attached or embedded. Engineering insights obtained from the data interpretation and numerical analysis are presented.

1 INTRODUCTION

In recent years, research and technology development on sensor and communications have been undergoing a revolution. In particular, we are starting to see certain innovative sensing techniques such as computer vision, fibre optic sensing, miniature sensors (Microelectro-mechanical systems (MEMS)) and wireless sensor network introduced in engineering practice for condition assessment and monitoring of geotechnical structures, and in some cases replacing the existing methods (e.g. Hoult et al. 2009; Bennett et al. 2010a& b; Ferri et al. 2009; Stajano et al. 2010; Soga 2012 & 2014; Hoult and Soga 2014; Stent et al. 2014). Recent advances in 3D printing, printed electronics, ultra-low power high performance microprocessors and wireless communication might radically alter the paradigm of sensing and monitoring systems in the near future. For example, inkjet printers can be used for prototyping and production of both individual sensors and printed circuit boards, whereas 3D printers will allow the production of bespoke sensor packaging capable of being tailored for particular applications. These will enable to realise the concept of 'intelligence on demand', in which sensors can rapidly be developed to produce the data required for decision making. If they can be used for a long time (i.e. equal to the lifetime of infrastructure), it could transform the industry by it taking a whole-life approach – design, commissioning, construction, maintenance and eventual de-commissioning (i.e. intelligence for life).

Using such innovations, there are great opportunities for geotechnical engineers to advance our understanding of the performance of geotechnical structures. Although there is a long history of developing robust monitoring methods for geotechnical engineering applications, emerging sensor and communication technologies provide a new way of understanding the performance of geotechnical structures.

Emphasis on monitoring is not new in geotechnical engineering. In fact, monitoring has been used extensively in geotechnical engineering for decades, ever since the development of the observational method where feedback from monitoring systems were used to inform and potentially modify design and construction (Peck 1969; Nicholson et al. 1999). Field monitoring is essential so that (i) the design is sound, (ii) the construction is executed safely, and (iii) the geotechnical structures we built satisfy the specifications set by the clients. Active monitoring will provide engineering intelligence when the actual behaviour of the structure is compared to the design prediction. As illustrated in this paper, by using recent advances in field instrumentation and monitoring systems, we can be more proactive than we used to be in closing the gap between theory and application.

Engineering design limits are often based on strain and/or stress developing in the structure. For structures interacting with soil (e.g. underground infrastructure such as foundations, tunnels or pipelines), the ground loads are distributed spatially (i.e. not point loads) and hence the state of the structure will be better understood if the complete in situ strain regime (or displacement profile) is known. Furthermore, capturing the continuous strain profile can be useful to pinpoint localised problem areas such as cavity collapse, non-uniformly distributed soil-structure interaction loads, and joint movements. Any technology that provides spatially continuous data will be useful, and distributed fibre sensing is one of such technologies.

This paper describes four case studies in which fibre optic based distributed strain measurement systems have been used to monitor the performance of geotechnical structures during construction.

2 DISTRIBUTED SENSING USING OPTICAL FIBRES

2.1 General background

Distributed fibre optics sensing technique takes advantage of the sensitivity of an optical fibre with respect to ambient parameters like temperature, strain, vibration and noise (acoustic). The ambient parameters to which the fibre is subjected influence the properties of a laser light signal travelling throughout the glass material in an optical fibre (Figure 1a). When a light travels through a transparent media, the majority of it travels through, but a small fraction is back-scattered (Figure 1b). Scattering occurs due to inhomogeneity of the refractive index of the glass medium and allows coupling to acoustic waves known as phonons. The scattered lights can either propagate in the same direction as the incident light or travel in the opposite direction to the incident light where the latter is called backscattered light.

There are three notable scattering processes (see Figure 1b): (i) Rayleigh, (ii) Brillouin, and (iii) Raman scattering. Rayleigh scattering re-radiates at the same frequency as the incident light and can be used to measure the loss distribution or attenuation along the length of the fibre by analysing the Rayleigh scattered light power. A decrease in the scattered light power corresponds to the loss of light along the optical fibre. Brillouin scattering light is temperature and strain dependent, in which the frequency shift of the Brillouin spectrum varies with longitudinal strain and temperature in a fibre. Raman scattering, on the other hand, has spectrum power levels that vary according to temperature changes.

A typical highly distributed fibre optic sensing system includes two major components: optical fibre cables and an optical fibre analyser that performs a number of tasks (including data acquisition, data processing, transmission, and storage). Different types of analyser detect different scattering signals in a different way (e.g. injecting a broadband frequency laser, or an extremely narrow linewidth laser with short pulses, analysing in-time domain or frequency domain, and using a high power pulse to take advantage of non-linear scatting).

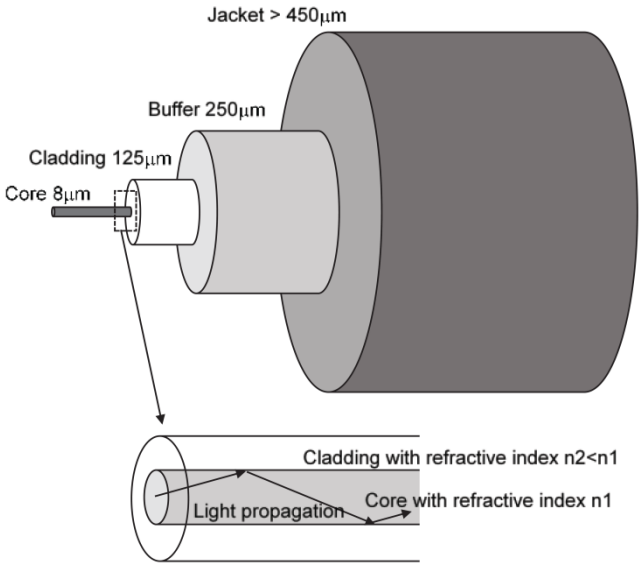

(a) Light propagation inside fibre optic cable

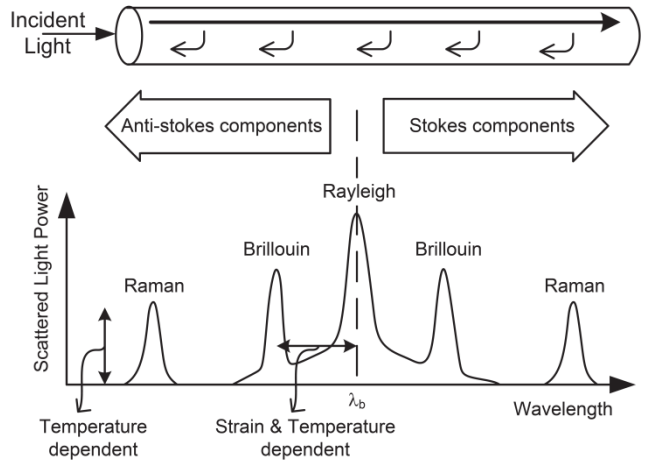

(b) Three back scattering processes

Figure 1. Light propagation and scattering.

For example, Phase-OTDR is capable of quantifying both acoustically induced and dynamic multiple strain perturbations. The technique is based on measuring the phase between the Rayleigh scattered light from two sections of the fibre which define the gauge length. It can perform long distance dynamic sensing for vibration and acoustics. Phase-OTDR can be used for security monitoring for long borders and perimeters at high-value facilities and high-level security locations, or real-time position and speed monitoring of trains.

The Raman Optical Time Domain Reflectometry (ROTDR) is a classical distributed sensing technology to measure temperature at many points along the length of an optical fibre. The distributed temperature sensing system (DTS) is a Raman scattering based system, which can be used for power cable and transmission line monitoring, fire detection, leakage detection at dikes, dams and sewers. It is widely used in downhole temperature monitoring of oil and gas wells.

The novel aspect of this new technology lies in the fact that a standard optical fibre becomes a sensor and tens of kilometres of fibre cable can be sensed at once for continuous distributed measurement of the conditions around the optical fibre such as temperature, strain, acoustic noise, etc. Because of its simple and quick installation, optical fibre based distributed sensing can be as equally practical as other conventional measurements. That is, the cost of a standard optical fibre is very low compared to other point measurement sensors. The material itself (i.e. Silica) is relatively inert and can be ideal for long-term monitoring by embedding the fibre inside structures. This implies that the quality of the data would increase with time as the capability of analysers is expected to improve with time. Such features can potentially provide a relatively cheap but highly effective monitoring system for both short and long term. Most of the capital investment relates to the analyser, which can be connected to a number of fibres or be shared at different sites. It is expected in the near future that a greater choice of analysers from more manufacturers would give a reduction in price with time.

2.2 Principles of distributed strain sensing

Brillouin scattering based techniques such as time domain techniques called 'Brillouin optical timedomain reflectometery (BOTDR)' and 'Brillouin optical time domain analysis (BOTDA)' are well-established for distributed strain measurement and are gradually coming into practice of civil engineering. BOTDR utilises the spontaneous back-scattering based sensing mechanism and works by injection a light from one end of the sensing fibre (Figure 2a), whereas BOTDA utilises the stimulated backscattering-based sensing mechanism and requires access to both ends of the sensing fibre (Figure 2b). As a comparison, the stimulated back-scattering (for BOTDA) offers much stronger signals than the spontaneous back-scattering (for BOTDR) and hence BOTDA gives better strain resolution than BOTDR. However, in BOTDA, the two ends of the sensing fibre need to be attached to the analyser in a loop configuration. This means that any accidental cut in the fibre cable results in no data, which is a major drawback for system reliability and robustness. However, with BOTDR, if a breakage occurs and both ends are accessible, it is still possible to obtain the whole strain profile.

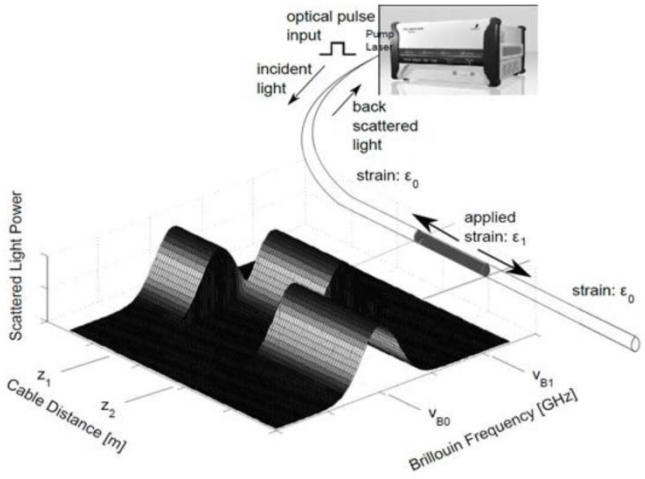

(a) Brillouin optical time-domain reflectometery (BOTDR)

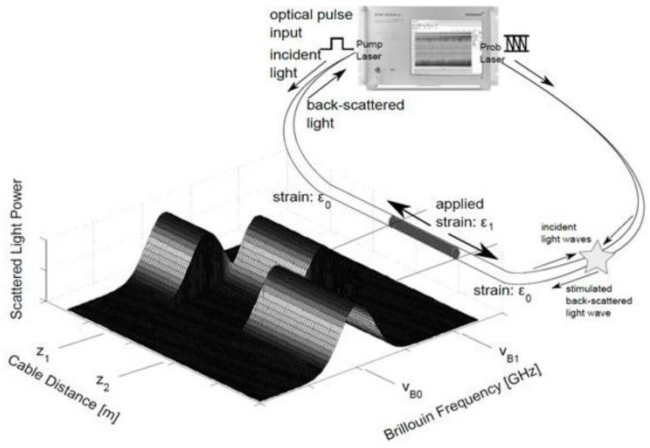

(b) Brillouin optical time domain analysis (BOTDA)

Figure 2. Distributed strain sensing techniques.

As shown in Figure 2a, when light (a wave length of 1550 nm) is pumped into an optical fibre, scattering is generated and the Brillouin spectrum of the back-scattered light can be analysed from the origin of the fibre. The Brillouin scatted light has roughly 25 to 30 MHz bandwidth and the central peak frequency is around 11 GHz for standard single mode fibres when no strain is applied, as shown in Figure 3. The back-scattered Brillouin central frequency υ_s is related to the input light based on the following equation.

$$\upsilon_s = (2\, n_f\, v_a) / \lambda_1 \qquad \text{Eq. (1)}$$

where n_f is the fibre core refractive index, v_a is the acoustic velocity in the fibre and λ_1 is the wave length of the input light.

Changes in temperature and/or strain induce density changes in the fibre, which in turn affect the acoustic velocity v_a and the refractive index n_f. As the strain or temperature at a given location changes, the frequency of the backscattered light is shifted by an amount linearly proportional to the applied strain or temperature (see Figure 3).

$$\upsilon_s = \upsilon_{so} + M\Delta\varepsilon + N\Delta T \qquad \text{Eq. (2)}$$

where υ_{so} is the central Brillouin peak frequency at zero strain and at a given temperature, $\Delta\varepsilon$ is the change in strain, ΔT is the change in temperature, and M and N are the proportionality constants for strain (about 500 MHz per percent strain) and temperature (about 1 MHz per degree Celsius). For the incident wavelength of 1550nm, the Brillouin frequency shift varies from 9GHz to 13GHz.

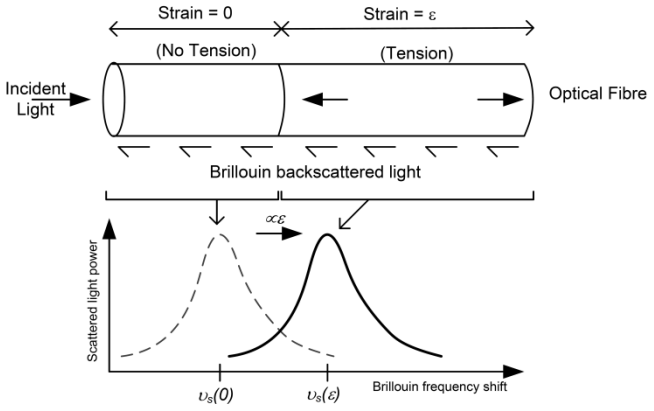

Figure 3. Frequency shift due to strain changes in the fibre.

In BOTDR, the length of the optical pulse determines the system spatial resolution. For example, 10 ns of pulse width will provide 1 m of spatial resolution. A longer pulse gives better back-scattered signal but the spatial gauge becomes longer. A shorter pulse would be better but the back-scattered signal tends to show high noise levels. A typical resolution of strain for a 10 ns pulse is ± 20 με after signal stacking operation to reduce the signal-to-noise ratio, which leads to longer data acquisition time.

As shown in Figure 2b, BOTDA utilises these two counter propagating waves coupled through a nonlinear parametric process where the energy transfers from the pump into the probe. The two waves propagate in opposite directions and generate an acoustic wave corresponding to their beat frequency. This allows better detection of the Brillouin scattering signal. The position-dependent information can be obtained by pulsing one of the optical waves and observing the local coupling on the counter-propagated wave. The spatial resolution can be improved to 0.5 m or less and the strain resolution to less than ± 5 με.

In summary, monitoring of this frequency shift in the Brillion scattering light gives information about strain and temperature change at the location where the back scattered light is generated. As the speed of light is constant, the location can be evaluated by measuring the time elapsed between when the light was pumped into the fibre and the time at which it comes back to the analyser. By resolving both time and frequency, it is therefore possible to generate a continuous strain or temperature change profile along the fibre for distances of a few kilometres or more.

The current state of the art distributed fibre optic strain measurement systems provide data in the micro-strain range with a spatial resolution (strain is averaged over a specified gauge length) of 0.2 m or less. This means that it is possible to have thousands of 'strain gauges' along a single cable connected to structures, or embedded in civil engineering infrastructure. Because of the simple and quick installation technique, distributed optical fibre sensing can be as equally practical as other conventional strain measurement systems.

2.3 Fibre optic cables for strain and temperature measurement

As described earlier, the fibre optic sensing cable itself is the sensor. A direct interpretation of the behaviour of a structure can be made by embedding fibre optic cables within it, or by attaching them to its surface. Fibre optic cables should be robust enough to survive in harsh construction environments, as well as sensitive enough to report the structural performance.

Typical strain measuring cables are shown in Figure 4a and 4b. The various coating layers and the inner glass core and cladding are bonded together so that the strain applied externally is fully transferred from the surface coating to the inner core. Additionally there should be no creep between the cable and the structure so that strain due to structure deformation is fully transferred to the cable.

Figure 4a shows a standard single fibre cable. It is very small (0.9 mm diameter). On the other hand, Figure 4b shows a reinforced cable, which is used for piling and diaphragm wall monitoring. It has steel wires on both sides and strong nylon is used for coating to protect the fragile optical fibres. However, it is more expensive than the former cable.

As the Brillouin frequency shift is sensitive to both strain and temperature, temperature compensation may be needed. In the case studies presented in this paper, a standard loose tube telecom cable, shown in Figure 4c, is installed alongside the strain sensing cable for temperature compen-

sation. It consists of several optical fibres installed in a gel filled tube so that any mechanical deformation applied to the jacket is not transferred to the cores (*M* in Eq. (2) is therefore zero). The cores contract or expand due to changes in temperature only. Further information on temperature compensation can be found in Mohamad et al. (2014). Advances in fibre optic cable manufacturing are rapid and both strain and temperature cables are expected to become more robust and less expensive as long as there is market demand.

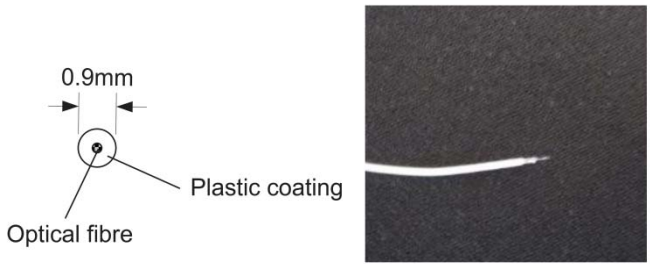

(a) Standard single strain measurement cable

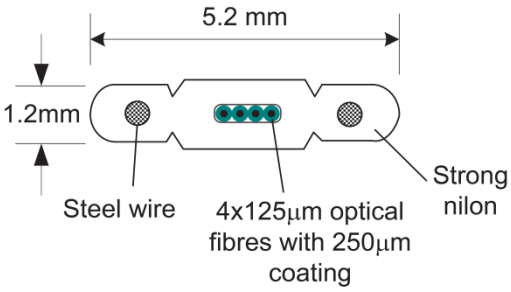

(b) Reinforced strain measurement cable

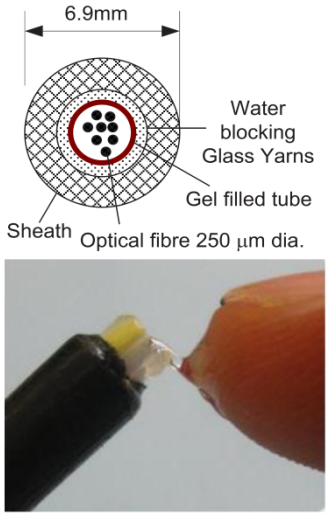

(c) Unitube temperature measurement cable

Figure 4. Fibre optics cables used in this study.

3 CASE STUDY 1 – PILE TESTING USING OCELLS

3.1 Site description

A pile load test was performed at a site in the Isle of Dogs, London. The proposed development comprises a 60-storey tower over underground tunnels. The soil stratigraphy is Made Ground, Alluvium and River Terrace Deposits overlying Lambeth Group, Thanet Sand and Chalk. The foundation design considers loads from the structure spanned across the tunnels and supported by piles on both sides. Due to heavy loading and limited space, the piles are required to be up to 2.4m in diameter, up to 60m deep founded in Chalk.

Eurocode 7 requires a pile load test to be carried out when past experience does not provide sufficient confidence in design. At this site, an Osterberg cell (O-Cell) pile load test was performed. O-Cell involves a sacrificial loading device being installed within a bored pile. It is usually placed at the bottom section of the pile to examine the pile shaft capacity and end capacity separately. During testing, it is hydraulically expanded and the pile is tested bi-axially. Resistance from the lower part of the pile provides reaction against the upper part of the pile and vice versa. This self-reaction system allows a pile to be tested to loads unreachable by traditional top-loaded systems. Typically the pile is instrumented with the conventional system of vibrating wire strain gauges and rod extensometers. In this study, a distributed fibre optic sensing system was also adopted so that better understanding of the load transfer mechanism along the pile could be gained.

The test pile at this site was 1.5 m in diameter and 51 m in length. As shown in Figure 5, the pile was socketed 13 m into Chalk. The pile bore was supported using bentonite and a temporary casing through the superficial layers. An O-Cell system was installed at 6m above the pile toe (see Figure 6). The pile reinforcement is continuous along the pile length, but separated into two sections to allow opening of the O-Cell. The reinforcement cage diameter was 1350 mm. The reinforcement cage was assembled in four sections spliced together using couplers as they were lowered into the shaft. An O-Cell system was built into the lowest cage section 5.8 m above the toe before construction. There is a funnel made of rebar above the O-cell to guide the tremie pipe through an off-centred hole in the O-cell assembly as shown in Figure 5.

Four fibre optics cable loops were installed; two loops (strain and temperature cables, as shown in Figure 7a) were placed through the O-cell assembly to the bottom of the pile and two loops (strain and temperature cables) to just above the O-cells. The cables ran along the length of the pile and were positioned on the cage perimeter 675 mm from the centre of the pile in two radial lines approximately 90° apart.

The cables are identified as T or S for temperature or strain, a numerical prefix and a numerical suffix. The prefix identifies the location around the pile, the suffix identifies the regiment, as shown in Figure 7b. For example, cable S-3-1 is a strain cable at location 3 that terminates below the O-Cell. T-2-2 is a temperature cable at location 2 that terminates above the O-Cell.

The bottom section of the cage was instrumented prior to lowering it into the drilled shaft. For the remaining three cage sections, the cables were attached to the cage as it was gradually lowered into the shaft as shown in Figure 8a and b. Cables were attached directly to the reinforcement cage using cable ties as shown in Figure 8c. The cables were coiled in 1.5 x diameter loops at points of termination within the pile. In summary, there were four points for distributed strain data as well as four for distributed temperature data. A BOTDR system was used for the measurement.

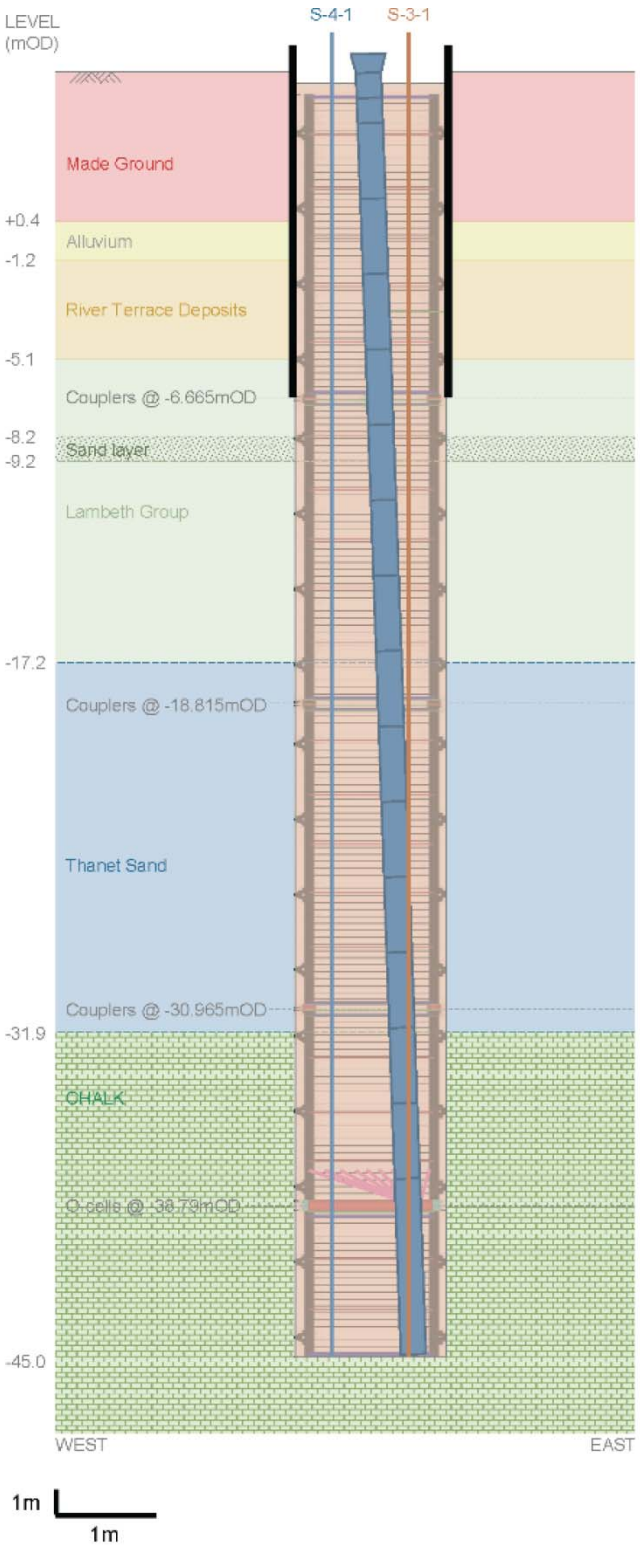

Figure 5. Pile geometry and soil stratigraphy.

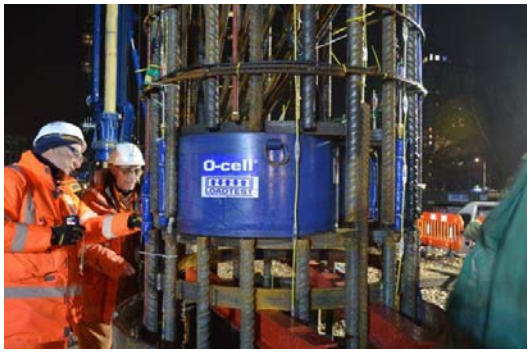

Figure 6. Osterberg cell (O-Cell).

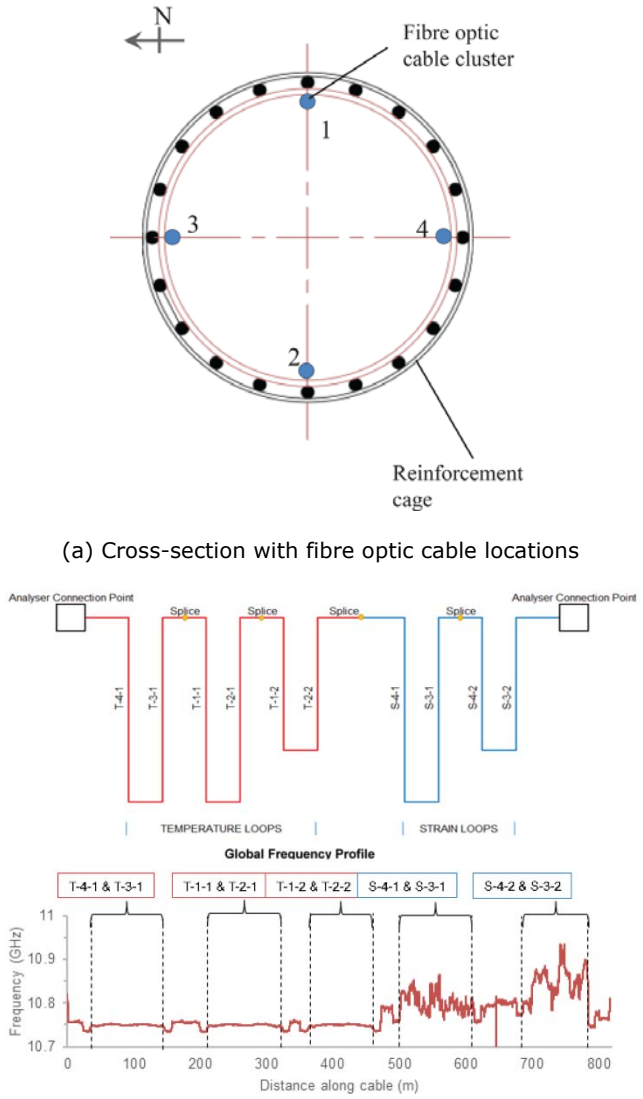

Figure 7. Pile cross-section and cable numbers.

It provided sampling interval of 5 centimetres and the spatial resolution was 50 centimetres. Further details of the installation can be found in Chunge (2015).

The conventional instrumentation included sister bar vibrating wire strain gauges (VWSGs), tell-tales, extensometers and LVDTs. The locations of the instruments are shown in Figure 9.

3.2 Data interpretation

The maximum applied load was 30.87 MN and the loading scheme had twenty-one stages including one intermediate unloading step, as shown in Figure 10. Several readings were taken at each load step, with a 14 minute measurement interval between successive readings.

The expected response of a pile in an O-Cell test is shown schematically in Figure 11. The O-Cell simultaneously generates an upward and a downward force as it expands under hydraulic pressure. Above the OCell, the applied force is resisted by downward acting shaft friction from the soil layers. The mobilised friction will vary depending on the properties of the soil and pile-soil interface. Below the O-Cell, the applied load will be resisted by upward-acting friction and typically a base reaction. The compressive internal axial load and pile strain will decrease in both of these regions due to friction.

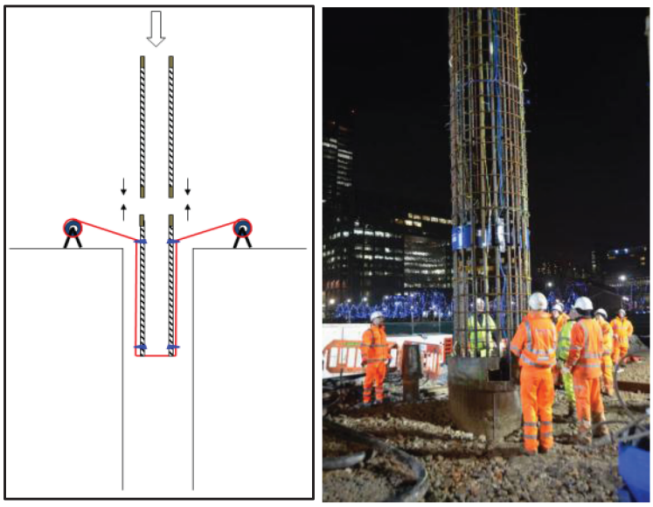

(a) Installation of reinforcement cage and optical fibres

(b) Coiled optical fibres fed into the borehole with the cage

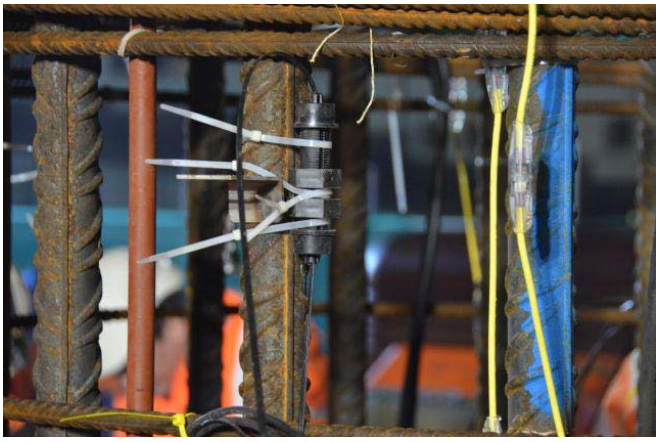

(d) Cable attachment to the cage

Figure 8. Optical fibre installation process during pile construction.

The progression of distributed strain profile development over all the load stages (except unloading) is shown in Figure 12 for two of the four strain cables. Negative values for strain change represent compression in the cable. Due to the hydration process of the concrete, the strain cables have different initial baseline strain profiles prior to applying an O-Cell load. The strain profiles plotted in these figures are the incremental strains from the baseline values to show the effect of loading only.

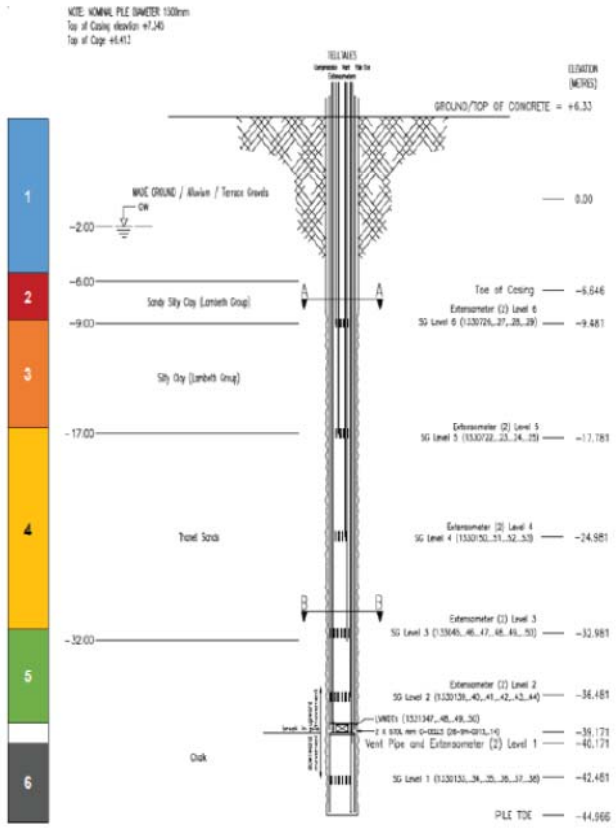

Figure 9. Location of conventional instrumentations (Reproduced from Fugro Loadtest drawing FLT20076-2 dated February 3 2014).

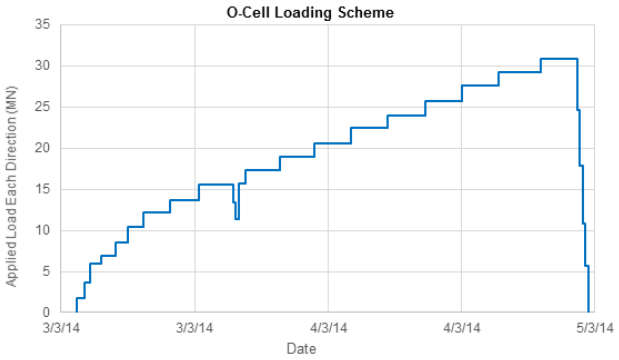

Figure 10. Loading Scheme.

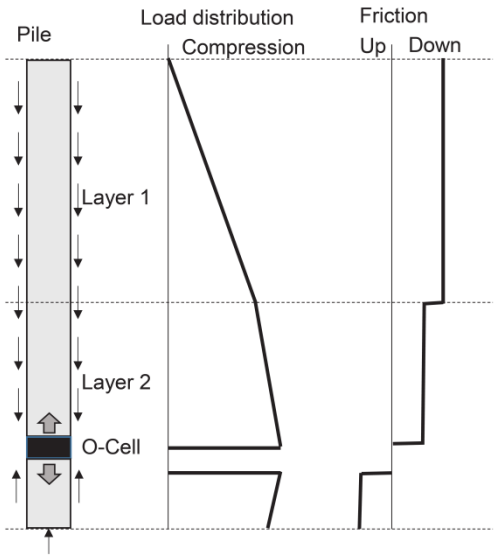

Figure 11. Expected response of a pile in an O-Cell test.

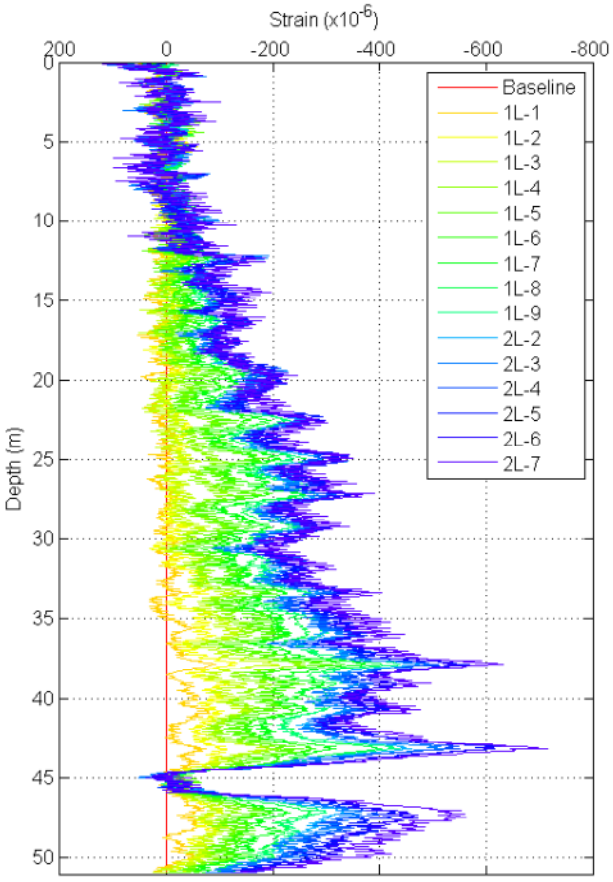

(a) Cable S-3-1

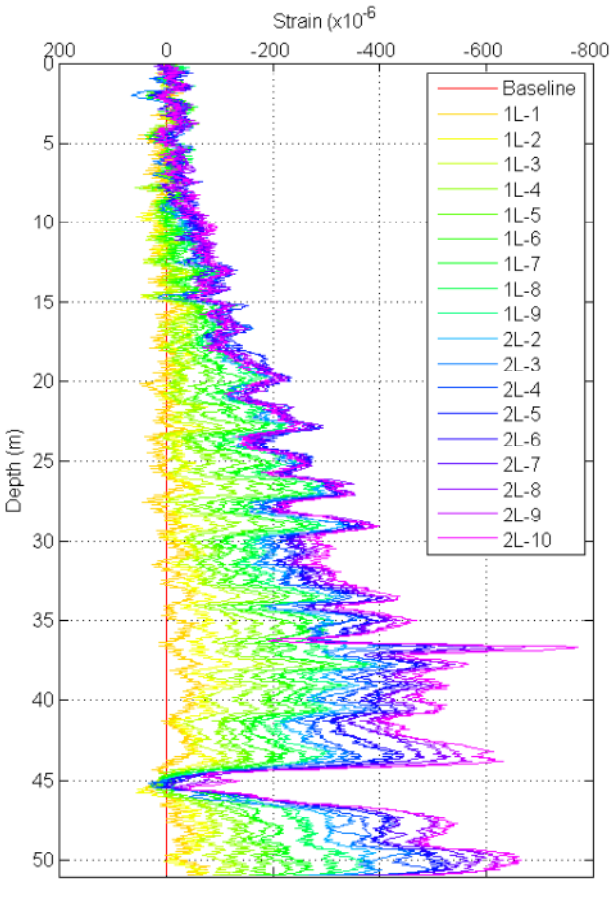

(b) Cable S-4-1

Figure 12. Increase in strains with load.

A plot of the strain in all cables at the 25.66 MN step is given in Figure 13. All cables show the largest compression directly above and below the O-Cell and the strain profiles generally follow the expected response. However, there are notable features such as large fluctuating strain profiles along the length of the pile as well as variable behaviour of different cables below the O-Cell and in the top cage section. It is interesting to note that the peaks and troughs of the four cables correspond well. These cables have independent baseline values but produce similar strain responses regardless of this. This suggests that the fluctuating response is potentially related to the real condition of the pile.

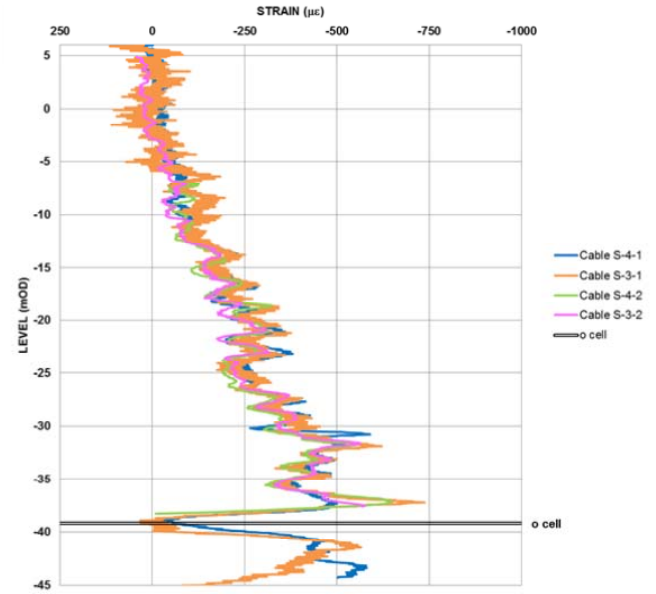

Figure 13. Strain distributions of four cables at the 25.66 MN step.

Six levels of VWSGs were installed in the pile; four gauges at each level for the top three levels, and six gauges at each level for the bottom three levels. The bottom-most level was installed below the Ocell. There were extensometers at VWSG levels and also to the top of O-cell and pile toe. Strain measurements from fibre optic sensors, VWSGs and extensometers at the maximum load (30.9 MN) are compared in Figure 14. The fibre optic strain profile compares reasonably well with measurements from VWSGs and also average 'strain' between the levels using the readings from the extensometers.

A displacement profile can be estimated by integrating the strain profile. The displacement profiles relative to the top of the pile is shown in Figure 15. The computed relative displacement at the bottom is compared to the difference in the extensometer readings at the top of the O-Cell and the top of the pile as shown in Figure 16. At the maximum loading stage, the pile experienced 11.48mm of compression over the 44 m of pile above the O-Cell. The two compares well up to the load of 20 MN or so, providing confidence in the distributed strain data.

The observed fluctuation in the data requires further investigation. The BOTDR system produces random noise of approximately 30 με at 0.05 m sampling intervals, which is very different from the waviness of approximately 2.5 m to 3 m apart shown in the profile. Most importantly, they are visible at the same locations in all cables despite each having an independent baseline profile. The peak and troughs typically develop over distances larger than the analyser spatial resolution, suggesting that the cable responses are representative of actual conditions.

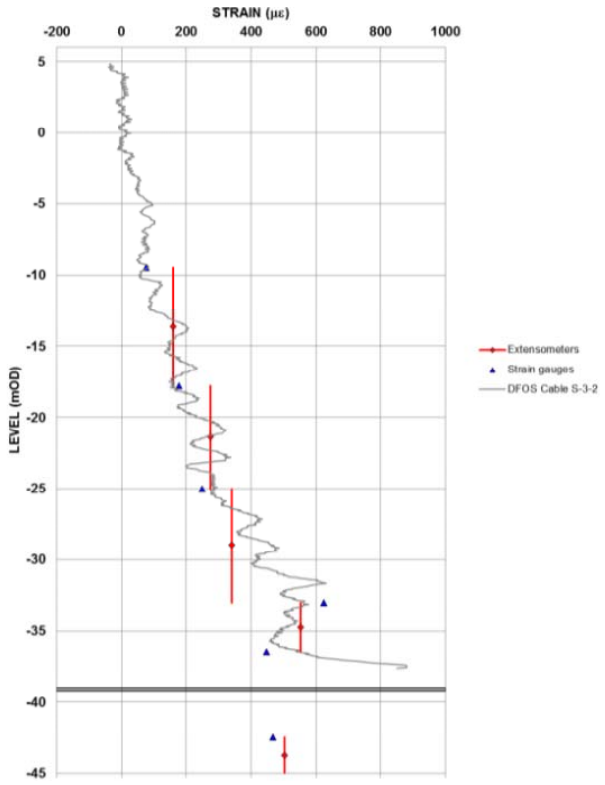

Figure 14. Comparison between FO strain data and conventional instrument data at the 30.9 MN step.

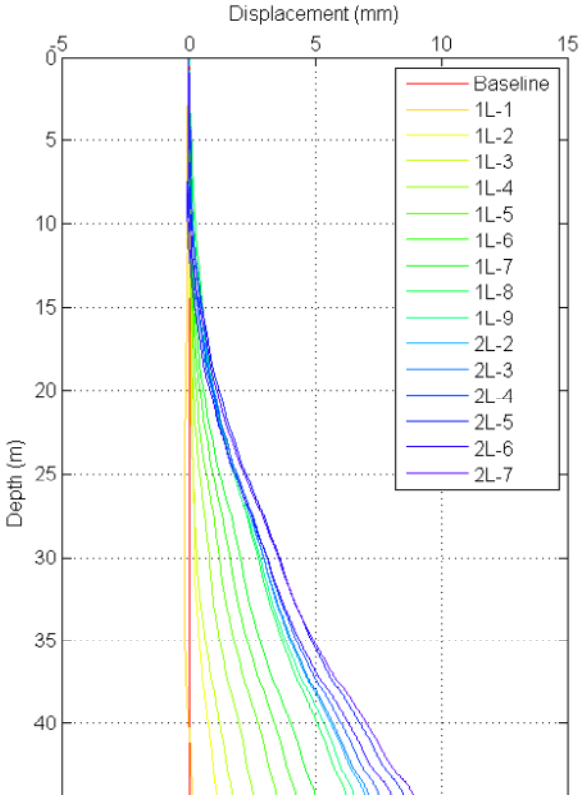

(a) Cable S-3-1

Figure 15. Displacement profiles at different loading stages. The displacement values are relative to the top of the pile.

The FFT analysis in the spatial domain did not reveal constituent signal frequencies. Most of the peak to trough ratios are between 1.1 and 2.1, suggesting that this variation in strain is unlikely to be purely due to variation in pile stiffness (*EA*) (caused for example by features such as local change in cross-sectional area, reinforcing links or isolated stiffening bands in the reinforcement cage). That is, there needs to be a substantial change in pile configuration for pile stiffness to be doubled or halved.

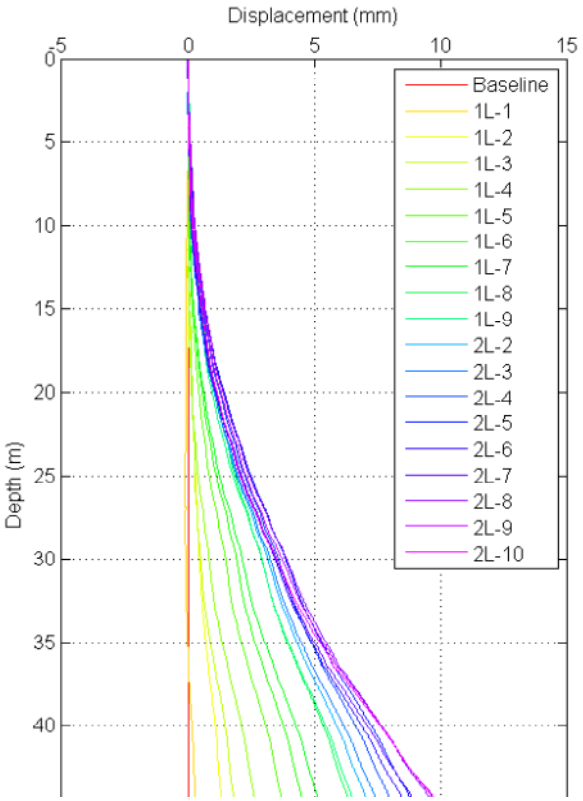

b) Cable S-4-1

Figure 15. Displacement profiles at different loading stages. The displacement values are relative to the top of the pile.

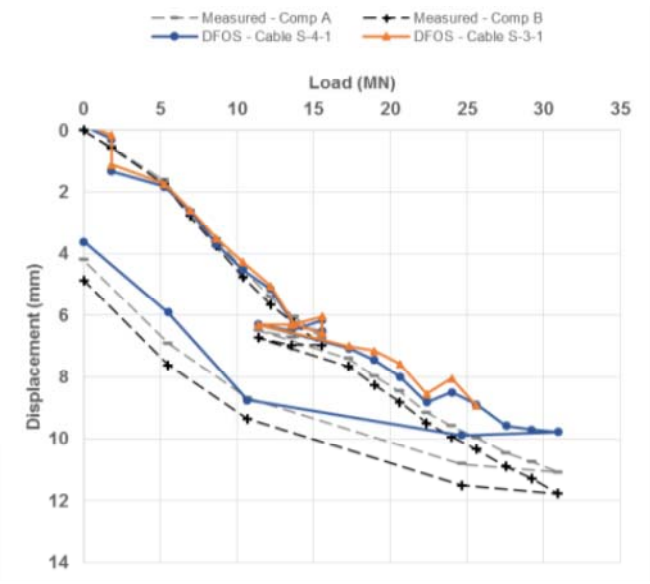

Figure 16. Displacement from integrated DFOS strain at the top of O-cells.

It also appears to correspond to the location of internal rings which were spaced roughly 2m apart in the cage as shown in Figure 17. Also, construction records were examined and the only thing identifiable is that many tremie pipe sections were in 3m segments. For each stage, the top of the concrete and rise in concrete level after each pour was

drawn adjacent to the strain profile. There might have been some correlations, but none were definitive. The major peak between 36m and 37m coincides with a number of occurrences, namely the boundary between Thanet Sand and Chalk, the splice connection between the bottom-most reinforcement cage and the one above, the top level of the third load of concrete and the bottom level of tremie pipe during the fifth load of concrete. Further investigation is required.

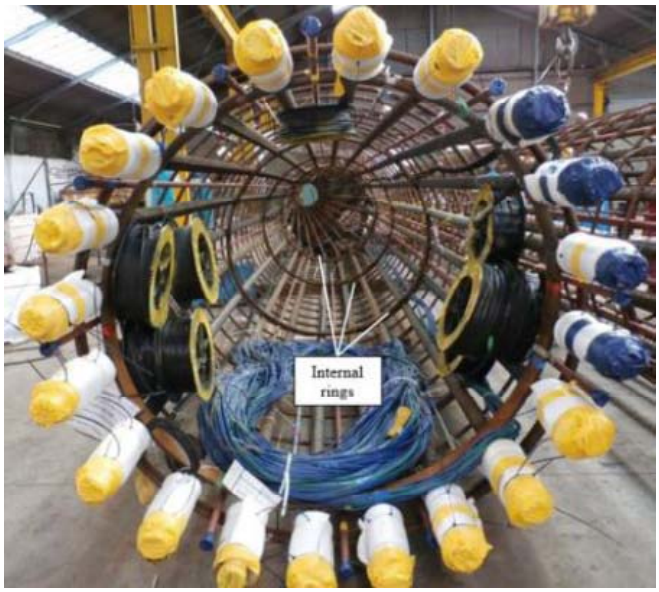

Figure 17. Internal rings spaced at 2m interval.

3.3 Engineering Analysis

Above the O-Cell, the pile strain responses show values of compressive strain in the range of 600-750 με immediately above the O-Cell, decreasing to a near zero value at the pile head. Although the strain profiles are wavy, the displacement profiles (see Figure 15) can be derived and they are very useful, in turn, to derive the shaft resistance-displacement (or *t-z*) characteristics of different soil layers. In this study, this was done by evaluating the shaft friction from the axial strain profiles of each soil layer at a given O-cell displacement and then plotting the values against representative layer displacements derived in Figure 15.

According to the core data logs, the subsurface was split into four layers (Made Ground, Silty-sandy clay, Thanet sand and Chalk). The t-z curves for the four layers derived directly from the FO-data are shown in Figure 18. The data from the Silty sandy clay layer and the Thanet sand layer give consistent *t-z* relations among different FO cables. It is interesting to note that the *t-z* relation of the Silty sandy clay layer shows initial slip-like behaviour before shaft friction mobilises with increasing shaft displacement. The *t-z* relations of the Made Ground layer and the Chalk Layer vary among different FO cables. This observed variation may be due to ground heterogeneity and variable construction effects.

In this study, a simple 1D *t-z* finite element model was developed as shown in Figure 19. A 45 m pile loaded from the bottom according to the loading schedule was modelled and an element size of 1 m was adopted (i.e. total number of elements: 45). The examination of the FO data suggested that the pile-soil interface of some layers required to have a small initial slip before shear resistance mobilises. To model this, the following 'modified' hyperbolic relation was used.

$$t = \frac{k_m z_0}{\left[1+\left(\frac{t_m z_0}{k_m}\right)^{hd}\right]^{\frac{1}{d}}} + \frac{k_m (z-z_0)}{\left[1+\left(\frac{t_m |z-z_0|}{k_m}\right)^{hd}\right]^{\frac{1}{d}}} \quad \text{Eq. (3)}$$

where z_0 is related to the initial slip, k_m, t_m, h and d are the model parameters, which are determined from calibration fitting of the data shown in Figure 18. When z_0 =0, the *t-z* relation becomes a standard hyperbolic curve.

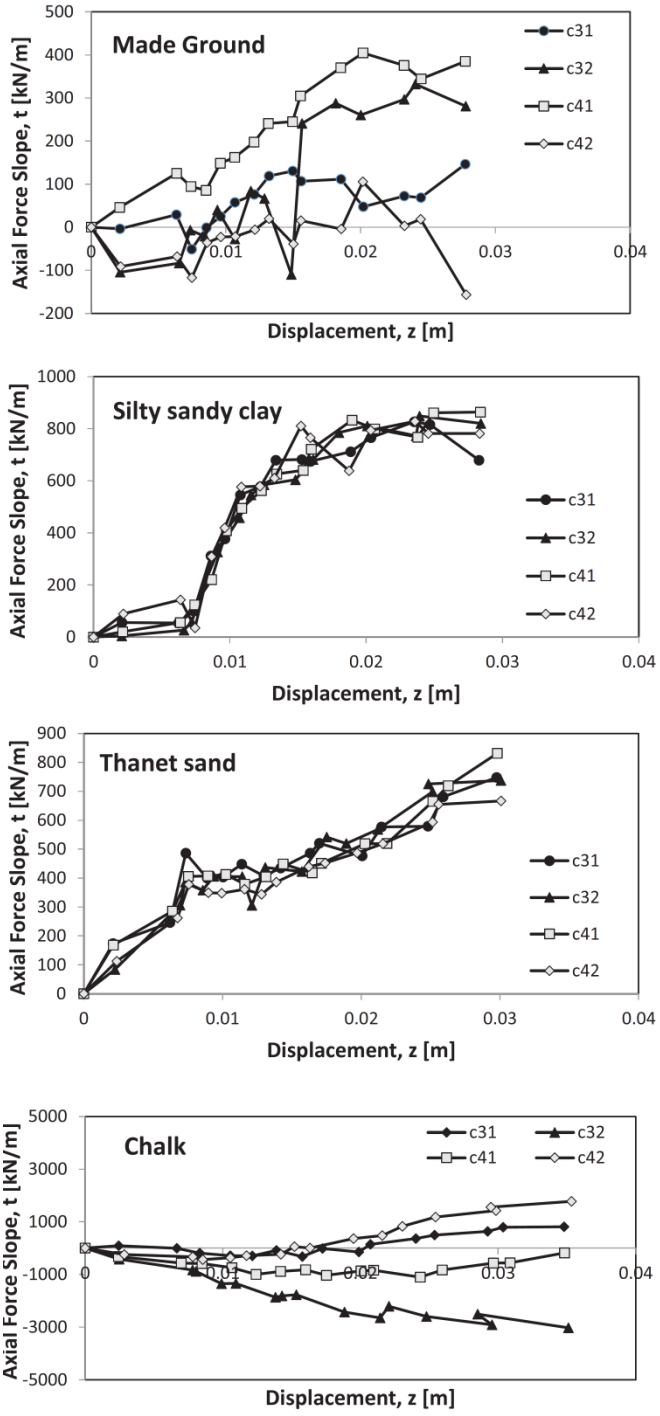

Figure 18. The *t-z* relations of the four soil layers derived directly from the FO data.

A value of 52,200 MN for *EA* was provided as an estimate for the friction calculations. Two models were used: (a) MODEL 1 which has a standard hyperbolic-type *t-z* curve (with *z0*=0) and (b) MODEL 2 which has a modified hyperbolic-type *t-z* curve that allows for an initial slip (for $z_0 \neq 0$).

The applied load was given as a boundary condition at the bottom of the pile and the equilibrium equations were solved to obtain the pile displacements. Some iterations were needed to reach convergence at each loading stage to satisfy both force equilibrium and displacement profile. At the end, using the local element (pile+soil spring) matrix,

the induced forces and resulting shaft frictions were obtained.

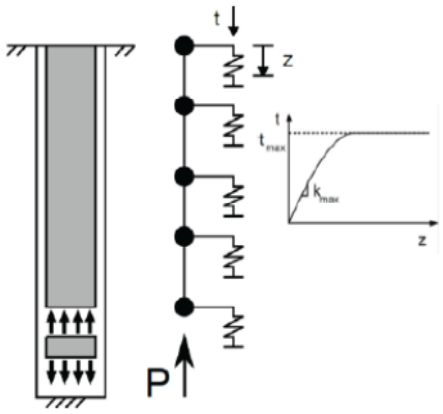

Figure 19. One dimensional t-z FE model for O-cell test.

Figure 20 shows that the computed displacement and axial strain profiles at four different loading stages match well to the measured data for the case of MODEL 2 considering the initial slip. This is more pronounced in the case of vertical displacements, where the standard hyperbolic case with no initial slip (MODEL 1) tends to under-predict the displacements for small load conditions (e.g. P=3.6 MN, 5.9 MN) and over-predict for larger load conditions (e.g. P=20.5 MN, 25.7 MN), i.e. overestimate the soil stiffness for small loads and underestimate it for larger loads. The displacement profiles are useful to calibrate the pile-soil interaction model to understand the shaft resistance mobilised in the different soil layers. It should be noted that the displacements are the actual displacements of the top section (not the relative displacements from the top as shown in Figures 15 and 16).

Figure 21 shows the back-calculated *t-z* relations of the four soil layers for the two models along with the *t-z* curves evaluated directly from the fibre optic strain data (in grey lines). The following observations can be made.

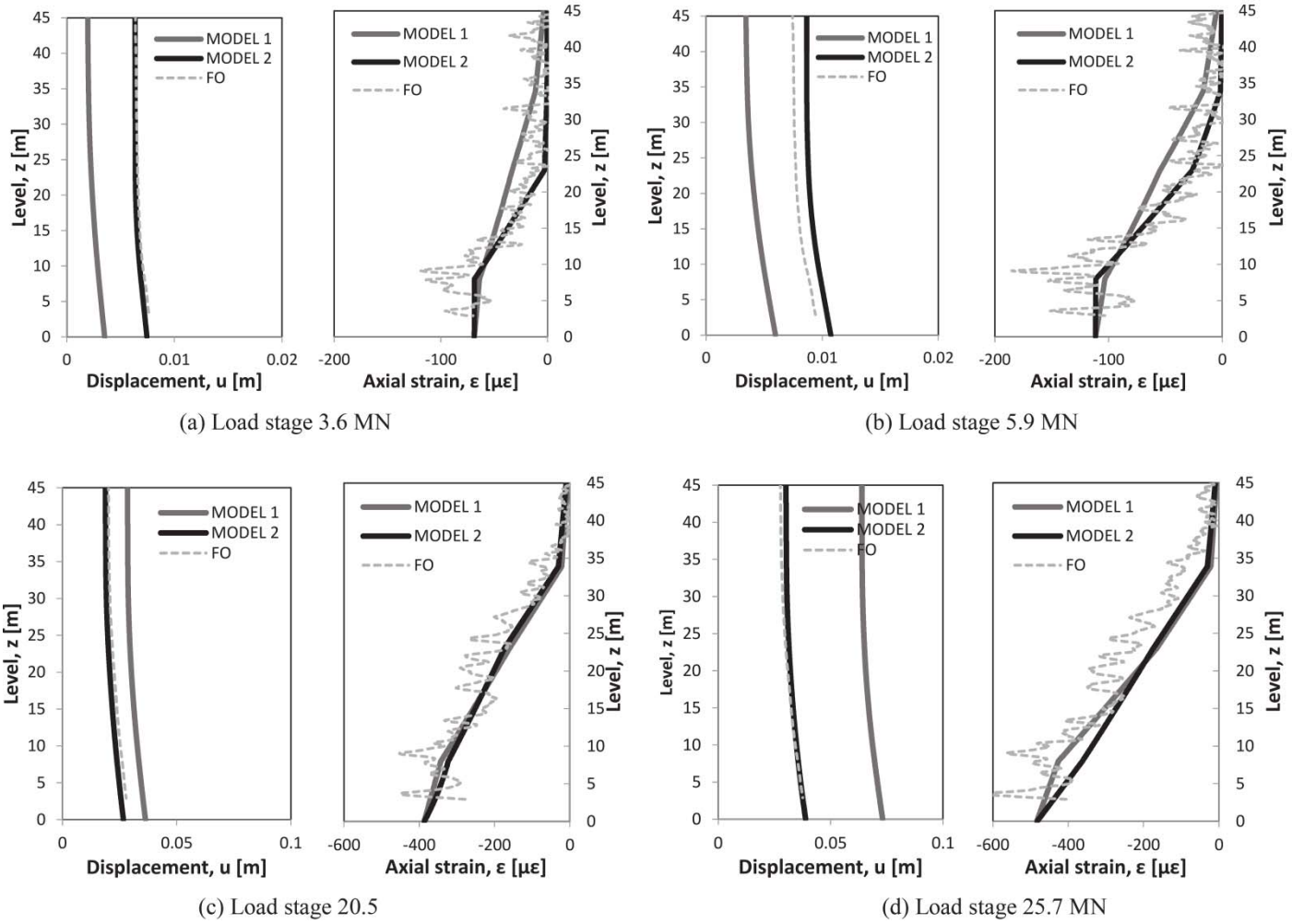

Figure 20. Field data versus model prediction for displacement profiles and axial strain distribution at four loading stages.

Made ground layer – The FO data from the 4 FO cables around the pile show variability in this relatively thin soil layer. The back-calculated *t-z* relation with a minor initial "slip" and then gradual development of shaft friction gave good fit to the displacement and axial strain profiles. The variation in the FO data and the initial slip may due to the construction process of casing installation and removal. The ultimate shaft resistance appears to have reached at around 100 kN/m (or 21 kPa).

Silty sandy clay layer – The *t-z* curves show significant development of shaft friction in this layer compared to the made ground layer. The FO data show very clearly an initial slip of the soil-pile interface. The ultimate shear resistance is about 700 kN/m (or 150 kPa). The FO data from the four FO cables around the pile show very good consistency for this relatively thick soil layer and also the comparison with the FE model is in good agreement.

Thanet sand layer - The *t-z* curves show significant development of shaft friction. The shear resistance at the maximum loading stage is about 700 kN/m (or 150 kPa). The shear resistance mobilisation is more gradual than the Silty sandy clay layer. No plateau is observed. The FO data from

the four FO cables around the pile show very good consistency for this thick layer and also the comparison with the FE model is in excellent agreement.

Chalk layer – Because the FO data gave variable *t-z* curves (see Figure 18), it was decided to assign a relatively small stiffness for the layer. The large compressive strains above the O-cell (between -35.5 moD and -37.5 moD in Figure 12) may be due to the complex interaction of the O-Cell loading plate, concrete and reinforcement, which requires further investigation. Between -35.5 moD and -32.0 moD in Figure 12, the strain values are almost the same, suggesting limited shaft friction maybe developing in the Chalk. Further investigation is needed to understand the engineering behaviour of this particular layer.

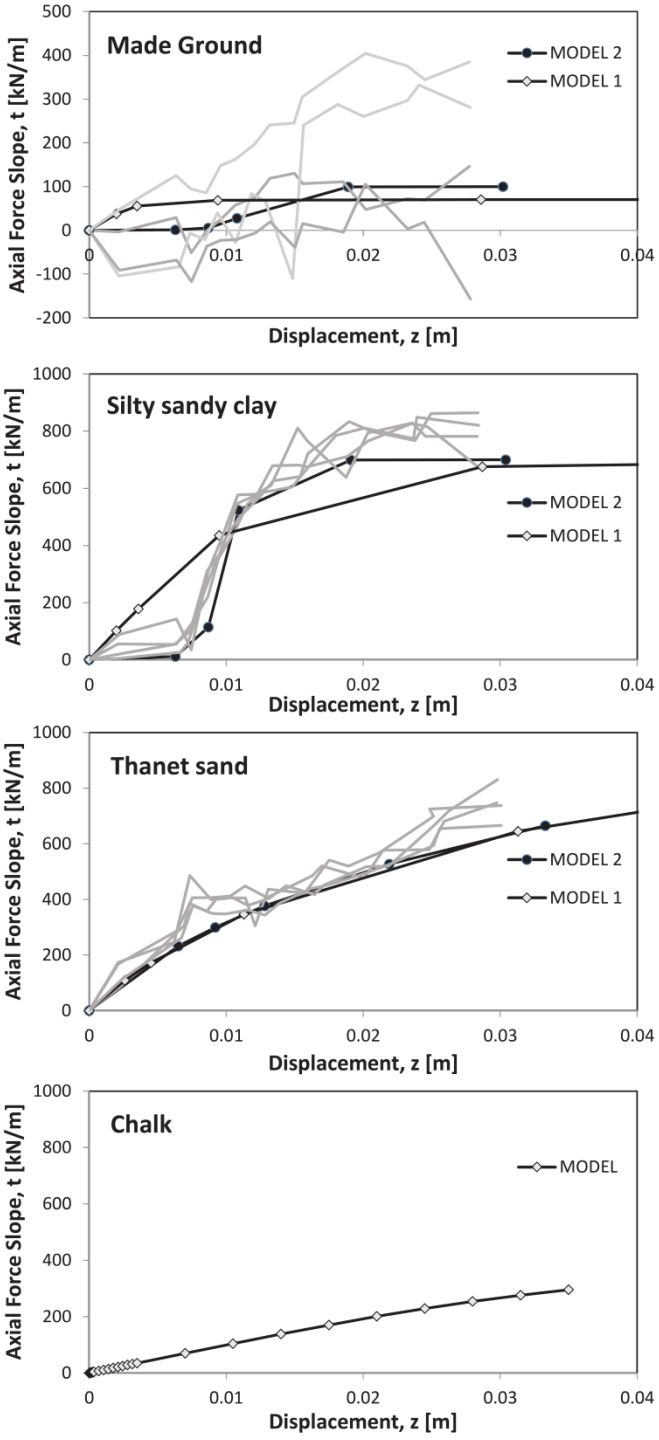

Figure 21. Back-calculated t-z relationships of five soil layers.

Coupled with the pile head displacement data, the distributed strain data gave the complete displacement profiles within the pile at different loading stages. This in turn provided a unique opportunity to derive the *t-z* relations of the soils along the pile shaft by back analysis.

4 CASE STUDY 2 – THERMAL PILES

4.1 Site description

A ground source heat pump (GSHP) system provides heating and cooling to buildings by using the ground as a heat source for heating in winter and a sink for cooling in summer. A typical GSHP system used in urban settings consists of a closed pipe system buried in the ground and a thermal transfer fluid travelling inside the pipe loops. In winter, a cold fluid is injected to absorb heat from the warmer ground. The heated fluid goes into a heat pump system to increase the temperature of the secondary loop heating system that is circulated inside the building. In summer, the reverse happens; a hot fluid generated from an air conditioning heat pump system is injected into the pipe system to dump the heat to the colder ground. By balancing the amount of heat injection and extraction similar within a year, the average ground temperature can be kept constant for long-term operation so that the system works efficiently.

GSHP itself is an established technology, even though the potential to cater for the heating and cooling demands of a city could be further exploited (e.g. Zhang et al., 2014). For new building and infrastructure developments, it is possible to incorporate this mechanism for heat transfer between the building and the ground through the foundation elements (e.g. piles and diaphragm walls). Since the mid-1980s, so called 'thermally active foundations' as shown in Figure 22 have found application across Northern Europe (Suckling & Smith, 2002; Brandl, 2006; Adam & Markiewicz, 2009). A thermal pile has a pipe network installed inside the structural piles of a building. The pipe loop is attached to the reinforcement cage of the pile before concrete is poured to create the pile. As concrete has excellent thermal conductivity and good storage properties, foundation piles are an ideal medium for heat transfer. In the UK, there have been a number of landmark thermal pile schemes constructed such as the 'One New Change' project (Garber et al., 2013b), as well as many smaller projects (Keeble college, Suckling & Smith, 2002; Lambeth college, Bourne-Webb et.al, 2009; Oxford Earth Science building, Garber et al., 2013a).

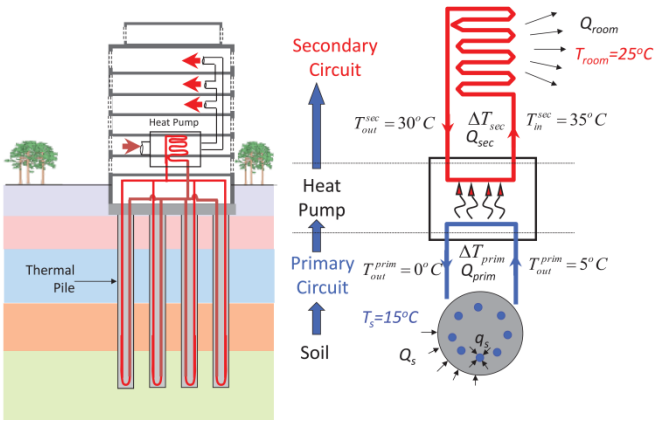

Figure 22. Thermal piles and heat pump system during heating.

The geotechnical performance of a thermal pile when it is heated or cooled gives rise to one design concern; that the change in temperature may induce pile settlement by cyclic thermal expansion and contraction of the pile. Or that the pile may generated large tension stresses during cooling by the strong soil resistance along the pile shaft.

To quantify the thermal influence on pile behaviour for use in engineering practice, a thermomechanical pile loading test was performed at the Clapham Centre of Lambeth College in South London in 2007. The pile load test scheme included (i) a non-mechanically loaded pile with a diameter of 600 mm and a length of 30 m (Pile 1) and (ii) a mechanically loaded pile with a diameter of 600 mm and a length of 23 m (Pile 2). The ground conditions were a superficial layer of Made Ground (1–1.5 m thick), River Terrace Deposits (3–4 m thick) and the London Clay Formation, which extends well below the toe level of the piles. The ground water table was found within the river terrace deposit which was about 3 m below ground level. The piles were installed in London clay and different temperature cycles were applied. Figure 23 shows the schematic layout of the field test.

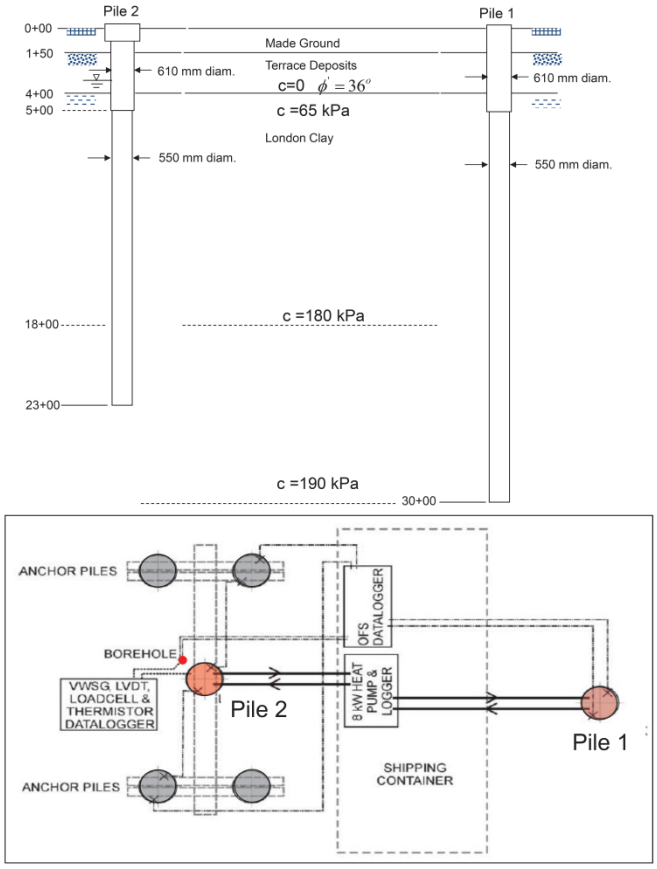

Figure 23. Thermal pile test layout.

Figure 24 shows the instrumentation layout of the mechanically loaded pile (Pile 2). A fibre optic system and vibrating wire strain gauges were used to record temperature and strain change throughout the test. Other measurements included pile head movement, ambient air temperature and the input or output temperature of fluid in the heat pump system.

Before conducting the thermal test, Pile 2 had a mechanical loading cycles of 1800 kN to zero and then to 1200 kN. The thermal test then lasted for about seven weeks with sequences of heating and cooling for Pile 1, as shown in Figure 25. The thermal sequence of Pile 2 was the opposite; for example, the heat extracted from Pile 1 was dumped into Pile 2. The initial ground temperature on site was about 19 degrees, which was roughly 3 to 5 degrees higher than the average range of ground temperature in London. For Pile 2, cooling commenced first from 18 June to 18 July. Heating was subsequently applied from 19 July to 30 July, during which the heating was interrupted on 23 July due to power failure. After 30 July, several cooling and heating cycles were applied. It is believed that the temperature was raised by the heat from the surrounding London underground tunnels. Further details of the test can be found in Bourne-Webb et al. (2009); Amatya et al. (2012) and Ouyang (2014).

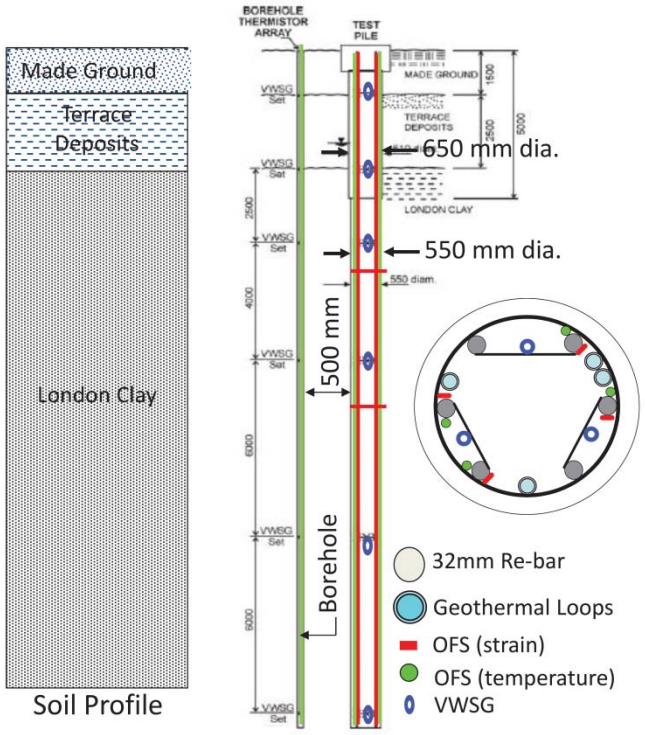

Figure 24. Instrumentation layout.

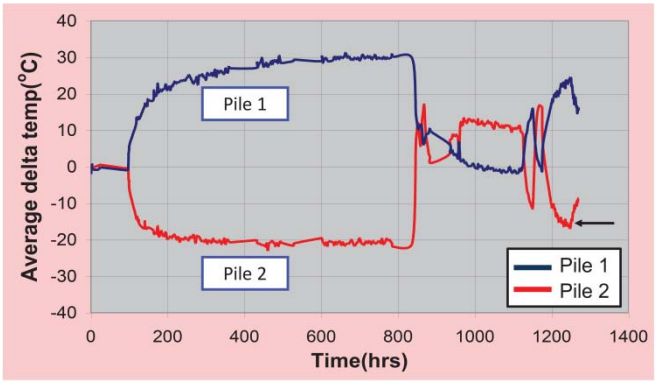

Figure 25. Changes in temperature with time for Pile 1 and 2.

4.2 Site description

Figure 26 shows a strain profile of Pile 1 during heating of ΔT = 30 ºC. The pile expanded during the first heating phase. The top expands freely upwards (e.g. thermal expansion coefficient of concrete x change in temperature) and the bottom also expands downwards. The expansive strain reduces from the two ends and becomes the smallest in the midsection. Therefore, the thermal expansion of the pile is resisted by negative soil friction at the top and positive soil friction at the bottom as shown by a simple mechanism presented in Figure 27.

The thermally induced force (ΔP_T) in the pile can be computed by the following equation.

$$\Delta PT = EA(\Delta\varepsilon_{measured} - \alpha\Delta T) \qquad \text{Eq. (4)}$$

where E is the Young's modulus of the pile material, A is the cross-sectional area, $\Delta\varepsilon_{measured}$ is the measured strain shown

in Figure 26, α is the thermal expansion of the concrete and ΔT is the change in temperature.

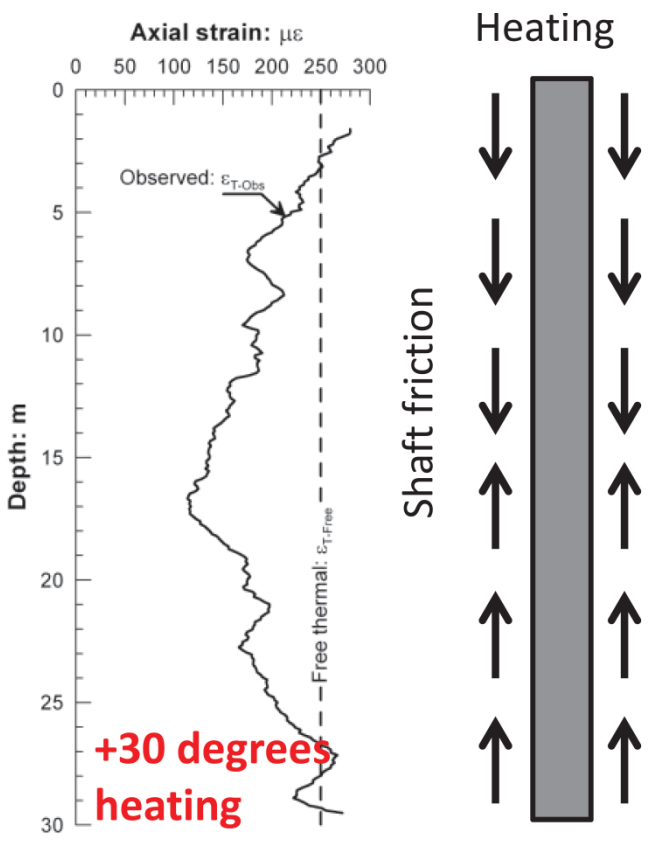

Figure 26. Strain distribution in Pile 1 by heating of ΔT = 30 ºC.

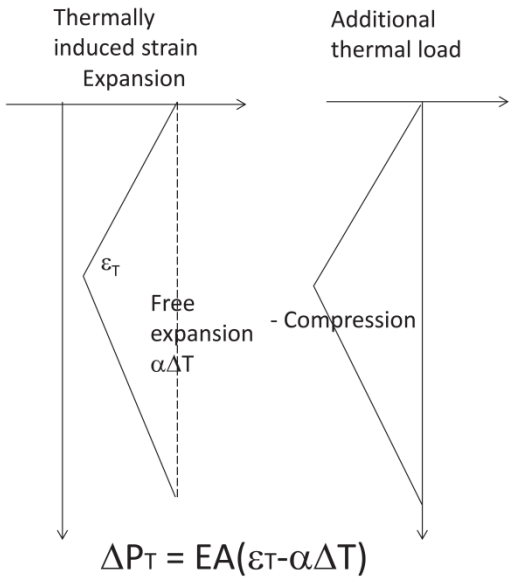

Figure 27. A mechanism of heating of a pile.

Using Eq. (4) and the FO strain data, the load distribution within the pile during heating can be shown in Figure 28 (tension positive). The distributed strain data gives the complete distributed nature of the heating effect on the thermally induced stresses. Upon heating, the top portion develops negative friction as the pile tends to expands upwards, whereas the bottom portion develops positive friction as the pile tends to expands downwards.

From the load profiles at different temperatures, the development of shaft friction with temperature can then be estimated. The mobilisation of shaft friction increases with temperature as shown in Figure 29. For this case study, the amount of mobilisation appears to be proportional to temperature increase.

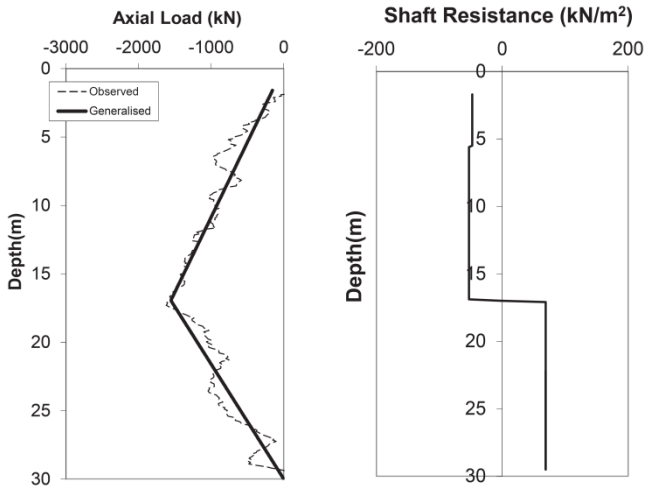

Figure 28. Thermally generated load and shaft friction distribution in Pile 1 by heating of ΔT = 30 ºC.

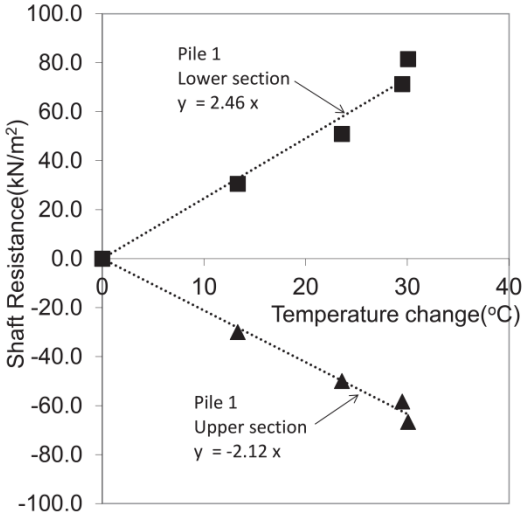

Figure 29. Thermally generated shaft friction.

Pile 2 was loaded to 1200 kN prior to the thermal test, and maintained at the same magnitude throughout the thermal testing period. Based on the FO distributed strain data, the pile load profiles at the stages of cooling and heating are shown in Figure 30a and b, respectively.

The load profile during the initial mechanical loading test phase (thin solid lines) follows the typical characteristics of a long slim pile in London clay; the majority of the external loading is resisted by the pile shaft mobilization and there is very little base resistance. The average mobilised shaft resistance prior to the thermal test is found to be around 30 kPa along the pile. This is shown by the dotted line in the shaft friction profile of Figure 31.

Figure 30a shows the cooling phase load profile obtained from the FO strain data. When the pile is cooled for ΔT = -20 ºC, it tends to contract. There will be thermally induced tensile stress as the shaft friction remobilizes to resist the contraction. As the pile contracts at both ends, positive incremental friction develops at the top half section, whereas negative incremental friction develops at the bottom half section. This changes the pile load distribution as shown by the thick solid line in the figure. At the top section of the pile, the compressive stress due to a 20 degrees drop in

temperature results in the mobilisation of a greater amount of the shaft friction to around 60 kPa, as shown in Figure 31. At the bottom section, the overall shaft resistance reduces and tensile stress develops inside the pile in extreme conditions as shown in Figure 30a.

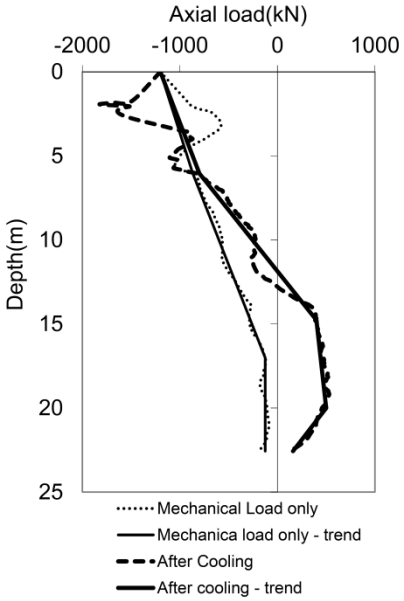

(a) Cooling of ΔT = -20ºC

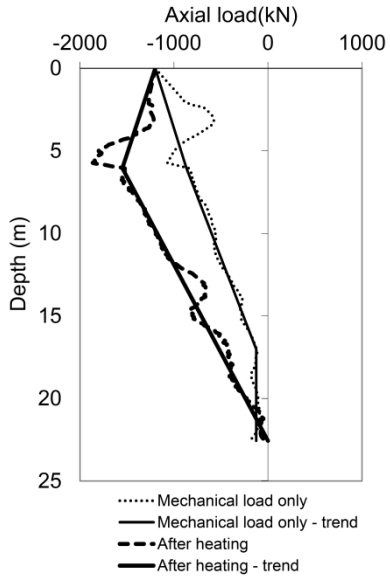

(b) Heating of ΔT = +10ºC

Figure 30. Thermally generated load distribution in Pile 2.

Figure 30b shows the heating phase profile obtained from the FO strain data. The pile was heated for ΔT = +10 ºC. The thermally induced expansion is resisted by shaft remobilisation; the shaft resistance at the top half section reduces, whereas that at the bottom half section increases. The pile is therefore subjected to a greater compressive load at the midway than is evidenced at the pile head. The shaft resistance at the bottom increases up to around 70 kPa with roughly 10 degrees increase in thermal load as shown in Figure 31.

In summary, in Pile 2, the heating and cooling effects observed in Pile 1 can be superimposed only on the mechanical loading state. For a frictional pile with negligible base resistance, a conceptual model of load distribution by heating and cooling can be illustrated in Figure 32. When the pile is cooled, the mobilised shaft friction increases in the upper part of the pile, but decreases in the lower part of the pile. An opposite trend is observed in the heating phase; shaft resistance decreases at the top and increases at the bottom. The distributed fibre optic strain data allowed the development of this conceptual model.

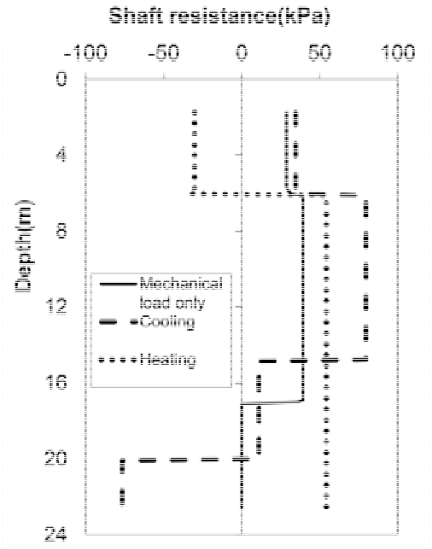

Figure 31. Shaft friction profiles in Pile 2.

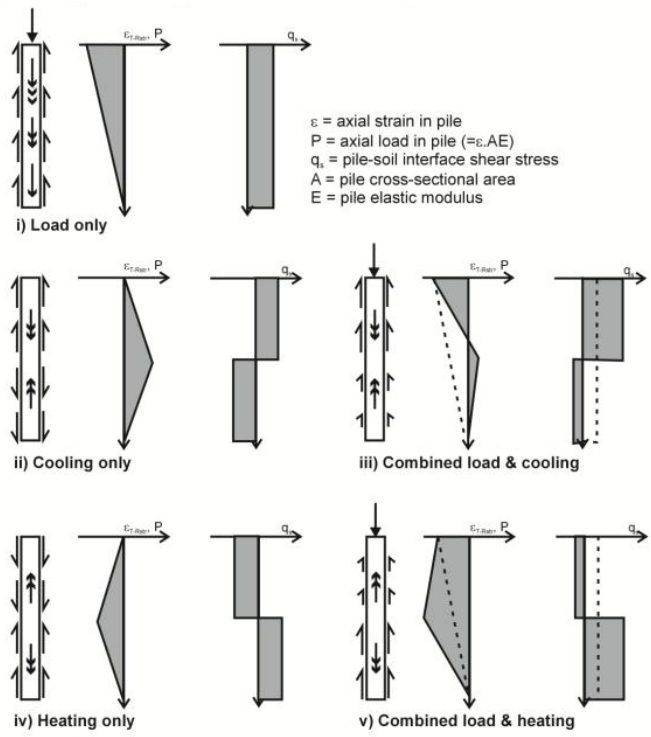

Figure 32. Conceptual model for thermo-mechanical behaviour of a frictional pile (after Bourne-Webb et al., 2009).

The continuous strain profile provided a full understanding of the soil-pile interaction when thermal loads are applied. The forces mobilised in the pile and the resistance mobilised at the pile-soil interface were inferred from the optical fibre distributed strain data response, and a simplified conceptual model for thermal pile behaviour was proposed (Amatya et al., 2012; Bourne-Webb et al., 2013). Although this model explains the pile response in an idealised situation, it provided straightforward guideline to interpret the pile behaviour. It also formed the basis for extending knowledge about the thermal pile with different restrained end cases such as end bearing piles and pile groups (see Bourne-

Webb et al., 2013 and Ouyang 2014). This finding led to the development of the thermal pile standard recently published by the UK Ground Source Heat Pump Association (2012). The standard is considered to be the most comprehensive document on thermal piles in the world.

4.3 Engineering Analysis

Figure 33 shows the movement of the pile head of Pile 2 during a series of thermal cycles. Immediately after application of 1200 kN load, the pile settled about 2.5 mm. During the first cooling phase, the settlement continued and reached about 4.5 mm by a temperature decrease of 20 degrees. When the pile was heated to ΔT = +10 degrees from the original ground temperature, the pile heaved about 2 mm and the overall settlement became about 2.5 mm, which is similar to the original settlement due to the mechanical load only. This implies that the pile movement is not entirely recoverable. The subsequent cooling and heating cycles produce cycle movements of the pile, but the magnitude of movement is very small (a few mm) even by the extreme thermal cycles applied in this particular test.

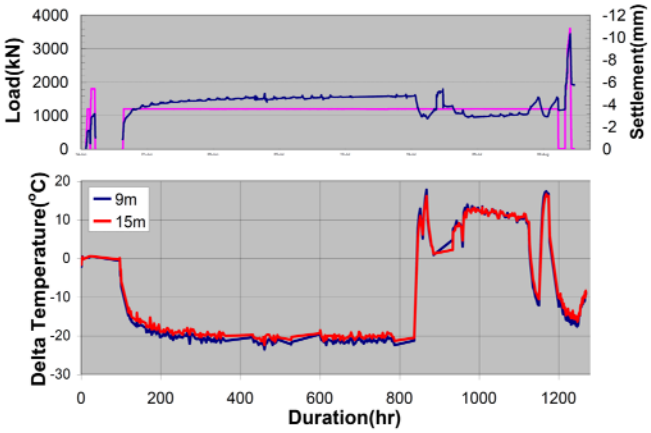

Figure 33. Pile settlement with time and temperature (negative means vertical movement downwards).

The change in thermally induced stress with temperature is evaluated at three locations: 6 m depth where the compressive stress was largest in the heating phase, 12 m depth the mid-depth of the pile, and 15 m depth where the tensile stress was largest in the cooling phase. The results are shown in Figure 34.

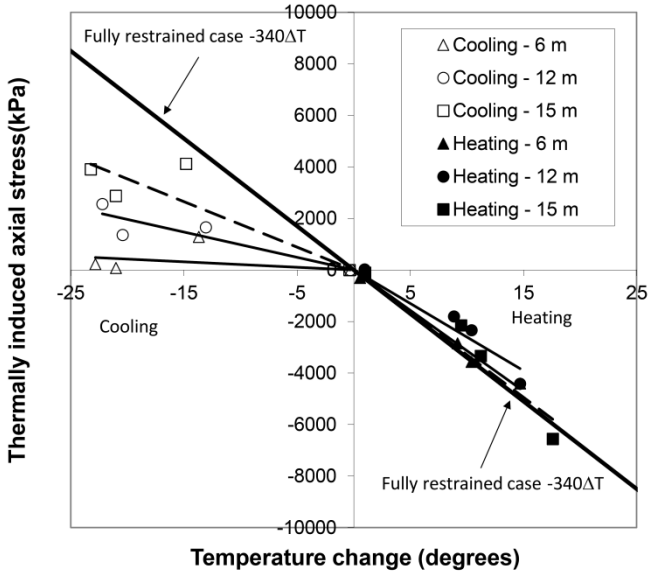

Figure 34. Thermally induced stresses in Pile 2 by temperature change.

During the heating phase, a unit degree change in temperature mobilised an additional axial stress within the pile of between 261 kPa/°C (77% of fully restrained value) and 329 kPa/°C (97%). On the other hand, during the cooling stage, the maximum stress (at 15 m depth) in the pile equates to an additional axial stress of about 177 kPa/°C. This means that the magnitude of shaft resistance during pile expansion by heating is greater than that during pile contraction by cooling. This interesting behaviour may be due to (i) increase in radial stress by pile expansion in the radial direction during heating or vice versa in cooling, and/or (ii) stress reversal along the shaft which result in stiffer response when the relative displacement increment direction becomes opposite to the previous loading condition (such as top portion during heating and bottom portion during cooling after a mechanical load is applied).

A thermo-hydro-mechanical coupled finite element analysis of the problem was conducted by Rui (2015). As the Cambridge in-housed developed THM code does not have an axisymmetric model, a 3D finite element model of the thermal pile as shown in Figure 35 was developed. A quarter of the pile and the surrounding ground were modelled using the symmetry. Further details of the code and the model can be found in Rui (2015).

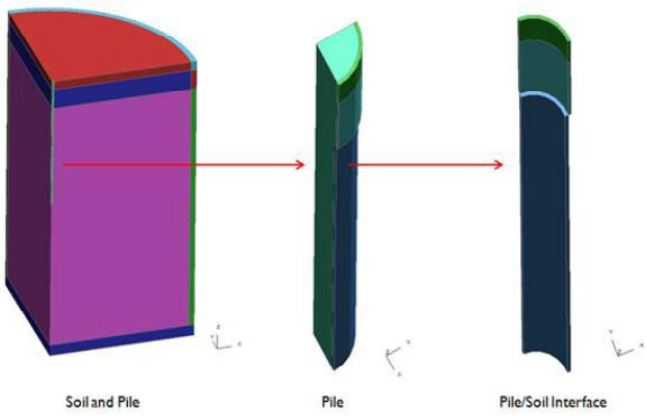

Figure 35. Geometry of the finite element model of Pile 2.

The soil-structure interface zone is divided into 3 layers, which are used to simulate the interactions between the pile and the different ground layers. The radius of the top part of pile is 300 mm, and decreases to 275 mm when elevation is below -4 m. The radius of the whole ground model is 10 m, incorporating three parts: Made Ground, Terrace Gravel, and London Clay. This model has about 40,000 elements in total.

A thermo-non-linear elastic Mohr Coulomb model was used to simulate the made ground and Terrace gravel, whereas the thermo-elasto-plastic advanced Cam-clay model was used for London Clay. The pile concrete stiffness was 40 GPa, and the thermal expansion coefficient was assigned as 8.5 x 10^{-6}/ºC. The soil's thermal conductivity was given as value of 1.5 W/m/K based on the thermal response test conducted at the site (Amis et al., 2008). Further details can be found in Rui (2015).

Figure 36 shows the comparison between the simulated results and the monitored data, representing the displacements of the pile head caused by loading and the cooling/heating cycle. The grey line is the monitoring data, whereas the black line is the model result. At the beginning, the pile is subjected to a working load of 1800 kN, and its settlement is about 3 mm. After the load is decreased to 1200 kN, the pile head rebounds and gives 2.4 mm settlement. The data from the model is larger than the monitoring data. This is probably because the monitored thermal

pile underwent several loading/unloading cycles and unloaded to 0 kN in the test, which was not modelled in the FE model. During the cooling and heating cycle, as the concrete and soil expands and contracts, the pile heat moved upward and downward accordingly. The cooling cycle begins after unloading to 1200 kN. The settlement is 4.5 mm during the first two days of cooling caused by the shrinkage of both the pile and the soil. After this, the movement increases to 5.0 mm during the 30 day cooling period. This is due to the lower temperature propagation through the ground and excess pore pressure dissipation. The opposite movement is recorded during the next heating stage, during which the pile expands and the pile settlement decreases to about 2.8 mm. There was an interruption to heating, which increased the settlement to 4 mm. After heating was resumed, the settlement rebounded to about 2.8 mm. After this another heating and cooling cycle was applied. The model results closely match the monitoring data.

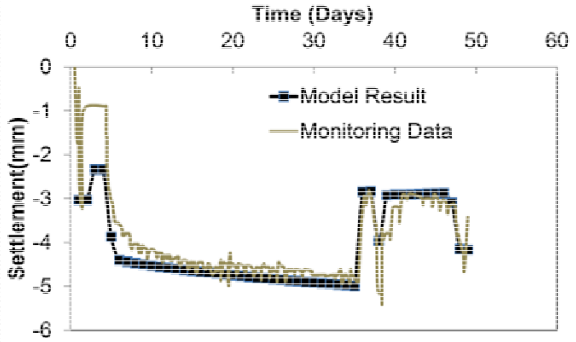

Figure 36. Simulated pile head displacements versus monitoring data.

Figure 37 shows the axial stress in the pile during mechanical loading only. The simulation results are similar to the monitoring data. It is important to note that the upper 5 m of the pile has a larger diameter than the remainder of the pile. Because of this, there is a step change in pile stress at 5 m depth.

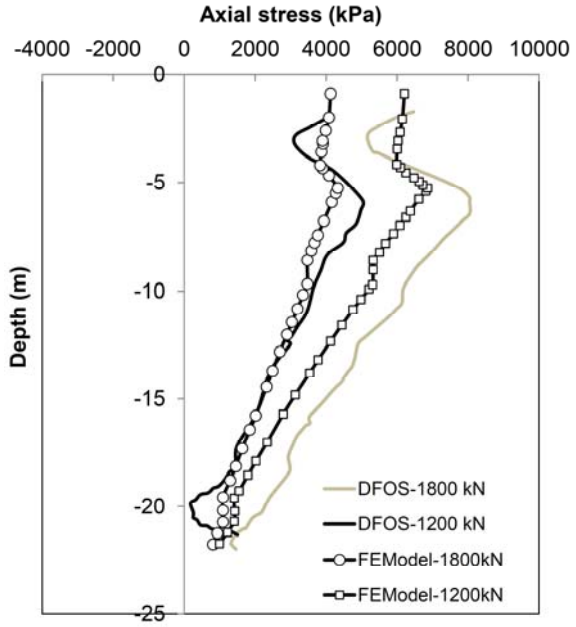

Figure 37. Axial stress profile during the mechanical loading stages of Pile 2

Figure 38 shows the vertical stress changes in the pile during the first cooling cycle. The numerical simulation results match well with the monitored data. A large negative (tensile) stress of about -1800 kPa develops at 17 m depth. After 10 days this value decreases to -1400 kPa, and after another 10 days reaches -1100 kPa. At the end of the cooling cycle, the largest negative stress is about -950 kPa. This result indicates that the pile stress varies with the heat transfer during the thermal pile test. As the low temperature propagates to the surrounding soil, the soil also shrinks. This change decreases the relative displacement between the pile and the soil, resulting in a decrease in tensile stress.

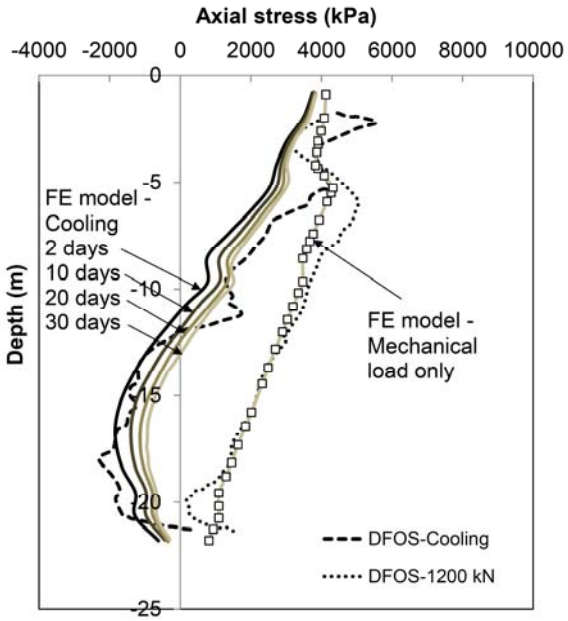

Figure 38. Axial stress profile during the first cooling stage.

Figure 39 shows that the compressive axial stress in the shaft increases during the heating phase. The largest change in the pile stress during 10 days of heating is about 300kPa. As discussed in the previous section, the maximum axial stress in the pile is greater than the mechanical load applied to the pile head, and it reaches to a maximum about 6500kPa between 6 m and 10 m in depth. When higher temperature propagates through the ground, the ground expands and hence, in time, reduces the relative displacement of the pile and ground in the vertical direction. This in turn reduces the shaft friction along the pile. The simulation result does not match the monitoring data at the lower section. One possible reason is that the stiffness of London clay was slightly underestimated during the heating cycle, which requires further investigation.

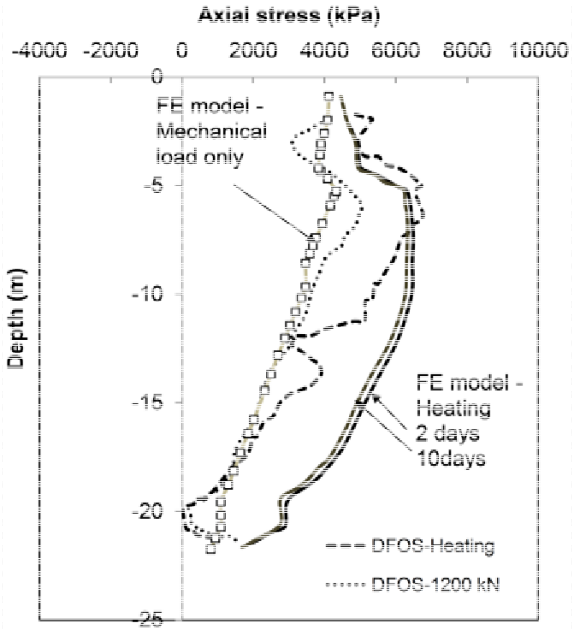

Figure 39. Axial stress profile during the first heating stage.

Rui (2015) shows from his numerical simulation that the shaft resistance in the heating phase is larger than that of the cooling phase. He demonstrated that this change in soil stiffness is due to the strain reversal. Figure 40 shows the shaft friction along the pile. The black line is the shaft friction at the end of loading cycle, the black dotted line is at the shaft friction at the end of the cooling phase, and the grey dotted line is the shaft friction at the end of the heating phase. The computed values are similar to the values derived from the DFOS data as shown in Figure 31.

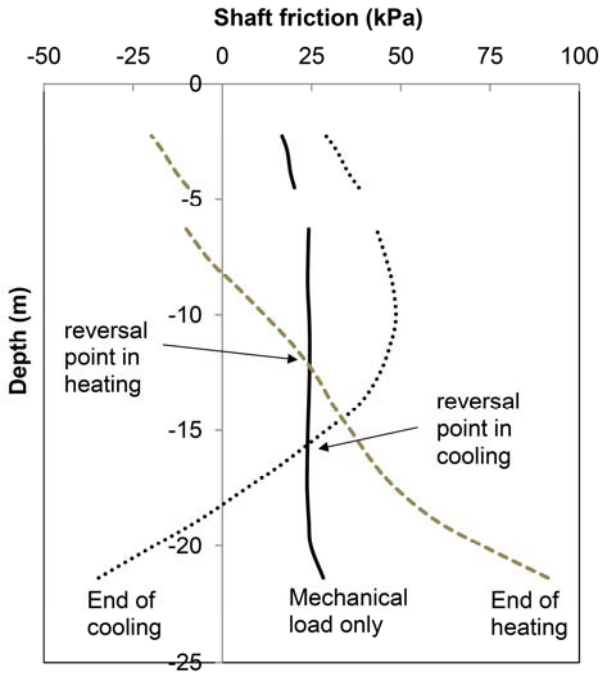

Figure 40. Computed shaft friction profiles in Pile 2.

During the cooling phase, the shaft friction increases in the upper section. The largest friction is about 48 kPa at an elevation of -10 m. In the lower section, the shaft friction decreases with depth, and the smallest friction is about -40 kPa at the bottom of the pile. In the upper section, the shear strain increment is in the same direction with that in the loading process. The shear stress increases in the upper section and the soil becomes more plastic. As the stiffness degradation characteristic is implemented into the constitutive model, the stiffness of the soil in the upper section decreases further. In the lower section, the stiffness of the soil adjacent to the pile shaft increases due to the strain reversal effect. A larger magnitude of friction develops in the lower section compared to the upper section. Therefore, the stress reversal point moves downwards.

During the heating phase, the additional friction caused by thermal expansion is negative above the reversal point and positive below the reversal point. The shaft friction decreases in the upper section, and the smallest friction is about -20 kPa at the pile top. The shaft friction in the lower section increases with depth, and the largest friction is about 100 kPa at the bottom of the pile. Due to the strain reversal effect, the stiffness of the soil adjacent to the pile in the upper section increases. In addition, the absolute value of shear strain in this zone decreases and therefore this part of the soil still behaves elastically. Hence, the soil in this area provides a large friction by heating and the reversal point moves upwards as shown in Figure 40.

In summary, the continuous strain profiles were essential to develop a conceptual thermo-mechanical mechanism of a thermal pile behaviour and to verify the mechanism from the thermo-hydro-mechanical finite element analysis of the problem.

5 CASE STUDY 3 - DIAPHRAGM WALL

5.1 Site description

A FO monitoring was conducted at Abbey Mills Shaft F, which is an integral part of Thames Water's Lee Tunnel project in London. The circular shaft as shown in Figure 41 was the largest ever constructed in the UK, providing a unique opportunity for a well-documented case history of a circular excavation. Its primary lining was made from twenty 1.2 m thick and 84 m deep diaphragm wall panels, constructed between September and December 2011, with a capping beam constructed at the top of the diaphragm wall. As shown in Figure 41, the depth of excavation was 73 m deep creating a 30 m diameter circular wall. The wall penetrated into a series of soil layers (Terrace Gravel, London Clay, Lambeth Group, Thanet Sand Formation, and Chalk Formation). The hydrogeological conditions comprised two aquifers; a shallow and a deep aquifer separated by the London Clay and the Lambeth Group clay.

Excavation started in April 2012 and was completed in September 2012. Following excavation to a depth of 73 m, a 2 m-thick base slab was cast and a secondary lining (using a double sided slipform shutter) was cast inside the shaft. The annulus, approximately 0.6 m wide gap between the diaphragm wall panels (which constitute the primary lining) and the secondary lining was filled with grout in April 2013.

The comprehensive monitoring scheme at Abbey Mills includes FO instrumentation and inclinometers in the shaft wall, as well as inclinometers and extensometers in the surrounding ground (see Figure 40). During the diaphragm wall installation, three out of the twenty 1.2 m thick and 84 m deep diaphragm wall panels were instrumented with fibre optic cables as shown in Figure 42. It was designed to measure the development of the bending strain and the circumferential hoop strain of the wall during shaft excavation.

Six cages were spliced together to form a long reinforcement inside the trench, as shown in Figure 43. Fibre optic cables were first attached on both sides of the bottom reinforcing cage in the vertical direction with pretension up to 2000 με. The remaining length of cable needed for the subsequent cages were coiled on cable drums which were temporarily fixed to the top of the bottom cage. While the bottom cage was placed in the bentonite-supported trench and spliced to the second cage, the FO cables in the drums were attached to the second cage. As the cage was lowered into the trench, the FO cables were gradually unrolled from the drums and were attached to the cage using a special clamp. The four remaining cages were instrumented in a similar manner.

The strain measurements were done at two sides of the wall, which allowed evaluations of the bending strain $\Delta\kappa$ profiles at different excavation levels. The circumferential hoop strain cable was attached either on the second or third cage, where the hoop stresses were expected to be largest. Further details on the installation, data acquisition and data processing of the FO instrumentation can be found in Schwamb et al. (2014) and Schwamb (2014)

5.2 Data Interpretation

The actual movement of the wall by the excavation was very small. The lateral wall displacement was less than 4 mm after the whole excavation, demonstrating the robustness of the circular shaft for deep excavation.

Selected curvature profiles are shown by the green and red lines in Figure 44 in which an incremental curvature change between different construction stages is given. As the overall bending strain was small, the incremental plots provided better view of the effect of the excavation on the bending

behaviour. A positive curvature value indicates tension on the soil face and compression on the excavation face. As expected, the wall was bending towards the shaft below the excavation level and away from the shaft above the excavation level. Around the excavation level, there were incremental curvatures of approximately 1.5 x 10^{-4} m^{-1}, which equates to a bending moment change of about 800 kNm between the two excavation level stages. The absolute curvature values (not shown) were slightly smaller with 1 x10^{-4} m^{-1}.

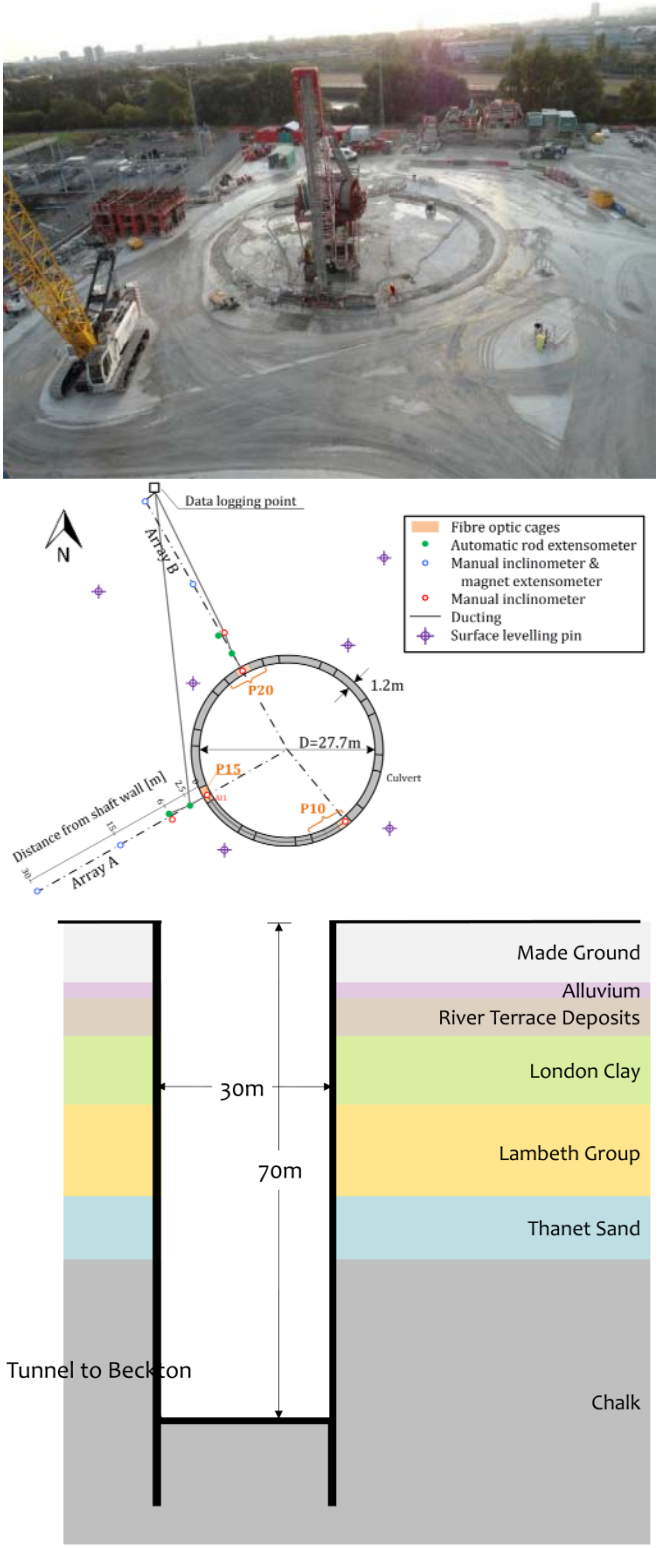

Figure 41. Plan view and subsurface profile for Abby Mills shaft F.

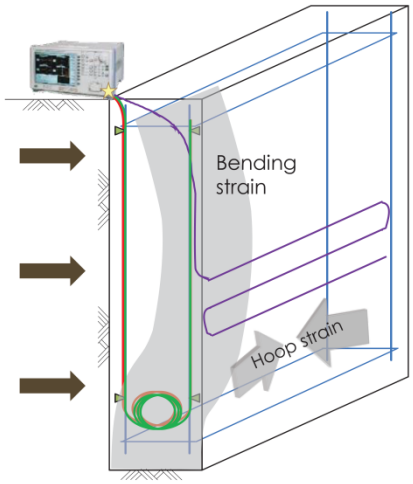

Figure 42. Schematic diagram of FO sensing instrumentation.

The design prediction is also plotted as the black lines in Figure 44; the incremental curvatures exceeded the predictions when the excavation was done in Chalk. This is discussed further in the next section.

The hoop strain data at around 60 mbgl against different excavation levels is shown in Figure 45. In both Panel 10 and 20, four levels of FO cable were installed in the hoop direction between 55 m and 65 m below the ground level (bgl). When the excavation depth reaches the monitoring level, there is a significant increase in compressive strain. Approximately - 500 ±130 με (tension positive) is measured at the final excavation depth. It is also noted that a smaller compressional hoop strain develops at the beginning of the excavation. Strains between 0 and -200 με (tension positive) are measured at an excavation level of 15 mbgl.

Figure 45 also presents the design predictions. The measured hoop strain was approximately twice as large as that predicted at the final excavation depth. This is related to the increase in hoop strain when excavation is made at shallow depths. This early increase in hoop strain is surprising because the clay layers present a hydraulic barrier that hinders the sump dewatering to affect the pore water pressures below them. Although speculative, this surprising behaviour may be related to creep in the Chalk. The wall installation changed the stress states in the Chalk, and may have led to time-dependent deformation associated with gradual increase in earth pressure applied to the wall. Further investigation is needed to better understand the performance of the wall.

In summary, the distributed fibre optics monitoring of the shaft gave valuable information on the bending and hoop response of the structure for the design of future similar shafts. As shown in the next section, the data was used to assess the design.

5.3 Engineering Analysis

As shown in Figure 44, the curvature predictions using the original design values (the solid black line) differed from the measurements when the excavation was done in Chalk (the two dashed lines). Schwamb (2014) conducted a series of numerical analyses of the circular shaft using FLAC to investigate the causes of this difference. The FLAC model with dimensions, mechanical and fluid boundary conditions and pore water pressure profile is displayed in Figure 46.

In the original design, all ground layers were modelled with a Mohr-Coulomb (MC) soil model. For the investigation, advanced soil models were applied for some soil layers. For the London Clay and Lambeth Group clay, the pre-yield

behaviour was modelled using a hyperbolic stiffness degradation function. The model parameters were selected based

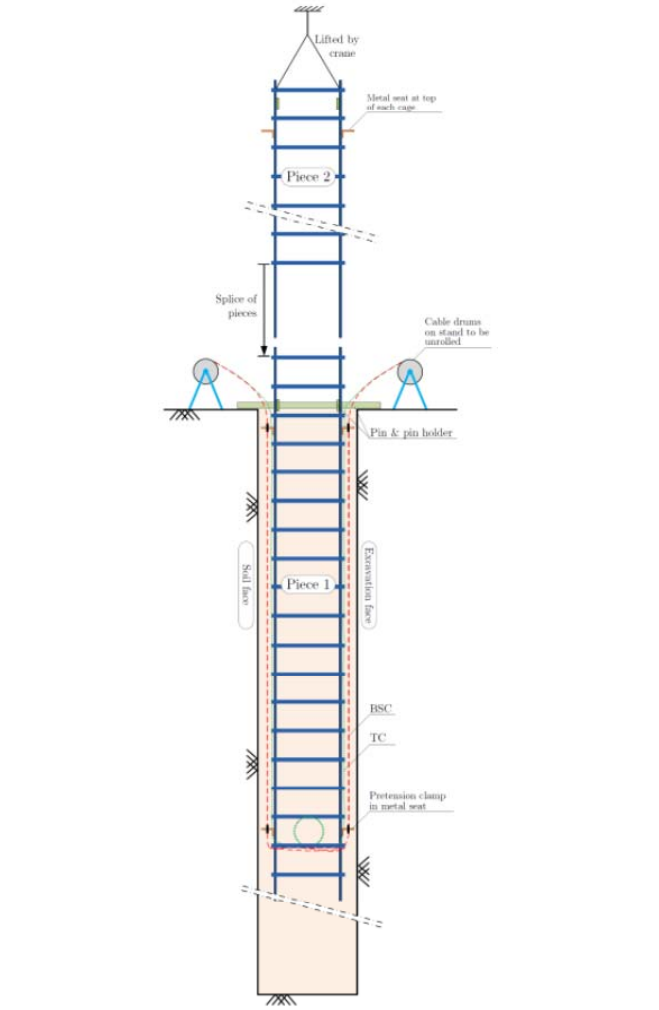

Figure 43. Installation of FO cables at Abby Mills.

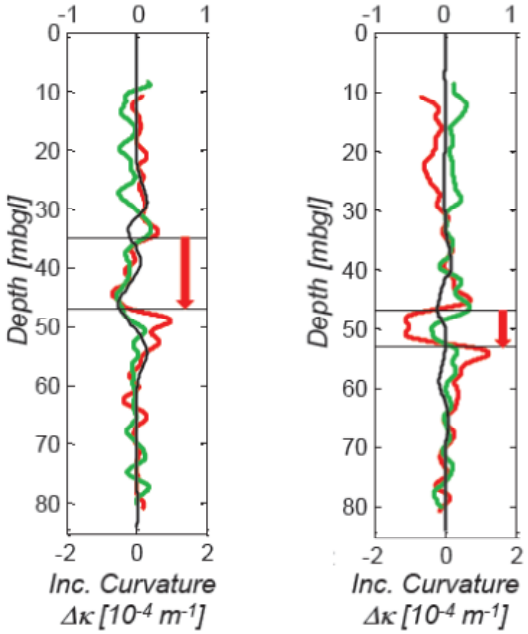

(a) between 35m to 47 m (b) between 47m to 53 m

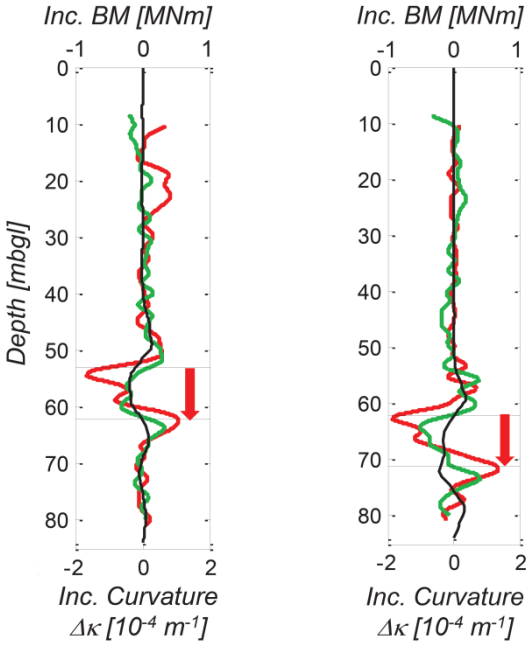

(c) between 62m to 53 m (d) between 71 m to 62 m

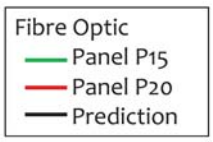

Figure 44. Changes in curvature between different excavation levels. The green and red lines are the FO data, whereas the black lines are FE predictions.

on triaxial tests from Gasparre (2005) and recommendations from CIRIA C583 (Gaba et al., 2003). For the failure criterion, a simple MC model was used. The mechanical behaviour of Lambeth Group Sand and Thanet Sand layers was modelled with FLAC's inbuilt strain-hardening/softening model. Friction and dilation were modelled with piece-wise linear functions according to the data of Ventouras' (2005) triaxial tests. To capture the strain hardening, and then softening, behaviour after the onset of yield observed in the

test data, the variations of the effective stress friction angle φ' and the dilation angle ψ with plastic axial strain were modelled. For the wall, an anisotropic elastic material model was implemented, which reduced the circumferential wall stiffness relative to the stiffness values in the vertical and radial directions, so that the possible discontinuous nature of diaphragm walls can be modelled.

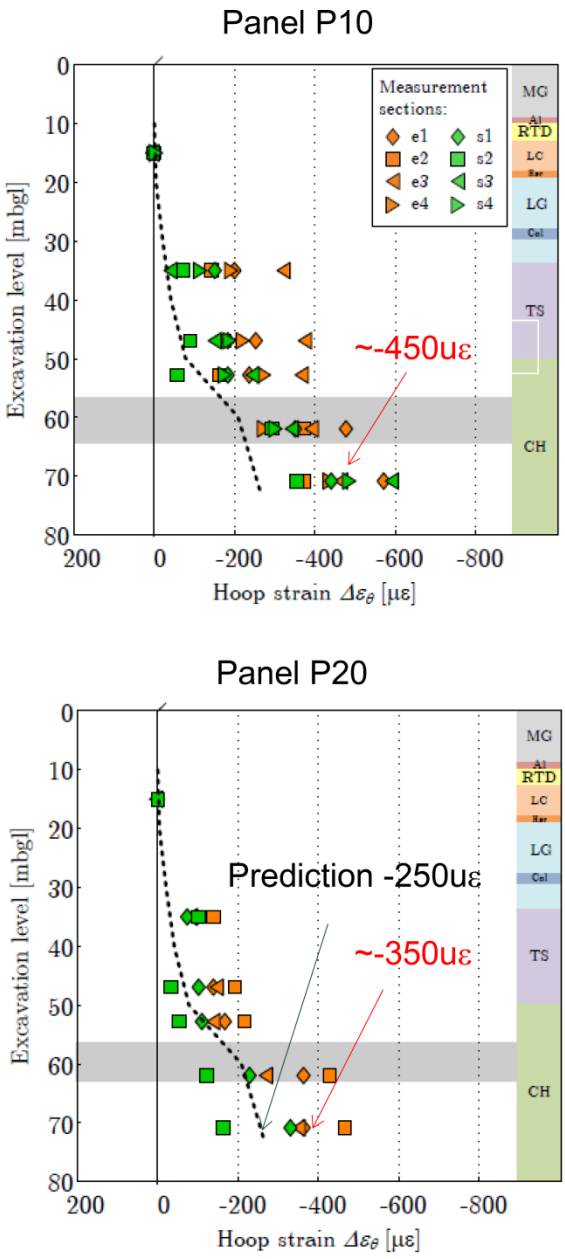

Figure 45. Development of hoop strains at different excavation levels.

For the Chalk, the original design used Mohr Coulomb model with a cohesion c' of 20 kPa and a friction φ' of 35°. Numerical simulation results show that, when the excavation reached the Chalk layer, plastic yielding occurred, making the chalk deformable, as shown schematically in Figure 47. As a consequence, the wall gradually bulged around the excavation level, which resulted in small bending moments.

When much larger yield stress was assigned, the chalk behaved elastically during the excavation, which resulted in a sharper wall bulge (see the "Adv" blue lines in Figure 48) and hence larger curvatures and bending moments, (see the "Adv" blue lines in Figure 49). It therefore appears that the assumed yield surface was unrealistic with a small cohesion of c' = 20 kPa.

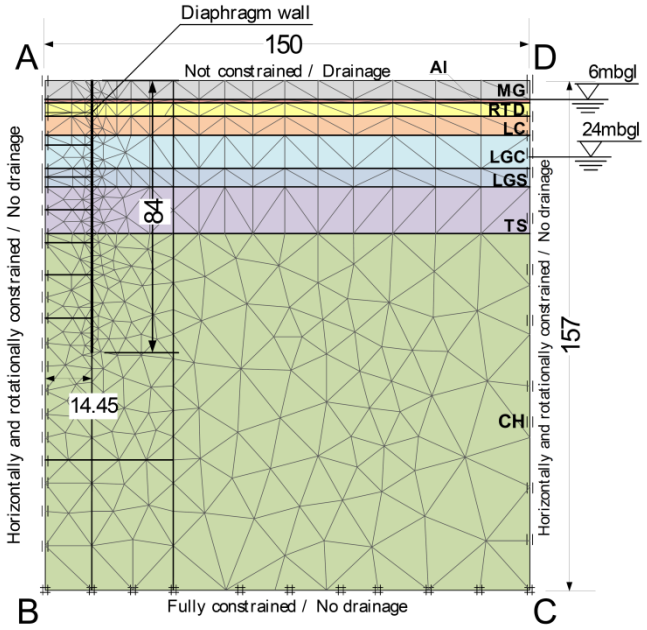

Figure 46. Axisymmetic model of the shaft in FLAC.

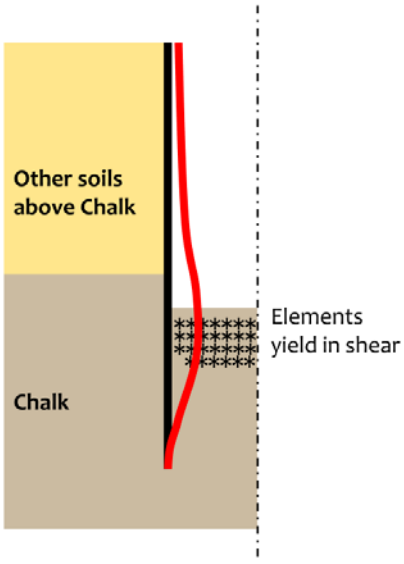

Figure 47. Plastic yielding in Chalk at the excavation depth.

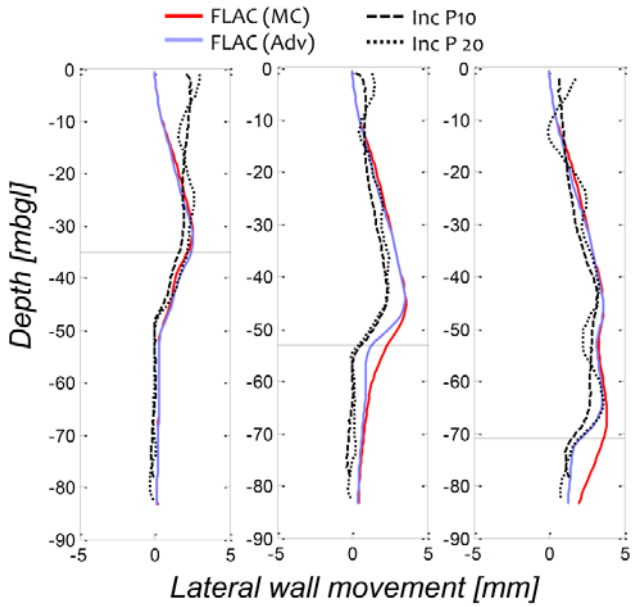

Figure 48. Model predictions versus monitoring data on lateral displacements of the D-wall. The excavation level is given by the horizontal line in the plots.

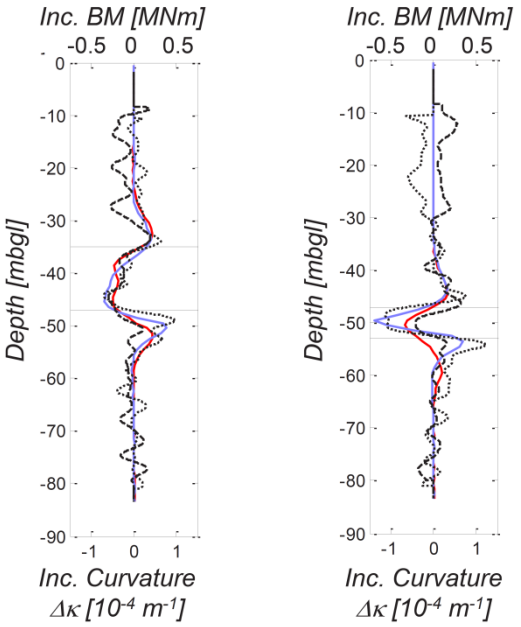

(a) between 35m to 47 m (b) between 47m to 53 m

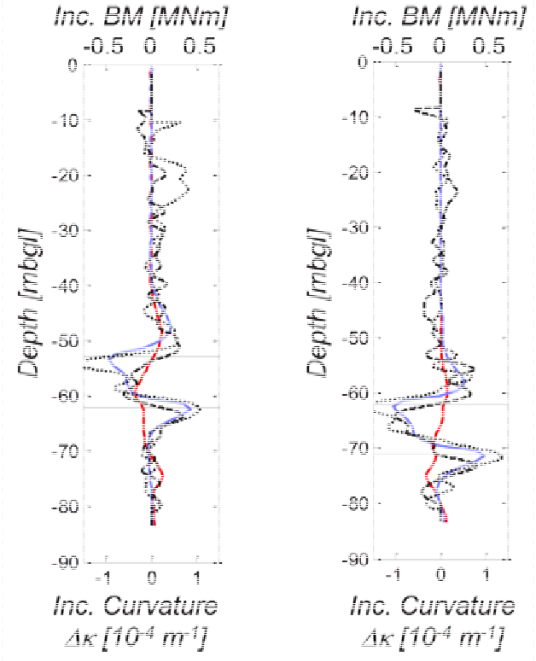

(c) between 62m to 53 m (d) between 71 m to 62 m

Figure 49. Model predictions versus monitoring data on the changes in curvature between different excavation levels.

The original design value was recommended in the Geotechnical Interpretative Report as 'moderately conservative' based on CIRIA C574 (Lord et al. 2002). Results show that, while it is conservative for ground movement estimates, this is not the case for the structure. It should be noted here that, although the measured bending moments exceed the SLS predictions, the reinforcement in the wall was sufficient enough to carry the larger bending moments, as it has been designed according to the more conservative ULS loading. Further study is required for better understanding of the mechanical behaviour of the Chalk in London and modelling of it (including creep).

Based on a series of parametric study and comparing the results with the monitoring data, Schwamb (2014) and Schwamb and Soga (2015) concluded the following in addition to the observation made for the behaviour of the Chalk layer as discussed earlier.

- This particular diaphragm wall behaved isotropically, not anisotropically due to the joints. The hydrofraise cut into the concrete of the adjacent panels seem to guarantee direct contact and strong joints.
- The design assumption of K_0 = 1.0 for the Chalk was reasonable for a wished-in-placed wall model. When the wall installation was modelled, using the pressure distribution suggested by Gourvenc and Powrie (1999), the numerical simulation results matched well with the field data irrespective of initial K_0 values (ranging between 0.5 and 1.5). This suggests that the performance of circular diaphragm walls during excavation is largely influenced by the installation process of the wall.
- The ground movements during wall installation were significantly overestimated by the 2D numerical simulation. This is because the 2D axisymmetric model simulates the wall installation for all panels at the same time. It does not allow the adjacent soil to provide support through arching.
- The numerical simulation predicted that the shaft excavation causes small heaves behind the shaft wall (approx. 5 mm) which was confirmed by level measurements of the diaphragm wall head.

6 CASE STUDY 4 - TUNNEL LINING

6.1 Site description

Concrete tunnel lining segments embedded with optical fibre cables were installed and monitored during the construction of the new 'National Grid Power Tunnel' project in London. Fibre optic cables were installed within 36 segments during manufacture in order to monitor strain following installation of the segments into the ground. The aim of the project was to quantify the tunnel lining behaviour subjected to the short term loading during and immediately following construction.

The tunnelling scheme consists of some 32km of new deep level tunnels, 15 large diameter shafts and 14 head house buildings that will sit atop the shafts. Construction work started in 2011 and the first section of cabling will come online in 2015 with the scheme due to be fully operational by 2018. The tunnelling was conducted using earth pressure balance (EPB) tunnel boring machine (TBM). Installation of fibre optics embedded tunnel linings was conducted in the 4 m diameter tunnel running between St Johns Wood and Hackney. The lining is tapered trapezoidal in type, with 6 segments forming each ring of 1.3 m width, as shown schematically in Figure 50a.

The tunnel segments were manufactured away from the construction site. The segments were made from concrete with steel fibre reinforcement and were cast within machined steel moulds. Because the tunnel segments did not have any reinforcement cage, a simple support frame was constructed to attach the fibre strain and temperature cables within the segment mould during casting, as shown in Figure 51a. The frame was intentionally made as light as possible because the influence of the steelwork should not have a global stiffening effect on the instrumented segments.

As shown in Figure 50b&c, the strain sensing cable was installed along the top and bottom of the respective frame bars, such that the cable was orientated as close to the outsides of the segment following casting as permitted by cover requirements. The reason for this was to have maximum differential of strain across the section so that a more accurate calculation of segment curvature / bending moment

could be attained. Pre-straining is frequently used when installing the fibre optic system to the external surface of an existing structure in order to measure compressive strain. A pre-straining of approximately 1000 με was applied.

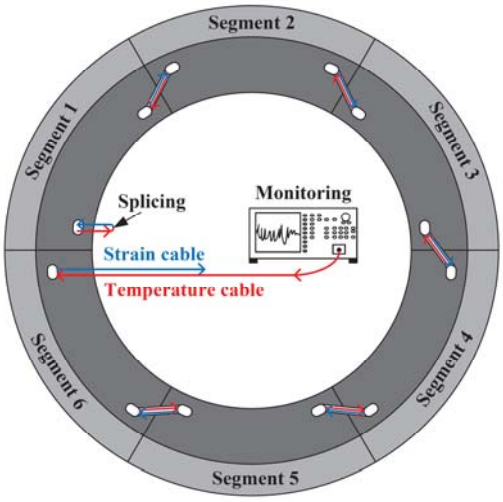

(a) Geometry of the tunnel linings

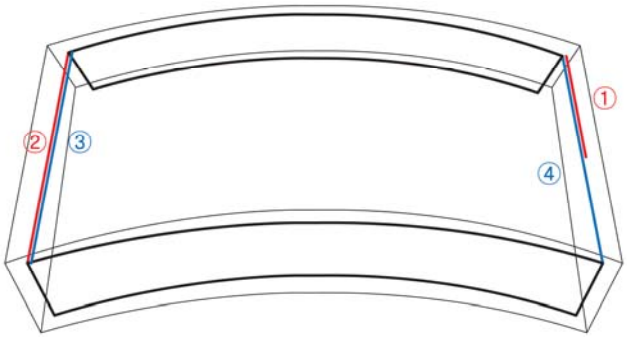

(b) FO cables in the longitudinal direction

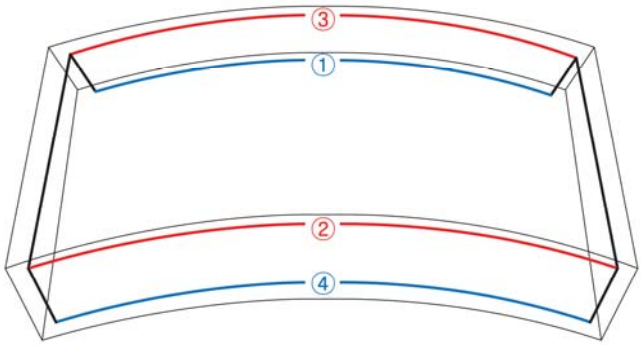

(c) FO cables in the circumferential direction

Figure 50. Conceptual diagram of FO embedded concrete lining.

The 36 instrumented segments were constructed into 6 (fully instrumented) tunnel lining rings (see Figure 51b) and these were incorporated into construction at 4 locations along the 4m St Johns Wood to Hackney tunnel alignment (see Figure 51c); two locations within London Clay, one within Lambeth Group and one within the Thanet sands.

6.2 Data interpretation in the longitudinal direction

This section discusses the short term loading of the fibre optic embedded segments installed within Thanet sands, as shown in Figure 52. The data and their interpretation from the other instrumented rings will be published in a future publication.

(a) Installation of fibre optic cables inside the casting mould

(b) A segment embedded with fibre optic cables

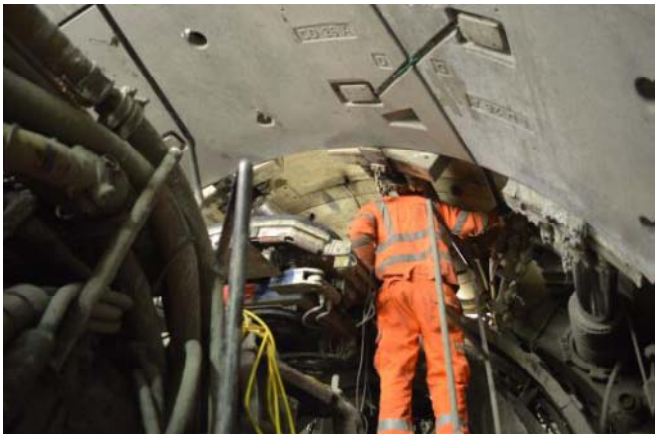

(c) Installation of instrumented segments

Figure 51. Manufacturing and installation of instrumented concrete segments.

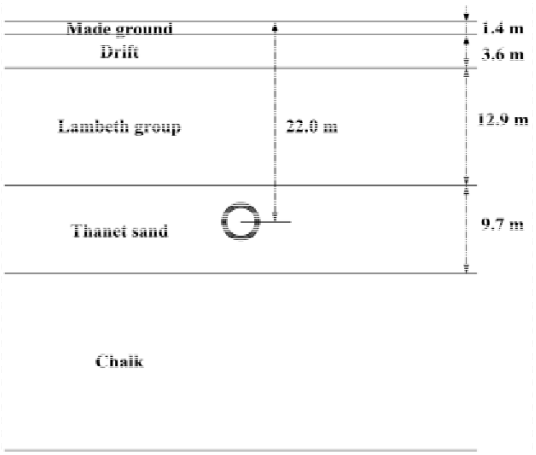

Figure 52. Ground conditions and the location of the instrumented segment.

During tunnel construction, segmental tunnel linings resist the tunnel boring machine loading regime to advance and hold back the overburdening earth pressure at the face of the machine. The TBM loads are transmitted through a number of hydraulic thrust rams. In certain circumstances, differential ram pressures and manufacture irregularities may result in damages of the concrete tunnel segments.

A TBM relies on maintaining reactive support to the earth through which it mines in order to minimise ground disturbance. As shown in Figure 53, the loading alternates between (i) TBM advance (shove) and (ii) segment installation (holding). The former gives the upper loading condition, whereas the latter give the lower static condition: the period whence a new tunnel ring is installed by withdrawing a minimum number of rams (~3) to permit placement a single segment at a time.

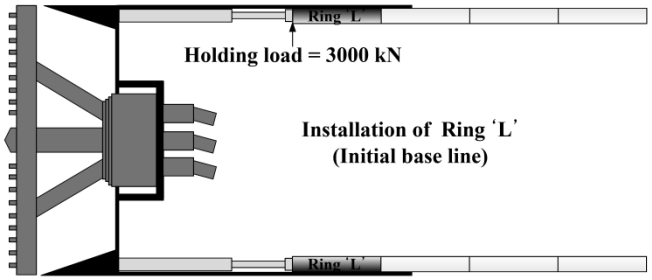

(a) Installation stage

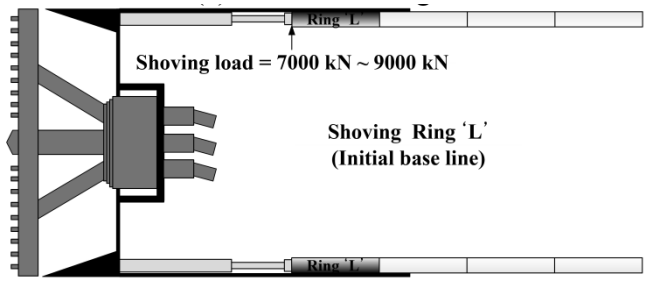

(b) Initial shoving stage

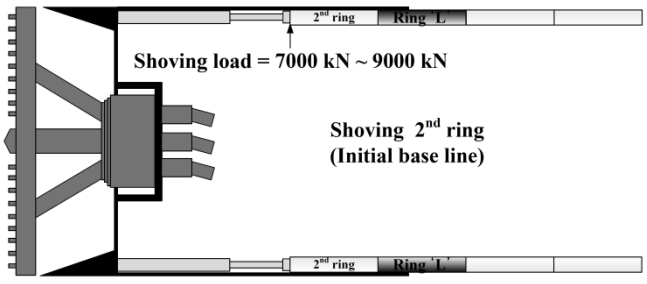

(c) Shoving stage of 2nd ring

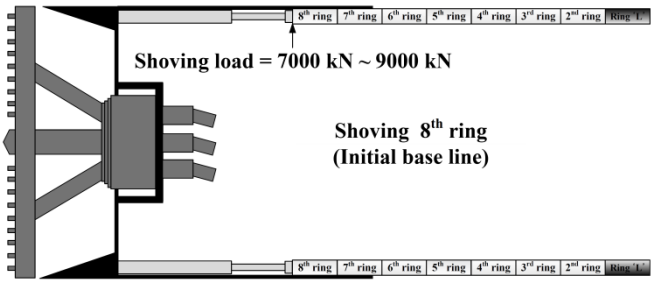

(d) Shoving stage of 8th ring

Figure 53. Construction stages after the installation of the instrumented segment.

Figure 54 shows the strain data for shove 1 through 8 for a single segment (segment 4 right knee in Figure 50a) against the initial baseline reading taken immediately after the ring was constructed inside the TBM. A single segment is analysed here for clarity. Longitudinal data are selected from the segment data and highlighted in Figure 50b. The averaged data of the middle point readings from longitudinal section ① to ④ are shown for Shove 1 to 8 in Figure 54a. After shove 2, the compressive strain dramatically decreases, as shown in shove 3 and shove 4 result; with strain returning to near base-line level. From shove 5 to 8, the longitudinal loading can be seen to have stabilized.

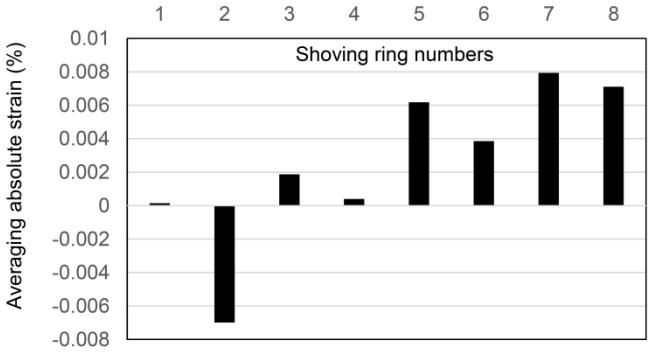

(a) Measured strain data

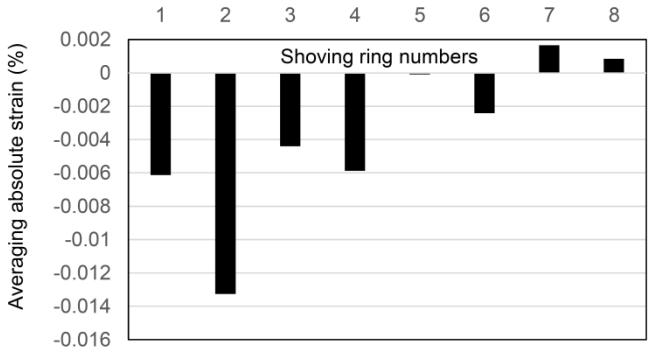

(b) Re-aligned strain data

Figure 54. Construction stages after the installation of the instrumented segment.

It was not possible to have a zero load condition base-line reading, as the segments had to be in-situ for connection to the analyser, hence an initial best estimate 'lower static' condition is taken based on available typical lower static condition from the TBM telemetry. The base-line longitudinal loading is approximately 3000 kN. The data show a clear levelling off of strain after shove 5 and hence the base line is re-estimated by their (fifth to eighth shove data) averaged values with the assumption that thrust road was exhausted in the fifth to eighth ring. The realigned plot is shown in Figure 54b.

The TBM telemetry data during this approximate period of tunnelling show that a loading between 7000 and 9000kN is applied (see Figure 53). The TBM has 12 thrust rams, each ram acts on the tunnel segments. When the area of contact is the full circumferential joint bearing area, a lower and upper bound loadings, say 7000kN and 9000kN, give the respective longitudinal straining in the segment is 0.0108% and 0.0138%, assuming the elastic modulus E = 30 GPa. Figure 55 shows the geometry used in this calculation. The measured strain value during the second shove is about 0.012%, which is between the two bounds.

The strain value at Shove 1 is smaller than that at Shove 2. This is probably due to the TBM rams acting directly upon the instrumented ring. Because the segments have a 1:6

taper to the radial joints, it is likely that the interaction of segment to segment during Shove 1 will mobilise shearing friction within the joint, effectively inducing counteracting tensile force within the longitudinal strain cables. The diagram in Figure 55 illustrates the position of the TBM rams and Figure 56 shows the region where shearing is likely to manifest. Detailed analyses using a finite element, solid element model are being conducted at present to investigate and better understand this interaction. From these analyses, peak compressive loads may be derived for segments being directly acted upon by the TBM thrust rams.

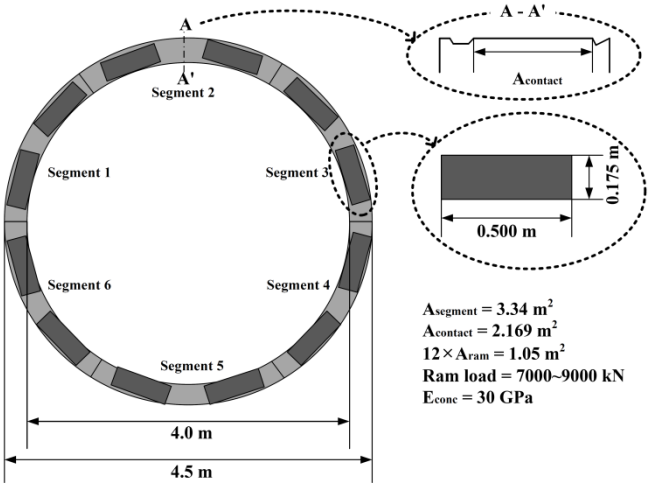

Figure 55. Estimate of strains from the shove loading.

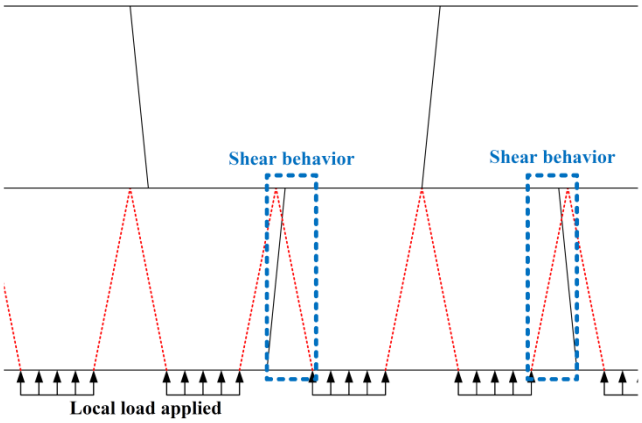

Figure 56. Possible shearing of a segment in the first shove.

6.3 Data interpretation in the circumferential direction

This section discusses the loading of the fibre optic embedded segments installed within London clay, as shown in Figure 57. Figure 50c illustrates the position of the fibre optic strain cables within the tunnel segments. Figure 58 shows the differential strain profile for Segment 1 with respective position of fibres within the segment. Two sets of data are presented; (i) when the segments inside the TBM and (ii) 93 days after construction with earth pressure acting on the tunnel lining. The data shows that large compressive strain is developing within the extrados of the segment when compared to the strains within the intrados. This indicates that the lining has both compressive axial stresses as well as bending moment.

By selecting a single data point in the middle of the circumferential strain cable, points A, B, C, D, E, F, G, and H (Figure 59a) bending moment and axial force are quantified. Segment 1 is located at the tunnel shoulder, whereas Segment 2 is located at the tunnel crown. The results of Segment 1 show compressive behaviour is dominant as shown in Figure 59b and c, and that compressive strain of the extrados is significantly greater than the intrados. The relative strain difference between points A and B is ~0.0087% and between points C and D ~0.021%. The relative strain difference between points C and D is on the longer side of the segment, whereas A and B is on the shorter side. Figure 59d and e show the result for Segment 2 at each selected point. Contrary to the results of Segment 1, there is tensile strain (point E) and small compressive strain (point G) in the extrados of Segment 2. The larger compressive strain occurs in the intrados of Segment 2. The relative strain difference between points E and F is ~0.016% and between points C and D ~0.0093%.

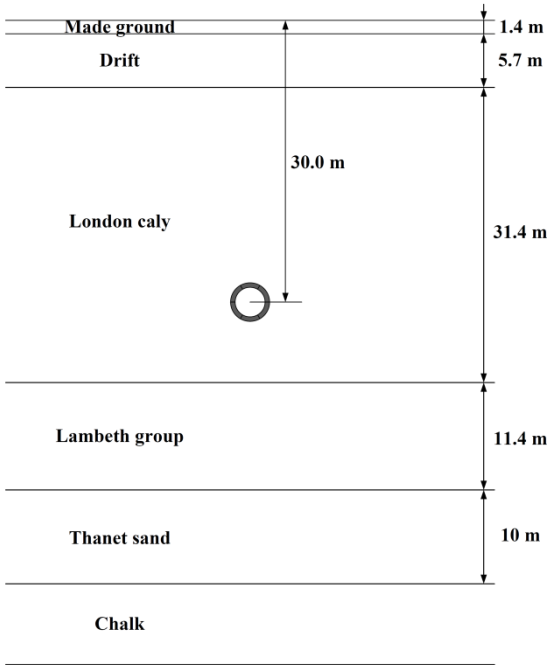

Figure 57. Ground conditions and the location of the instrumented segment.

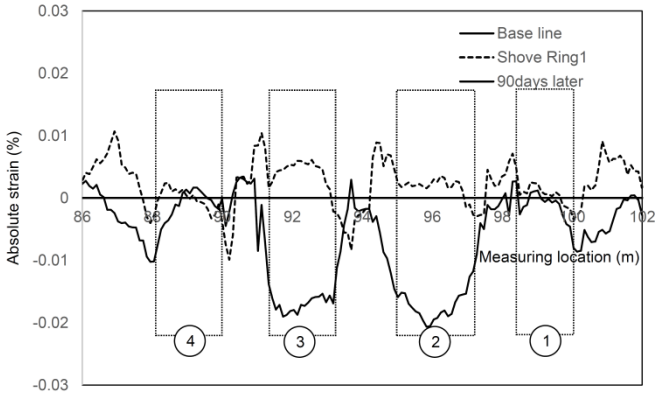

Figure 58. Measured strain relative to the baseline (i) after the first shove and (ii) 93 days later.

The tunnel design was conducted using methods of Muir Wood (1975) and Duddeck and Erdmann (1985). Figure 60 presents the moment / axial force (M/N) envelope, showing the ULS load cases for Muir Wood and Duddeck and Erdmann for zero shear and full shear interaction with the ground. It can be seen that the 90 day axial loadings for Segment 1 and 2 are within the envelope and are smaller than those calculated within the design. For Segment 1, the bending moment reaches 29.2 % of the section capacity. In Segment 2, it reaches 43.3 % of the section capacity. The instrument recorded bending moment and axial force are significantly smaller than those generated in the design. The axial force at 93 days is relatively small, but it is expected

to increase with time. As the un-reinforced tunnel lining segments have little tensile capacity, it must rely on axial force in order to sustain bending moments. The long-term performance monitoring of the lining is currently conducted.

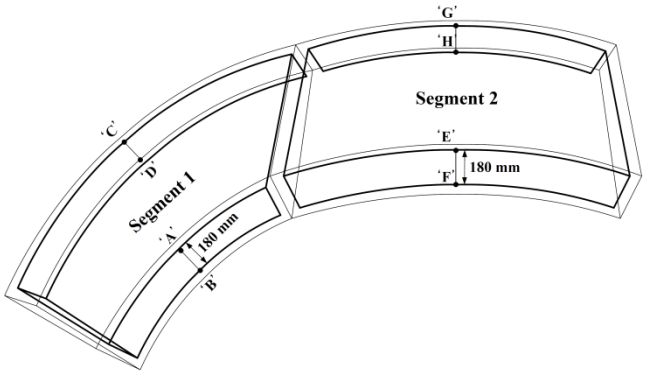

(a) Locations of Segment 1 and 2

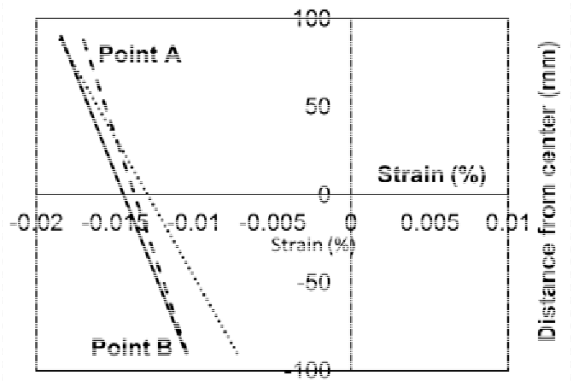

(b) Strains in A and B

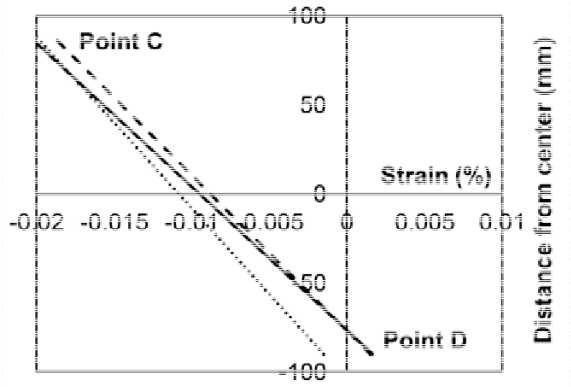

(c) Strains in C and D

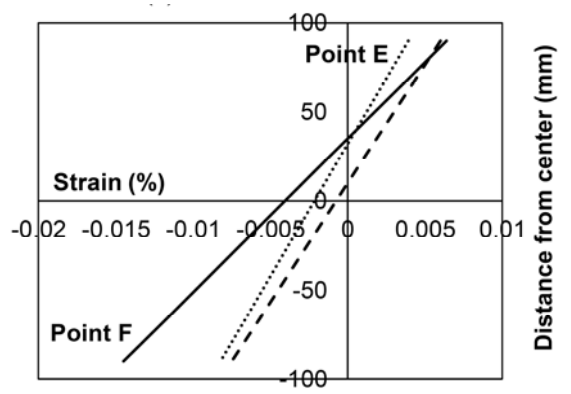

(d) Strains in E and F

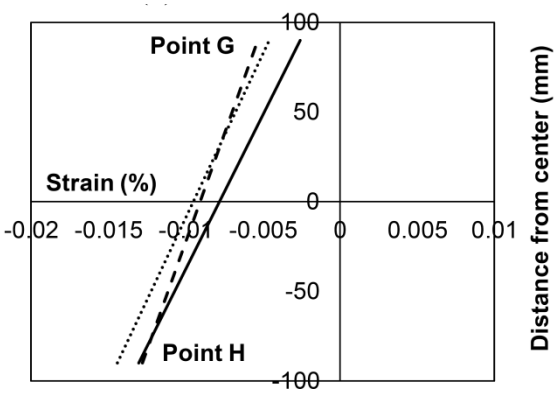

(e) Strains in G and H

Figure 59. Measured strains at 93 days after installation.

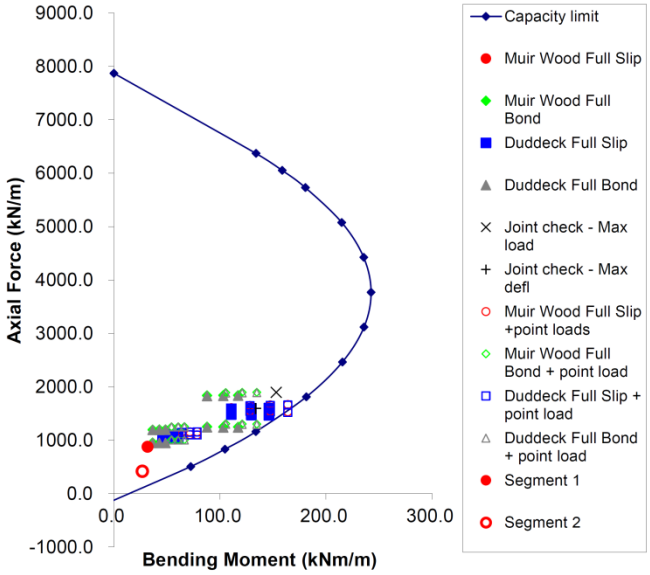

Figure 60. Moment / axial force (M/N) values after 93 days.

The data presented in this paper is preliminary and further data analysis is being conducted for the other segments and rings. Further long term readings will be taken to investigate whether the loads upon the lining are increasing with time. The distributed optical fibre strain measurement system allows sensing cables to be embedded inside the segment as part of the manufacturing process. The embedded sensor material itself (Silica) is relatively inert and can be ideal for long-term monitoring of structures. This implies that the quality of the data is expected to increase with time as the capability of analyzers should improve with time. Such features can potentially provide a relatively cheap but highly effective monitoring system for both short and long term.

7 CONCLUSIONS

In recent years, sensor and communications research has been undergoing a quiet revolution, promising to have significant impacts on new generation of monitoring technologies for geotechnical structures. An innovative distributed fibre optic strain measurement system was introduced in this paper. It can have thousands of "strain gauges" along a single cable connected to structures, embedded in soil or grouted into boreholes. Because of the simple and quick installation technique, distributed optical fibre sensing can be as practical as the other conventional measurements. They can provide a highly effective monitoring system for both the short and the long term, creating 'smart' geotechnical structures', in which strain measurement becomes

more routine than at present, and cost is particularly important. As the cost of a standard optical fibre is very low compared to other point measurement sensors, most of the capital investment relates to the analyser, which can be connected to a number of fibres or be shared at different sites. More choice from more manufacturers will give a reduction in price of analysers.

To accelerate the usage of emerging technologies, however, field demonstrations such as the ones shown in this paper are essential so that confidence within the community can be built. A large number of such field demonstrations on distributed FO strain monitoring, not presented in this paper, have been carried out by the Cambridge Geotechnical Group and the Cambridge Centre for Smart Infrastructure and Construction. Some examples are:

- Monitoring of water main pipeline during construction of a tunnel underneath (Vorster et al., 2006),
- Ground movement monitoring of clay cuttings and embankments along motorways (Janmonta et al., 2008),
- Performance monitoring of soil nails for stabilizing steep highway curt slope (Amatya et al., 2008)
- Lateral movement monitoring of a secant piled wall (Mohamad et al., 2011)
- Movement monitoring of existing tunnels affected by nearby underground construction (Cheung et al., 2010; Mohamad et al., 2010; Mohamad et al., 2012; Alhaddad, et al., 2014; Gue et al, 2014&2015).

It is hypothesized in this paper that the future of infrastructure relies on smarter information; the rich information obtained from embedded sensors within infrastructure will act as a catalyst for new design, construction, operation and maintenance processes for integrated infrastructure systems linked directly with user behaviour patterns. This fully integrated approach starts from designing sensor systems that provide better information for decision makers and finally enables more effective management of assets, cities and infrastructure systems throughout their life. Infrastructure owners need to provide the market 'pull' for smart technologies in response to the challenging targets set by the public. That is, the new infrastructure needs to be constructed and maintained more economically and safely than before. Our existing aging infrastructure requires a better understanding of its extent of ageing and the consequent remaining design life. There is a need to assess the safety levels in extreme events such as flooding and earthquakes. Ultimately the development of 'smart' infrastructure means true realization of performance-based design and maintenance.

ACKNOWLEDGEMENT

Firstly the authors would like to thank their Cambridge colleagues who conducted the field instrumentation work presented in this paper. These include Mehdi Alhaddad, Binod Amatya, Musa Chunge, Nicky de Battista, Njemile Faustin, Saleta Gil-Lorenzo, Chang Ye Gue, Koson Janmonta, Peter Knott, Mahul Patel, Masanari Nakashima, Echo Ouyang, Jason Shardelow, Seda Torisu, Taro Uchimura, Fei Wang, Yifei Yu, and Dan Zhang. We would also like to thank Prof. Robert Mair, Dr. Mohammed Elshafie, Dr Cedric Kechavarzi and Dr Jennifer Schooling for their initiative and support for the field studies. The field studies could not be performed by generous contributions and commitments from our industry partners. These include Arup (Duncan Nicholson, Paul Morrison and Lohini Ganesharatnam), Cementation Skanska (Peter Bourne-Webb, Andrew Bell, Martin Pedley, Rab Fernie), CH2M HILL (Peter Wright), Geothermal International (Tony Amis and Chris Davidson), JV MVB (Morgan Sindall, Vinci Construction Grands Projets and Bachy Soletanche) & AECOM & SolData & Thames Water (Ba Dan Nguyen, Clotilde Boquet, Jean-Christophe Galan, John Greenwood, Julian Gatward, Martin Stanley, Richard Sutherden and Sivilay Sayavong), National Grid (Mark Farmer), Costain (Christopher Gannon, Tim Embley, Andy Firth, Sam Simons) and Buchan Concrete (Trevor Cobby). The first author thanks Dr Cedric Kechavarzi and Ms Sandy Yatteau for their editorial check of the paper. The funding of the projects partly comes from the Cambridge Centre for Smart Infrastructure and Construction, which is supported by The Engineering and Physical Sciences Research Council (EPSRC) and Innovate UK.

REFERENCES

Adam D. & Markiewicz R. 2009. Energy from earth-coupled structures, foundations, tunnels and sewers, *Geotechnique* **59**(4), 229-236.

Alhaddad, M., Wilcock, M., Gue, C.Y., Bevan, H., Stent, S., Elshafie, M.Z.E.B., Soga, K., Devriendt, M., Wright, P. & Waterfall, P. 2014. Multi-suite monitoring of an existing cast iron tunnel subjected to tunnelling-induced ground movements. *Geotechnical Special Publication*. pp. 293-307. ISSN 0895-0563

Amatya, B.L., Soga, K. Bennett, P.J., Uchimura, T., Ball, P. & Lung, R. 2008. Installation of optical fibre strain sensors on soil nails used for stabilising steep highway cut slope, *Proceedings of 1st ISSMGE International Conference on Transportation Geotechnics,* pp. 276-282

Amatya, B., Soga K., Bourne-Webb P.J., Amis T. & Laloui L. 2012. Thermo-mechanical behaviour of thermal piles. *Geotechnique* **62**(6), 503-519

Bennett, P.J., Kobayashi, Y., Soga, K. & Wright, P. 2010a. Wireless Sensor Network for Monitoring of Underground Tunnel, *ICE, Geotechnical Engineering* **163**(GE3), 147–156.

Bennett, P.J., Soga, K., Wassell, I.J., Fidler, P., Abe, K., Kobayashi, Y. & Vanicek, M. 2010b. Wireless Sensor Networks for Underground Railway Applications: Case studies in Prague and London, *Smart Structures and Systems* **6** (5-6), 619-639

Bourne-Webb P.J., Amatya, B., Soga K., Amis T., Davidson, C. & Payne, P. 2009. Thermal pile test at Lambeth College, London: geotechnical and thermodynamic aspects of pile response to heat cycles. *Geotechnique* **59**(4), 237-248

Bourne-Webb P.J., Amatya, B. & Soga K. 2012. A framework for understanding thermal pile behaviour. *Proceedings of the ICE - Geotechnical Engineering* **166**(2), 170-177

Brandl H. 2006. Energy foundations and other thermoactive ground structures. *Geotechnique* **56**(5), 81-122.

Cheung, L.L.K., Soga, K., Bennett, P.J., Kobayashi,Y., Amatya, B. & Wright, P. 2010. Optical fibre strain measurement for tunnel lining monitoring, *Proceedings of ICE, Geotechnical Engineering* **163**(GE3), 119–130

Chunge, M.P.M. 2015. *Monitoring the Integrity of Bored Concrete Piles using Distributed Fibre Optic Sensors*, MPhil thesis, University of Cambridge

Duddeck, H. & Erdmann, J. 1985. On structural design models for tunnels in soft soil. *Underground Space* **9**, 246–259.

Ferri, M., Mancarella, F., Seshia, A., Ransley, J., Soga, K., Zalesky, J. & Roncaglia A. 2009. Development of MEMS strain sensors for crack monitoring in ageing civil infrastructures, *Smart Structures and Systems* **6**(4), 225-238.

Gaba, A., Simpson, B., Powrie, W. & Beadman, D. 2003. *CIRIA C580 Embedded retaining walls - guidance for economic design*. CIRIA, London.

Garber D., Choudhary R. & Soga, K. 2013a. Risk based lifetime costs assessment of a ground source heat pump (GSHP) system design: Methodology and case study, *Building and Environment,* **60**(2), 66-80

Garber D., Soga, K. & Choudhary, R. 2013b. Post-occupancy assessment of thermal-pile and open-well Ground Source Heat Pump, *ASHRAE Transactions* **119**(7), 2

Gasparre, A. 2005. *Advanced Laboratory Characterisation of London Clay.* PhD thesis, Imperial College London.

Gue, C.Y., Wilcock, M., Alhaddad, M.M., Elshafie, M.Z.E.B., Soga, K. & Mair, R.J. 2014. Monitoring the effects of tunnelling under an existing tunnel-fibre optics, *Geotechnical Aspects of Underground Construction in Soft Ground - Proceedings of the 8th Int. Symposium on Geotechnical Aspects of Underground Construction in Soft Ground,* TC204 ISSMGE - IS-SEOUL 2014. 357-361

Gue, C.Y., Wilcock, M., Alhaddad, M.M., Elshafie, M.Z.E.B., Soga, K. & Mair, R.J. 2015. The monitoring of an existing cast iron tunnel with distributed fibre optic sensing (DOFS), accepted for publication in *Journal of Civil Structural Health Monitoring* Ground Source Heat Pump Association. 2012. *Thermal Pile Design, Installation & Materials Standards*, National Energy Centre, http://www.gshp.org.uk/pdf/GSHPA_Thermal_Pile_Standard.pdf

Hoult, N.A., Bennet, P.J., Stoianov, I., Maksimović, C., Middleton, C.R., Graham, N.J.G. & Soga, K. 2009. Wireless Sensor Networks: creating 'Smart Infrastructure', *Proceedings of ICE, Civil Engineering* **162**, August 2009, 136–143.

Hoult, N.A. and Soga, K. 2014. Sensing solutions for assessing and monitoring tunnels, in "*Sensor Technologies for Civil Infrastructures: Applications in Structural Health Monitoring*" (edited by Ming L. Wang, Jerome P. Lynch, Hoon Sohn), Vol. 2, pp. 309-346

Janmonta, K. Uchimura, T. Amatya, B.L., Soga, K. Bennett, P.J., Lung, R. & Robertson, I. 2008. Fibre Optics Monitoring of Clay Cuttings and Embankments along London's Ring Motorway, *GeoCongress 2008, Characterization, Monitoring and Modeling of Geosystems,* ASCE Geotechnical Special Publication No. 179, pp. 509-516

Lord, J., Clayton, C. & Mortimore, R. 2002. *CIRIA C574 Engineering in chalk*. CIRIA, London.

Mohamad, H. 2008. *Distributed Optical Fibre Strain Sensing of Geotechnical Structures,* PhD thesis, University of Cambridge Mohamad, H., Bennett, P.J., Soga, K. Mair, R.J. & Bowers, K. 2010. Behaviour of an Old Masonry Tunnel Due to Tunnelling Induced Ground Settlement, *Géotechnique* **60**(12), 927 –938

Mohamad, H., Soga, K. & Pellow, A. 2011. Performance Monitoring of a secant piled wall using distributed fibre optic strain sensing, *Journal of Geotechnical and Geoenvironmental Engineering* **137**(12), 1236-1243

Mohamad, H., Soga, K., Bennett, P.J., Mair, R.J. & Lim, C.S. 2012. Monitoring Twin Tunnel Interactions Using Distributed Optical Fiber Strain Measurements, *Journal of Geotechnical and Geoenvironmental Engineering*, American Society of Civil Engineers **138**(8), 957-967

Mohamad, H., Soga, K. & Amatya, B. 2014. Thermal Strain Sensing of Concrete Piles Using Brillouin Optical Time Domain Reflectometry, *Geotechnical Testing Journal,* ASTM, **37**(2), 333-346

Muir Wood, A.M. 1975. The circular tunnel in elastic ground, *Géotechnique* **25**(1),115 –127

Nicholson, D., Tse, C., Penny, C., O'Hana, S. and Dimmock, R. 1999. *The Observational Method in Ground Engineering: Principles and Applications*. CIRIA, London, Report 185.

Ouyang, Y. 2014. *Geotechnical behaviour of energy piles*, PhD thesis, University of Cambridge

Peck, R. B. 1969. Advantages and limitations of the Observational Method in applied soil mechanics, *Geotechnique* **19**(2), 171–187

Rui, Y. 2015. *Finite Element Modelling of Thermal Piles and Walls*, PhD thesis, University of Cambridge

Schwamb, T. 2014. *Performance Monitoring and Numerical Modelling of a Deep Circular Excavation*, PhD thesis, University of Cambridge

Schwamb, T., Soga, K., Mair, R. J., Elshafie, M. Z., Sutherden, R., Boquet, C. & Greenwood, J. 2014. Fibre optic monitoring of a deep circular excavation, *Proceedings of the ICE - Geotechnical Engineering* **167**(2), 144-154

Schwamb, T. & Soga, K. 2015. Numerical Modelling of a Deep Circular Excavation at Abbey Mills in London," accepted for publication in *Geotechnique*

Soga, K. 2012. Emerging sensing technologies for geotechnical engineering – a case study, *Proc. of the International Workshop on ICT in Geo-Engineering,* Miyata, Y., Okayasu, T., Furuya, H., Uchimura, T. and Otani, J. (eds.), pp. 13-23

Soga, K. 2014. Croce Lecture: Understanding the real performance of geotechnical structures using an innovative fibre optic distributed strain measurement technology, *Rivista Italiana di Geotechnica*, Vol. 4, pp. 7-48

Stajano, F., Hoult, N., Wassell, I., Bennett, P., Middleton, C. & Soga, K. 2010. Smart Bridges, Smart Tunnels: Transforming Wireless Sensor Networks from Research Prototypes into Robust Engineering Infrastructure, *Ad Hoc Networks* **8**, 872-888.

Stent, S., Gherardi, R., Stenger, B., Soga, K. & Cipolla, R. 2014. Visual change detection on tunnel linings, *Machine Vision and Applications* 28 Nov 2014

Suckling T.P. & Smith P. 2002. Environmentally Friendly Geothermal Piles at Keble College, Oxford, UK. *9th Intl Conf. on Piling and Deep Foundations*, Nice France

Ventouras, K. 2005. *Engineering Behaviour of Thanet Sand.* PhD thesis, Imperial College London.

Vorster, T.E.B. 2005. *The Effects of Tunnelling on Buried Pipes, PhD thesis*, University of Cambridge

Vorster, T.E.B., Soga, K., Mair, R.J., Bennett, P.J., Klar, A., & Choy, C.K. 2006. The use of fibre optic sensors to monitor pipeline behaviour, *ASCE Geocongress 2006.* pp. 1-6. doi: 10.1061/40803(187)33

Zhang, Y., Soga, K. & Choudhary, R. 2014. Shallow geothermal energy application with GSHPs at city scale: study on the City of Westminster. *Geotechnique Letters* **4**(2): 125-131.

Creeping faults: Good news, bad news?

Kate Huihsuan Chen and Roland Bürgmann

Abstract The motion of the Earth's tectonic plates drive fault slip. Some faults slip in sudden movements, releasing great amounts of energy during large earthquake ruptures, while others slip in steadier movements which release energy more slowly. The latter, known as creeping faults, are believed to be less hazardous but there is mounting evidence that they are more complex than previously thought and can also pose a significant hazard. A recent review by Harris [2017] documents the earthquake potential of creeping faults in shallow continental fault zones from worldwide data. She presents a comprehensive review of prior studies; key insights into when, where, and why fault creep takes place and under which conditions creeping faults may represent high seismic hazard and suggests some directions for future research.

1. What Are Creeping Faults?

Earthquake faults are everywhere. They are near homes, schools, and places where our families and friends live. Often times, damaging earthquakes occur in unexpected places where no historical records of large earthquakes have been reported, or only small earthquakes have been recorded. Some unusual faults that produce frequent small earthquakes at depth while slipping slowly (creeping) at the Earth's surface may be the last to worry about.

Creeping faults are often assumed to be less hazardous, incapable of producing major destructive earthquakes, as much of the fault surface slides steadily, and thus cannot build up the potential for a large slip event. However, some faults that were understood by many to be such relatively benign structures turned out to produce destructive earthquakes. The Hayward fault in California and the Chishang fault in Taiwan are examples of faults that rapidly creep at the surface but are also known to have produced magnitude 6.8 earthquakes. Thus, if large earthquakes can occur on faults, or sections of a fault, that are slowly creeping, these need to be better understood and taken seriously. In the recently published review article by Harris [2017], the nature and hazard of creeping faults are comprehensively addressed.

2. Where Do Creeping Faults Occur and What Damage Do They Cause?

Thanks to improved measurement techniques and increasing damage to manmade structures built across faults, we have come to realize that creeping faults are not uncommon. As summarized by Harris [2017], creep on major continental faults has been observed in the U.S., Mexico, Italy, Turkey, Israel, Afghanistan, Pakistan, China, Philippines, Japan, and Taiwan.

Along the extensively studied San Andreas fault system, California, creep has resulted in significant structural damage where faults traverse urban areas, such as to the Berkeley Memorial Stadium at the University of California Berkeley, which required extensive retrofitting due to the creep damage from the Hayward fault (Figure 1). Another example is the thrust-faulting Chihshang fault in eastern Taiwan, where rapid surface slip at 2–3 cm/yr has damaged houses, roads, fences, and utility pipes built across the fault in recent decades (Figure 2). The impact of creeping faults on infrastructure should be seriously considered, as buildings generally cannot accommodate such ground offsets, even if they occur at very low rates.

3. Why Do Faults Creep?

As reviewed in Harris [2017], there are some specific types of rock that can increase a fault's frictional strength as slip accelerates, thus forcing slip to slow down and allowing the fault to slip stably and quietly without ever generating earthquakes. Fault sections filled with these materials (e.g., serpentinite, talc, some clay minerals, and salt) may fully resist faster slip and represent persistent barriers to propagating earthquake ruptures.

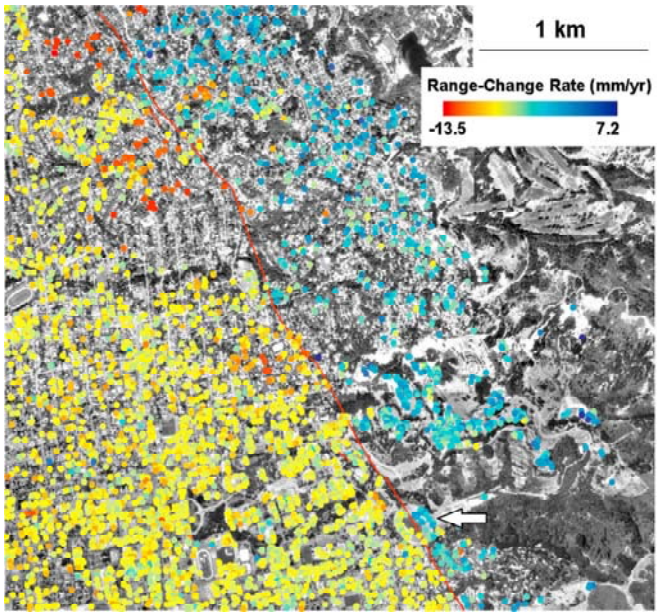

Figure 1. The creeping Hayward fault in Berkeley, California. Color circles indicate surface motions during 1992–2001 measured with satellite radar interferometry from the European Remote Sensing (ERS-1/ERS-2) satellites. The red line is the surface trace of the fault with different circle colors on either side reflecting fault creep. Areas with fast moving red circles on west side of the fault lie on active landslides [Hilley et al., 2004]. The creep rate at Memorial Stadium at the University of California, Berkeley (oval in the bottom right, as indicated by arrow) is ~5 mm/yr, about half its long-term rate. Credit: Roland Bürgmann.

However, other factors that may enable a fault to creep include fluid pressure, temperature, the chemical environment, fault geometry, and sudden stress changes from nearby earthquakes [e.g., Avouac, 2015].

A variety of numerical modeling studies and some laboratory experiments indicate that there are specific physical conditions that allow creep to be switched on and off. Noda and Lapusta [2013] pointed out the role of fluids at depth; a creeping segment may lose its resistance to slipping seismically through frictional heating of pore fluids. Experiments show that even serpentinite, which is famous for enabling faults to creep, can switch from creep to seismic slip under high slip speeds [e.g., Kohli et al., 2011; Proctor et al., 2014]. Uchida et al. [2015] also noted that such mode-changing behavior took place in a seismic-to-aseismic transition zone of northeast Japan's subduction zone, a conditionally stable area where slip behavior changes with loading rate.

4. Are Creeping Faults a Seismic Hazard?

Creeping faults very often are found to not slip at their expected full long-term rate. So when and how do creeping faults catch up with this slip deficit? There are a number of possibilities: (1) They slip as part of large earthquakes that initiate on neighboring, fully locked sections of a fault, but with a reduced amount of slip. (2) They catch up via accelerated but still slow (aseismic) slip following rupture of adjacent locked sections. (3) They spontaneously accelerate in slow-slip episodes without ever reaching seismic slip speeds. (4) They change their character and accelerate into an earthquake rupture after all.

Precise surface deformation measurements allow us to deduce if creep is halted elsewhere on the fault deep in the Earth. While it may be relatively good news that some faults release tectonic energy by slow creep that only damages structures built across them (Figures 1 and 2), the bad news is that most of these creeping faults are still capable of hosting large earthquakes. Both the Hayward fault [e.g., Chaussard et al., 2015] and the Chishang fault [Thomas et al., 2014] were found to have large locked fault sections hidden at several kilometer depth, some of which have already slipped in damaging earthquakes.

Figure 2. View of the fast creeping Chihshang fault (black line) that bounds Longitudinal Valley and Coastal Range in eastern Taiwan. With 2–3 cm/yr surface slip rate, this is the most rapidly creeping continental reverse fault in the world. The east dipping thrust fault separates by Lichi Mélange in the hanging wall and young river deposits in the foot wall. Fault creep damage of utility pipes (1 and 2), a road (3), and a brick wall (4) along the Chihshang fault in eastern Taiwan. Surface slip on the Chihshang fault is monitored with creepmeters [Lee et al., 2003] (1 and 2). Credit: Hao-Tsu Chu and Chung-Hsiang Mu.

For faults that slowly move at a rate of a few millimeters to centimeters every year, the physics of fault slip is mechanically different from faults that remain locked for decades or centuries before catching up in a sudden great earthquake. So the question is, does the fault creep reduce the amount of slip during a large earthquake and therefore cause less ground shaking? The Harris [2017] review provides a partial answer: earthquakes on creeping faults ruptured a similar-size fault section and produced similar peak ground shaking compared to earthquakes of the same magnitude on locked faults. Harris [2017] pointed out, however, the magnitude and ground motion statistics were mainly derived from magnitude <6.7 earthquakes in the San Andreas fault system, and additional investigation of other regions and dip-slip earthquakes is needed.

5. Can Fault Creep Stop or Limit Earthquakes?

When an earthquake occurs, the longer and further a rupture is allowed to grow, the greater is the resulting fault slip and damaging ground shaking. When this happens, how "freely" the fault surface allows the slip to continue is mainly controlled by the rupture velocity and frictional properties of the fault. Through simulations, scientists are learning how the presence of fault creep affects the growth of earthquake rupture. Harris [2017] addresses different simulation approaches and outcomes that give us a different answer: great ruptures may penetrate through creeping sections or can be stopped by them depending on a complex set of model variables. The physical processes responsible for such differences can be better understood through more and more detailed observations of fault creep and large earthquake ruptures.

6. What Further Research Is Needed to Better Understand Fault Creep?

In tectonically active continental regions, well-documented fault creep has mostly been found on strike-slip faults but only on a few thrust and normal faults. As summarized in Figure 3 derived from the worldwide creeping faults data in Table 1 of Harris [2017], a correlation between wider creeping depths and higher creep rate appears (Figure 3). It is worth noting that there are only a few documented cases of dip-slip creeping faults. This may partly reflect the difficulty of recognizing creep on dip-slip faults and points to the need to collect more data in the future, for the better understanding of what controls the creeping behavior in different tectonic environments.

We do not know if the faults that rapidly creep over most of their surface area continue to represent substantial seismic hazard. It is important to further assess if creeping faults, such as the central San Andreas fault, have in the past and may again rupture in rare great earthquakes that "bulldoze" through. Whether there exists a universal rule for what controls the creep rate also requires further exploration.

Finally, a number of large earthquakes appear to have occurred after a precursory phase of slow fault creep [Bouchon et al., 2013, Uchida et al., 2016; Obara and Kato, 2016], suggesting that understanding slow slip is essential to understanding the timing of earthquakes. Harris [2017] encourages an expanded thinking and investigation on the nature and effects of fault creep: what we have seen and what we expect from creeping faults around the world. Continuous collection and analysis of geologic, geodetic, and seismic data will help clarify the role of creeping faults in causing earthquakes, and contribute to seismic hazard assessment.

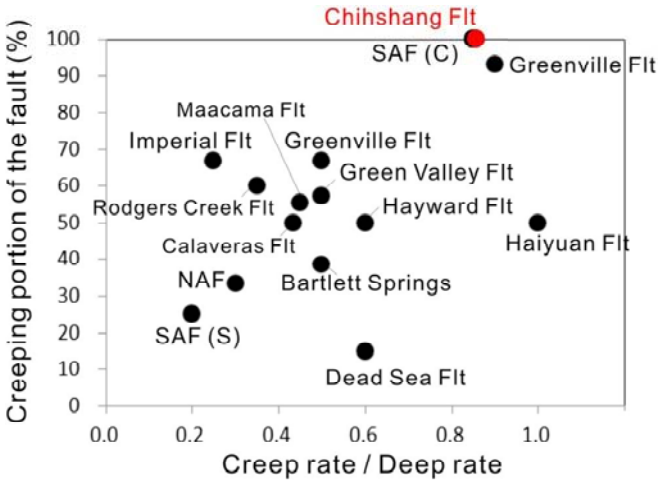

Figure 3. Depth extent of creep on faults versus creep rate from worldwide data summarized in Table 1 of Harris [2017]. Here the depth extent is expressed as the average depth to which surface creep is understood to extend divided by the depth to the base of the seismogenic zone. The creep rate ratio is the shallow creep rate divided by the long-term fault slip rate at depth below the seismogenic zone. Black circles indicate the data from strike-slip faults. Black circles indicate data from strike-slip faults; the Chihshang fault (red circle) is one of the very few well documented creeping dip-slip faults. Note that five faults with only limited data in Table 1 of Harris [2017] are excluded in this figure.

Acknowledgments

We thank Editor Mark Moldwin's invitation for this commentary. We acknowledge useful suggestions from Mark Moldwin, Jenny Lunn, Ruth Harris, and Kathryn Materna to

improve the presentation. We also appreciate the effort by Chung-Hsiang Mu to make Figure 2.

References

Avouac, J. P. (2015), From geodetic imaging of seismic and aseismic fault slip to dynamic modeling of the seismic cycle, Annu. Rev. Earth Planet. Sci., 43, 233–271, doi:10.1146/annurev-earth-060614-105302.

Bouchon, M., V. Durand, D. Marsan, H. Karabulut, and J. Schmittbuhl (2013), The long precursory phase of most large interpolate earthquakes, Nat. Geosci., 6, 299–302, doi:10.1038/ngeo1770.

Chaussard, E., R. Bürgmann, H. Fattahi, C. W. Johnson, R. Nadeau, T. Taira, and I. Johanson (2015), Interseismic coupling and refined earthquake potential on the Hayward-Calaveras fault zone, J. Geophys. Res. Solid Earth, 120, 8570–8590, doi:10.1002/2015JB012230.

Harris, R. A. (2017), Large earthquakes and creeping faults, Rev. Geophys., 55, 169–198, doi:10.1002/2016RG000539.

Hilley, G. E., R. Bürgmann, A. Ferretti, F. Novali, and F. Rocca (2004), Dynamics of slow-moving landslides from permanent scatterer analysis, Science, 304, 1952–1955.

Kohli, A. H., D. L. Goldsby, G. Hirth, and T. Tullis (2011), Flash weakening of serpentinite at near-seismic slip rates, J. Geophys. Res., 116, B03202, doi:10.1029/2010JB007833.

Lee, J.-C., J. Angelier, H.-T. Chu, J.-C. Hu, F.-S. Jeng, and R.-J. Rau (2003), Active fault creep variations at Chihshang, Taiwan, revealed by creep meter monitoring, 1998–2001, J. Geophys. Res., 108(B11), 2528, doi:10.1029/2003JB002394.

Noda, H., and N. Lapusta (2013), Stable creeping fault segments can become destructive as a result of dynamic weakening, Nature, 493, 518–521, doi:10.1038/nature11703.

Obara, K., and A. Kato (2016), Connecting slow earthquakes to huge earthquakes, Science, 353(6296), 253–257, doi:10.1126/science.aaf1512.

Proctor, B. P., T. M. Mitchell, G. Hirth, D. Goldsby, F. Zorzi, J. D. Platt, and G. D. Toro (2014), Dynamic weakening of serpentinite gouges and bare surfaces at seismic slip rates, J. Geophys. Res. Solid Earth, 119, 8107–8131, doi:10.1002/2014JB011057.

Thomas, M. Y., J.-P. Avouac, J. Champenois, J.-C. Lee, and L.-C. Kuo (2014), Spatiotemporal evolution of seismic and aseismic slip on the Longitudinal Valley Fault, Taiwan, J. Geophys. Res. Solid Earth, 119, 5114–5139, doi:10.1002/2013JB010603.

Uchida, N., K. Shimamura, T. Matsuzawa, and T. Okada (2015), Postseismic response of repeating earthquakes around the 2011 Tohoku-oki earthquake: Moment increases due to the fast loading rate, J. Geophys. Res. Solid Earth, 120, 259–274, doi:10.1002/2013JB010933.

Uchida, N., T. Iinuma, R.M. Nadeau, R. Bürgmann, and R. Hino (2016), Periodic slow slip triggers megathrust zone earthquakes in northeastern Japan, Science, 351(6272), 488–492, doi:10.1126/science.aad3108.

(Rev. Geophys., 55, doi:10.1002/2017RG000565, https://www.researchgate.net/publication/316342097_Creeping_faults_Good_news_bad_news)

Earthquake science in resilient societies

T. Stahl, M. K. Clark, D. Zekkos, A. Athanasopoulos-Zekkos, M. Willis, William Medwedeff, Logan Knoper, Kirk Townsend, and Jonson Jin

Abstract

Earthquake science is critical in reducing vulnerability to a broad range of seismic hazards. Evidence-based studies drawing from several branches of the Earth sciences and engineering can effectively mitigate losses experienced in earthquakes. Societies that invest in this research have lower fatality rates in earthquakes and can recover more rapidly. This commentary explores the scientific pathways through which earthquake-resilient societies are developed. We highlight recent case studies of evidence-based decision making and how modern research is improving the way societies respond to earthquakes.

1. What Are the Risks and Costs of Earthquakes?

Strong ground shaking in earthquakes has resulted in millions of deaths in the last century, with many millions more projected in the future [Holzer and Savage, 2013]. For many affected regions, destructive landslides and tsunami, fault ruptures that tear through unlucky homes, flooding and liquefaction in recurring aftershocks, fires, and disease can add up to sustained economic losses—let alone numerous casualties—that reach far beyond the initial earthquake and ground shaking. Since the beginning of just the 21st century, earthquakes and their secondary effects have caused over 700,000 deaths, millions of injuries, and hundreds of billions of dollars in damage [Bilham, 2009; Quigley and Duffy, 2016]. Worldwide, approximately 20–25% of earthquake related deaths are due to secondary effects, and some of the largest death tolls in natural disasters have been due to these phenomena (e.g., ~227,000 deaths in the 2004 Indian Ocean tsunami) [Marano et al., 2010].

As Earth's population continues to grow, so too does the fraction of the population exposed to earthquake hazards. On a global scale, earthquake-related fatalities and seismic risk have only increased through time [Bilham, 2009]. This trend is largely due to the increased urbanization, exposure, and vulnerability of economically developing regions prone to earthquakes. From 1900–2009, approximately 80% of all earthquake shaking related fatalities were caused by just 25 earthquakes in 11 countries [Jaiswal et al., 2009]. The costs of earthquakes are more economic in the developed world, where fewer casualties occur in events of similar intensity due to investment in earthquake science, engineering, and education [Bilham, 2009; Jaiswal and Wald, 2011]. Even in well-prepared regions, however, the scale of the economic toll can prolong or prevent recovery.

There is no immunity to earthquakes or related hazards, but scientists and engineers who study earthquakes can provide solutions that reduce the burden quakes have on society. This commentary explores the multidisciplinary pathways through which we have come to understand earthquakes and what constitutes an earthquake-resilient society. We provide a case study that highlights how this science has progressed along with promising avenues for future research.

2. What Causes Earthquakes and How Are They Measured?

Earthquakes are caused by rapid displacement on faults and the sudden release of accumulated strain in the form of seismic waves. These seismic waves cause ground shaking that collapse buildings, damage infrastructure, and can cause widespread landsliding in mountainous terrain. Earthquakes have been problematic for as long as humans have been building structures, to the point that some argue for tipping points in which the downfalls of entire civilizations were catalyzed by major earthquakes [cf. Sintubin, 2011]. But it was not until 1910 that Harry Fielding Reid, an American geologist studying the 1906 San Francisco earthquake, formulated a hypothesis by which earthquakes occur, eventually allowing earthquake hazard to be evaluated. Reid used seismology, structural geology, and survey data to postulate a mechanism for earthquakes called elastic rebound: that the slow buildup of forces on either side of a locked fault eventually results in its sudden rupture and release of seismic energy [Reid, 1910]. At the time, Reid used seemingly disparate bits of information to develop the now well-accepted elastic rebound theory, some 60 years before the acceptance of the theory of plate tectonics. We now recognize plate tectonics as the foundational principle of modern geology, which forms the basis of our understanding of where and how often earthquakes occur.

As Reid envisioned, the study of earthquakes requires information and expertise from several geologic and engineering disciplines (Table 1). Geodesists and geomorphologists use high-precision survey data from Global Positioning Systems (GPS), satellite-based radar, lidar, and image analysis to identify active faults at the Earth's surface and monitor how quickly they are accumulating tectonic strain on human timescales. Paleoseismologists date and measure previous episodes of fault motion and analyze the geologic record of earthquake ground shaking (e.g., earthquake-induced landslides or ancient tsunami deposits preserved on land) in prehistoric earthquakes. Seismologists detect modern earthquakes and map out the deeper structure of the Earth. Engineers measure the response of the Earth's surface to shaking and can design structures that are resistant to different levels and frequencies seismic shaking. Hazard modelers aggregate this data with geographic and historical information to more reliably predict the spatial distribution and magnitude of destruction in large events.

3. How Do We Plan for Earthquakes?

So, what use are all of these fields and the troves of data they produce? A common public misconception is that the end result is, or should be, earthquake prediction—precise dates, times, locations, and magnitudes of impending earthquakes. In fact, the lack of reliable quake precursors has infamously drawn geologists into legal problems [Cartlidge, 2015], propped up less-than-scrupulous hypotheses regarding the predictive power of astrology [Stahl, 2011], and led to an unfortunate public view that earthquake science is the "ambulance down in the valley" rather than as a series of fences at the top (or nets along the way).

The purpose of the work of earthquake scientists and engineers is to mitigate unnecessary damage and loss of life. Researchers and practitioners identify likely geologic hazards, inform policy on where and how to build structures, determine how to best divide resources and response teams in the aftermath of quakes, and educate policy makers and the public on how to best prepare for earthquakes. Detailing the contribution that each field makes toward these larger societal goals (Table 1) is outside the scope of this overview, but we hope to briefly highlight the hallmarks of good earthquake science through the hand lens of recent earthquakes in New Zealand.

4. Two Examples From New Zealand

4.1. The 2010–2011 Canterbury Earthquakes

New Zealand lies on a major tectonic plate boundary and is no stranger to large earthquakes. In 2010–2011, a magnitude 7.1 (M7.1) earthquake and its M6.3 aftershock dealt a devastating blow to one of its largest cities, Christchurch. Due to a "perfect storm" of geologic conditions, the M6.3

Table 1. Disciplines, Goals, and Outcomes of Earthquake Science

Discipline	Description	Goals as Applied to Earthquake Science	Examples of Tractable Research Questions
Paleoseismology	Assessment of prehistoric earthquakes and their environmental effects	Identify active faults, estimate the recurrence interval of large earthquakes throughout recent geologic time, anticipate the magnitudes of earthquakes on faults, and anticipate the response of Earth's surface to faulting and strong ground motions	Where will earthquakes occur in the future? How big will the earthquakes be, on average? Where have secondary hazards (tsunami, landslides, and liquefaction) occurred in the past?
Seismology	Assessment of the rates, size and locations of modern earthquakes; the structure of the Earth; and the response of Earth's surface to seismic waves	Identify active faults, monitor the location and frequency of earthquakes through time, determine the structure of the Earth, and determine the response of different sites to incoming seismic waves	What is the annual frequency of destructive earthquakes in a region? What is the probability of a magnitude 6 aftershock in the next month?
Fault/rock mechanics; Engineering geology	The physics of how rocks deform and fail under stress	Understand how earthquakes initiate, the controls on how large they can grow, and assess slope stability at the surface	How does rock type influence the size of the largest earthquake on a fault? Where are landslides likely to occur when subjected to shaking?
Geodesy	Remote sensing of Earth processes through space and time	Identify active faults and quantify rates and processes that lead to earthquakes	Where are large aftershocks likely to occur? Which faults a currently accumulating seismic strain and likely to rupture?
Tectonic geomorphology and structural geology	Numerical, field, and lab-based science for the tectonic evolution of a region over all timescales	Identify the processes and spatial distribution of faulting, slope failure, and erosion through geologic time, and quantify their rates and interactions	How do earthquake-induced landslides contribute to erosion? How do fault slip rates and earthquake hazards change through time?
Geotechnical engineering (subdiscipline of civil engineering)	The behavior and response of Earth materials	Determine the response of rocks and soils to seismic waves and seismic soil-structure interaction, and predict locations and type of ground failure (landslides, liquefaction, and rock fall)	Which areas and what types of sediment are prone to liquefaction? How do soils amplify seismic waves?
Civil engineering/ structural engineering	Design, construction, and maintenance of built environment	Reduce the vulnerability of structures to fault displacements, seismic shaking, and other secondary hazards	How can we prevent flooding due to earthquake subsidence? How can we isolate a building's foundation to prevent shaking-induced collapse?
Hazard and disaster management	Prediction and mitigation of negative outcomes of earthquakes on society	Model economic losses and fatalities for response and recovery operations, predict spatial distribution of adverse impacts on infrastructure, and interface with policy makers	Where are the most fatalities expected to focus response and relief efforts? What is the effect of earthquake-induced landslides on transportation networks?

aftershock resulted in some of the strongest ground motions ever recorded—nearly 5 times those that killed over 100,000 people in the 2010 Haiti earthquake. Despite the stronger ground motions in Christchurch, 185 fatalities occurred; 115 of those from the collapse of a single building that was not designed to code [Canterbury Earthquake Royal Commission, 2012].

Both Christchurch earthquakes occurred on previously unknown faults, which were buried beneath thick alluvial plain sediments [Quigley et al., 2010] and volcanic rocks. Because individual faults could not be identified from surface mapping, scientists planned for a "distributed source" M7 earthquake in the region instead of an earthquake on a single fault line [Stirling et al., 2008]. As anticipated, widespread liquefaction and flooding occurred throughout the city and was one of the most damaging components of the earthquake. The potentially hazardous areas were well documented, and largely identified as such, prior to the earthquake. Restrictions on the locations of buildings and infrastructure with engineered improvements to the ground will greatly improve the resilience of these areas during future earthquakes. Although economic recovery in Christchurch is still incomplete 6 to 7 years later, prior scientific data greatly mitigated what could have been a much worse outcome. Research conducted in the aftermath of this event has also spawned excellent case studies of faulting, rockfall, soil liquefaction, and hazard management [Massey et al., 2014; Potter et al., 2015; Quigley et al., 2016].

4.2. The 2016 Kaikoura Earthquake

In November 2016, a larger M7.8 earthquake struck New Zealand's South Island. Recently published data indicate that it was one of, if not the most, complex earthquakes ever documented. At least 12 faults and even more fault segments ruptured in quick succession, resulting in ground motions exceeding that of gravity and tens of thousands of landslides [GeoNet, 2016]. Approximately 200 significant landslides dammed or continue to dam rivers [GeoNet, 2016]. The earthquake ruptured across a 170 km stretch of faults about midway between New Zealand's capital Wellington and Christchurch. Despite the widespread faulting, strong shaking, landslides, and tsunami, only two people are reported to have died—one from a building collapse, the other from a heart attack.

We would be remiss to claim that the complexity of this earthquake was fully anticipated by geologists. However, it is a testament to the robustness and diversity of science that goes into seismic hazard assessments, engineering design codes, hazard planning, in addition to the low population density in the worst affected area, that so few casualties occurred. And, despite its complexity, the magnitude and location of this event was not unexpected. Emergency management systems generally worked. The rapid collection of data from an international network of engineers and scientists, led by the Institute of Geological and Nuclear Sciences (GNS) in New Zealand, allowed for a coordinated and targeted humanitarian response. Continued scientific monitoring of landslides, landslide dams, and flood hazards are underway and have provided valuable data to the public, transportation authorities, and civil services. Probabilistic aftershock forecasts have been continuously updated by GNS since November and have further informed the timeline of response and recovery efforts. This is how earthquake-resilient societies operate—on data, research, and planning.

5. How Can Science Better Prepare Us for Earthquakes in the Future?

Although we are unlikely to ever be able to predict earthquakes, we can improve our resilience to them. New data sets, technologies, computational power, and continued investment in Science, Technology, Engineering and Mathematics (STEM) advance our ability to react quickly to events and prioritize resources. For example, new methodologies can provide rapid assessment of the characteristics of earthquake-induced landslides from high-resolution satellite images and satellite-derived elevation models of the Earth. We can continue to improve our models of how ruptures "jump" onto other faults to generate larger earthquakes [Stahl et al., 2016; Hamling et al., 2017]. We can prevent avoidable catastrophes in the United States, where nearly 50% of the population faces some degree of earthquake hazard (Figure 1) [Jaiswal et al., 2015], and in developing nations where the seismic risk of exposed populations is far greater [Tucker, 2013]. This work requires a concerted effort from many scientific disciplines to provide the means to build resilient societies and educate the public and policy makers.

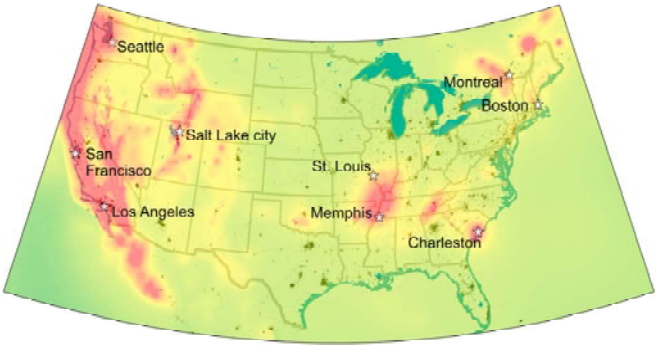

Figure 1. Seismic hazard of the conterminous United States. This map shows a 2%probability of exceeding a mapped peak ground acceleration (PGA, green to red colors) in 50 years. The darkest red colors represent PGAs of approximately 0.5–1.0 g. This map is a simple visual representation of the 2014 USGS hazard map (available at https://earthquake.usgs.gov/hazards/hazmaps/conterminous/) and should not be used for hazard purposes. Major population centers are shown with stars, and population density is shown in black and white (black = areas of densest population; data from GPWv4 by Center for International Earth Science Information Network [2016]).

Acknowledgments

The authors gratefully acknowledge the National Science Foundation and USGS for their commitment to funding and pursuing earthquake research. Work related to the Kaikoura earthquake was funded by NSF RAPID 1719496 and 1719524. Stahl and others thank all members of Geotechnical Extreme Event Reconnaissance (GEER) for the Kaikoura earthquake, along with the many New Zealand-based academic institutions and GNS that have worked on both the 2010–2011 and 2016 events. Stahl was supported by postdoctoral fellowship NSF EAR 1451466.

References

Bilham, R. (2009), The seismic future of cities, Bull. Earthq. Eng., 7(4), 839.

Canterbury Earthquake Royal Commission (2012), Final Report: Volume 6, Canterbury television building. [Available at http://canterbury.royalcommission.govt.nz/Final-Report-Volume-Six-Contents, (last accessed 2 April 2017).]

Cartlidge, E. (2015), Why Italian scientists were exonerated, ScienceInsider, doi:10.1126/science.aaa7841.

Center for International Earth Science Information Network (2016), Gridded Population of the World, Version 4 (GPWv4): Population Density. Palisades, NY: NASA Socioeconomic Data and Applications Center (SEDAC), doi:10.7927/H4NP22DQ (last accessed 2 April 2017).

GeoNet (2016), Landslides and landslide dams caused by the Kaikoura earthquake. [Available at http://info.geonet.org.nz/display/quake/2016/11/18/Landslides+and+Landslide+dams+caused+by+the+Kaikoura+Earthquake (accessed 2 April 2017).]

Hamling, I. J., et al. (2017), Complex multifault rupture during the 2016 Mw 7.8 Kaikōura earthquake, New Zealand, Science, 356(6334), doi:10.1126/science.aam7194.

Holzer, T. L., and J. C. Savage (2013), Global earthquake fatalities and population, Earthq. Spectra, 29(1), 155–175.

Jaiswal, K. S., M. D. Petersen, K. Rukstales, and W. S. Leith (2015), Earthquake shaking hazard estimates and exposure changes in the conterminous United States, Earthq. Spectra, 31(S1), S201–S220.

Jaiswal, K. S., and D. J. Wald (2011), Rapid estimation of the economic consequences of global earthquakes, U.S. Geol. Surv. Open File Rep., 2011–1116, 47 p.

Jaiswal, K. S., D. J. Wald, and M. Hearne (2009), Estimating casualties for large earthquakes worldwide using an empirical approach, U.S. Geol. Surv. Open File Rep., 2009–1136, 78 p.

Marano, K. D., D. J. Wald, and T. I. Allen (2010), Global earthquake casualties due to secondary effects: A quantitative analysis for improving rapid loss analyses, Nat. Hazards, 52(2), 319–328.

Massey, C. I., et al. (2014), Determining rockfall risk in Christchurch using rockfalls triggered by the 2010–2011 Canterbury earthquake sequence, Earthq. Spectra, 30(1), 155–181.

Potter, S. H., J. S. Becker, D. M. Johnston, and K. P. Rossiter (2015), An overview of the impacts of the 2010–2011 Canterbury earthquakes, Int. J. Disaster Risk Reduct., 14(Part 1), 6–14.

Quigley, M. C., and B. Duffy (2016), in Seismic Hazard, in Natural Hazards of Australasia, edited by J. Goff and C. R. De Freitas, pp. 105–143, Cambridge Univ. Press, Port Melbourne, Australia.

Quigley, M., et al. (2010), Previously unknown fault shakes New Zealand's South Island, Eos. Trans. AGU, 91(49), 469–470.

Quigley, M. C., M. W. Hughes, B. A. Bradley, S. van Ballegooy, C. Reid, J. Morgenroth, T. Horton, B. Duffy, and J. R. Pettinga (2016), The 2010–2011 Canterbury earthquake Sequence: Environmental effects, seismic triggering thresholds and geologic legacy, Tectonophysics, 672–673, 228–274.

Reid, H. F. (1910), The mechanics of the earthquake, in The California Earthquake of April 18, 1906, Report of the State Investigation Commission, vol. 2, pp. 1–192, Carnegie Institution of Washington, Washington, D. C.

Sintubin, M. (2011), Archaeoseismology: Past, present and future, Quat. Int., 242(1), 4–10.

Stahl, T. (2011), Lunar eclipse prompts lunatic quips but is not going to rock your world, The Conversation. [Available at http://theconversation.com/lunareclipse-prompts-lunatic-quips-but-is-not-going-to-rock-your-world-556 (last accessed 2 April 2017).]

Stahl, T., M. C. Quigley, A. McGill, and M. S. Bebbington (2016), Modeling the maximum moment magnitudes of earthquakes on imbricate reverse faults: Results from a paleoseismic study of the Fox Peak and Forest Creek faults, South Island, New Zealand, Bull. Seismol. Soc. Am., 106, 2345–2363.

Stirling, M. W., M. C. Gerstenberger, N. J. Litchfield, G. H. McVerry, W. D. Smith, J. Pettinga, and P. Barnes (2008), Seismic hazard of the Canterbury region, New Zealand: New earthquake source model and methodology, Bull. N. Z. Soc. Earthq. Eng., 41, 51–67.

Tucker, B. E. (2013), Reducing earthquake risk, Science, 341(6150), 1070–1072.

ΠΡΟΣΕΧΕΙΣ ΓΕΩΤΕΧΝΙΚΕΣ ΕΚΔΗΛΩΣΕΙΣ

Για τις παλαιότερες καταχωρήσεις περισσότερες πληροφορίες μπορούν να αναζητηθούν στα προηγούμενα τεύχη του «περιοδικού» και στις παρατιθέμενες ιστοσελίδες.

3ο Πανελλήνιο Συνέδριο Φραγμάτων και Ταμιευτήρων - Διαχείριση Έργων και Προοπτικές Ανάπτυξης, 12 - 14 Οκτωβρίου 2017, Αθήνα, www.fragmata2017.gr

18 - 20 October 2017, Izmir, Turkey
www.zye2017.org

"The Third International Soil-Structure Interaction Symposium" will be held in Izmir on October 18 and 19, 2017. The symposium is hosted by Dokuz Eylül University Civil Engineering Department, and is organized on behalf of the Turkish Society for Soil Mechanics and Geotechnical Engineering (www.zmgm.ogr.tr). Turkish Chamber of Civil Engineers Izmir Branch also contributes to the organization. The symposium will be followed by a one-day Workshop on "Axial Load Response of Long Piles in Deep Alluvial Soils" which is in cooperation with TC212 Deep Foundations. Detailed information can be reached at its own web page (www.zye2017-pileworkshop.org).

Typical themes at The Third International Soil-Structure Interaction Symposium are: Shallow and Deep Foundations, Coastal Structures, Energy Structures, Tall Buildings, Transportation Structures, Embedded Structures, Deep Excavations and Retaining Structures. Proceedings covering static and dynamic aspects of soil-structure interaction including determination of strong ground motion are highly welcome.

Anybody interested in soil-structure interaction is invited to participate. Participation will benefit academic researchers, engineers working with companies and representatives from local authorities. Besides presenting their own research or professional work, participants will be informed from and discuss latest accomplishments, innovations and future directions in soil-structure interaction area. Also, participants connect with each other in order to develop networks and collaborations. We are looking forward to welcoming you at the **"The Third International Soil-Structure Interaction Symposium"** and **Workshop on "Axial Load Response of Long Piles in Deep Alluvial Soils"** in Izmir, Turkey.

Main Topics

Typical themes at The Third International Soil-Structure Interaction Symposium are:

- Shallow and Deep Foundations
  - Soil-pile interaction under lateral and vertical loading conditions
  - Piled rafts
  - Influence of soil improvement on foundation input motion
- Coastal Structures
- Energy Structures
  - SSI for offshore wind turbines
  - Soil-pile interaction for energy piles
- Tall Buildings
  - SSI in tall building design
  - Determination of foundation input motion for shallow and deep foundations
  - Dynamic response of deep alluvial soils
- Transportation Structures
- Embedded Structures
  - Influence of embedded structures on strong ground motion in urban areas
  - Lifelines
- Deep Excavations and Retaining Structures

Contact

CONFERENCE SECRETERIAT
Assoc. Prof. Dr. Yeliz Yukselen AKSOY
Dokuz Eylül University
Department of Civil Engineering
Tınaztepe Yerleşkesi Buca, Izmir Turkey
yeliz.yukselen@deu.edu.tr

4th International Conference on Long-Term Behaviour and Environmentally Friendly Rehabilitation Technologies of Dams, 17-19 October 2017, Tehran, Iran, www.ltbd2017.ir/en

The 15th International Conference of International Association for Computer Methods and Advances in Geomechanics, 19-23 October 2017, Wuhan, Hubei Province, China, www.15iacmag.org

XIII International Conference "Underground Infrastructure of Urban Areas 2017", 24-26 October 2017, Wroclaw, Poland, http://uiua.pwr.edu.pl/?lang=en

SIFRMEG 2017 Shaoxing International Forum on Rock Mechanics and Engineering Geology, October 28-29, 2017, http://forum.hmkj.com.cn/index.php/Index/show/tid/20

4th Underground Infrastructure & Deep Foundations Middle East Conference and Awards, 13 – 14 November in Dubai, UAE, www.undergrounduae.iqpc.ae

ISAUG 2017 2nd International Symposium on Asia Urban GeoEngineering, 24-27 November 2017, Changsha, China, www.isaug2017.org

International Symposium on Dam Safety
Nov. 9-10, 2017,Changsha, China
http://www.chincold.org.cn/dams/NewsEvents/webinfo/2017/06/1496391626559562.htm

Dams and reservoirs as important water storage infrastructure, with multiple water services, have played important role to support social economy development. As dam failure may cause extensive damage or even loss of lives, dam safety has obtained high concern and been a top priority. The crisis at Oroville Dam happened in Feb. 2017 has attracted attentions all over the world, which arouse reflection on considering how to keep dam safety in a changing world.

International Symposium on Dam Safety, organized by Chinese National Committee on Large Dams (CHINCOLD), will be held in Changsha, China on November 9 to 10, 2017. The aim of this symposium is to discuss and exchange the state of the art concepts, methods, technologies related to dam safety in a changing situation, such as considering of climate change and changing requirements, so as to advance the implementation of practice and to ensure the safe of dam projects.

This Symposium will be held together with the 2017 CHINCOLD Annual Meeting. The CHINCOLD Annual Meeting is one of the most important events in dams and hydropower society in China and has attracted 600-800 participants every year since 2011, including many high level experts such as Former Minister of Ministry of Water Resources of China Mr. Wamg Shucheng, ICOLD President Prof. Anton Schleiss, Hon. President Prof. Luis Berga, and Vice President M. Rogers. During the Annual Meeting, the 10th Round Table meeting on Sustainable Development for Africa, Round table meeting on Public Awareness, Youth Forum will be organized together with technical sessions. Post study tours will be arranged after the Symposium.

Topics

This symposium will focus on "dam safety in a changing world", topics are as following:

- New risk factors and safety assessment
- New requirements of urbanization and economic development on reservoir flood control and operation
- The state of the art: construction and reinforcement technologies for safety

Secretariat Contact
Ms Wang Xiao
Tel: +86 10-68585310 Fax:+86 10-68712208
Email address: chincold-en@vip.126.com

11ο Συνέδριο «Ελληνική Γλώσσα και Ορολογία», 9–11 Νοεμβρίου 2017, Αθήνα, www.eleto.gr/gr/Conference11.html

PARIS 2017 AFTES International Congress "The value is Underground", 13-16 November 2017, Paris, France, www.aftes2017.com

2nd International Conference "Challenges in Geotechnical Engineering" 2017 20-23 November 2017, Kyiv, Ukraine, www.cgeconf.com/en

2nd International Symposium on Asia Urban GeoEngineering, 24-27 November 2017, Changsha, China, hwww.isaug2017.org

6 - 7 December 2017, London, UK
https://tunnelling.newcivilengineer.com

New Civil Engineer's 11th Tunnelling Summit will bring together all major stakeholders and decision-makers from major clients, designers, contractors and their supply chain. Attend this year's event to pinpoint future opportunities and explore how the next generation of tunnels will be designed, delivered and maintained.

- Explore the pipeline of projects in the UK and pinpoint tunnelling opportunities
- Hear directly from key clients and understand their project needs and what they're looking for from the supply chain
- Take home practical learnings and best practice with insight from from UK and international project case studies
- Network with over 200 leaders and decision-makers from across the tunnelling industry, all under one roof
- Benefit from extended networking time with our post-event VIP drinks and dinner
- Plus, don't forget to book your seat at the Tunnelling Awards, taking place after the seminar on 7th December, to celebrate the very best in tunnelling expertise.

DELEGATE ENQUIRIES

Ilja Ryndin
T: 020 3033 2609
E: ilja.ryndin@emap.com

Civil Engineering and Development Department
The Government of the Hong Kong Special Administrative Region

Slope Safety Summit
11 December 2017, Hong Kong, China

Organizer: Geotechnical Engineering Office, The Government of Hong Kong Special Administrative Region and Geotechnical Division, The Hong Kong Institution of Engineers

Contact Person: Tony Y K Ho
Address: 11/F Civil Engineering and Development Building, 101 Princess Margaret Road, Homantin, Hong Kong
Phone: (852) 2762 5400
Fax: (852) 2714 0275
Email: tonyykho@cedd.gov.hk

ASIA 2018 Seventh International Conference and Exhibition on Water Resources and Renewable Energy Development in Asia, 15 March 2018, Danang, Vietnam, www.hydropower-dams.com/asia-2018-conference.php?c_id=303

World Tunnel Congress 2018 "The Role of Underground Space in Future Sustainable Cities", 20-26 April 2018, Dubai, United Arab Emirates, www.wtc2018.ae

EUROCK 2018 Geomechanics and Geodynamics of Rock Masses, 22-26 May 2018, Saint Petersburg, Russia, www.eurock2018.com/en

4th GeoShanghai International Conference
May 27-30, 2018, Shanghai, China
http://geo-shanghai.org

GeoShanghai is a series of international conferences on geotechnical engineering held in Shanghai every four years. The conference was inaugurated in 2006 and was successfully held in 2010 and 2014, with more than 1200 participants in total. Since the last conference, the geotechnical communities have witnessed many advances both in fundamental understandings and engineering practices. To show the latest developments and promote collaborations in geotechnical engineering and related areas, the organizers of the GeoShanghai International Conference would like to invite you to participate in the 4th GeoShanghai International Conference to be held in Shanghai in May 2018.

Themes

- Soil behavior & geomechanics
- Unsaturated soil mechanics
- Seepage and porous mechanics
- Rock mechanics and rock engineering
- Pavement mechanics and engineering
- Geohazards
- Geosynthetics
- Geoinformatics
- Geotechnical in-situ testing & monitoring
- Environmental geotechnics
- Transportation geotechnics
- Offshore geotechnics
- Mining geotechnics
- Energy-related geotechnics
- Behavior of biotreated geomaterials and foundations
- Geomechanics at macro & micro scales
- Ground improvement
- Soil dynamics & earthquake engineering
- Landfills and contaminated soil
- Sustainability in geotechnical engineering
- Deep excavations & retaining structures
- Shafts & deep foundations
- Tunneling and underground constructions
- Pavement materials and structures
- New frontiers in geotechnology
- Case studies

Contact Us

Ming Xiao, Ph.D., P.E., Associate Professor
Department of Civil & Environmental Engineering, 231P Sackett Building, The Pennsylvania State University, University Park, PA 16802, USA
Tel: 814-867-0044

Xiaoqiang Gu, Ph.D., Assistant Professor
Department of Geotechnical Engineering, College of Civil Engineering, Tongji University
1239 Siping Road, Shanghai 200092, P.R. China
Tel: + 86(21)-6598-4551
Fax: + 86(21)-6598-5210
E-mail: geoshanghai@tongji.edu.cn

XVI Danube-European Conference on Geotechnical Engineering: Geotechnical Hazards and Risks: Experiences and Practices
7 - 9 June 2018, Skopje, Former Republic of Yugoslav
www.decge2018.mk

In the year 1964 the Danube-European Conferences on Geotechnical Engineering were founded in Vienna by Austrian Society of Engineers and Architects (ÖIAV) with its branches for Geotechnical Engineering (Member Society of ISSMGE) and Road Engineering (Member Society of PIARC). The aim of these Conferences was to bring together colleagues from East and West along Danube region, from either side of the former "Iron Curtain". The vision of ÖIAV at that time was at least a mental, cultural, economic and scientific reunification of this region. Meanwhile, this took place in a newer scope, and now the "Danube-European Conference" comprises more than 20 countries, when – for historical reasons – Russia and Turkey are also included.

As a result of MAG's progressive and continuous work, during the Danube-European Conference on Geotechnical Engineering (DECGE) held in Vienna in September 2014, it was unanimously decided to allocate the organization of the XVI DECGE in 2018 to Macedonian Association for Geotechnics.

Conference Theme

The idea for the conference theme comes from the several catastrophic events during past years, not only in the re-

gion. So, it is more than evident that risk assessment and management are required in all aspects of geotechnical issues, such as planning, design, construction, maintenance and restoration of structures. International exchange of information is of vital importance today to advance knowledge and experience in this scientific and practical field.

Papers about influence of geotechnical hazards on infrastructure, landslides, man-made slopes, earthworks, deep excavations, dams, tailings dams, slope failure repair and remediation, flood hazards, earthquakes and seismic events, bridge foundations, tunnelling, karts environments, problematic materials and environments (glacigenic materials, peat, soft soils, collapsing soils, swelling soils, weak rocks, permafrost problems, weathered materials, freezing - thawing problems etc.), selection of parameters for physical and numerical modelling, soil structure interaction, behaviour of unsaturated and saturated materials, case histories etc. are welcomed.

Topics

A Methods for hazard assessment
B Risk assessment and management in geotechnical engineering
C Parameters and modelling
D Reliability of geotechnical predictions
E Construction risk management
F Repair and maintenance strategies of geotechnical structures
G Geotechnical codes and design methods

Contact: info@decge2018.mk

16th European Conference on Earthquake Engineering (16thECEE), 18-21 June 2018, Thessaloniki, Greece, www.16ecee.org

CPT'18 4th International Symposium on Cone Penetration Testing, 21-22 June 2018, Delft, Netherlands, www.cpt18.org

NUMGE 2018 9th European Conference on Numerical Methods in Geotechnical Engineering, 25-27 June 2018, Porto, Portugal, www.numge2018.pt

RockDyn-3 - 3rd International Conference on Rock Dynamics and Applications, 25-29 June 2018, Trondheim, Norway, www.rocdyn.org

ICOLD 2018
26th Congress – 86th Annual Meeting
1 - 7 July 2018, Vienna, Austria
www.icoldaustria2018.com

On behalf of the Austrian national Committee on Large Dams, it is my great honor to invite you to the 26th ICOLD World Congress in combination with the 86th ICOLD Annual Meeting and the ATCOLD Symposium Hydro Engineering, to be held in Vienna, Austria.

The conference program will include interesting study tours to high-head pumped storage plants, run-of-river plants and excellent examples of Austrian dams at high elevation in the Alps.

The cultural program for participants and accompanying persons will comprise musical performances and excursions to some of Austria's most impressive sites.

Participants in 2018's ICOLD Congress can take advantage of the event's special location and enjoy Austria's renowned hospitality, cultural heritage and landscape. Vienna is a pleasant and safe city with outstanding conference facilities as well as comfortable international travel connections and a well-developed local transportation network.
A great number of national institutions, the dam owners and the members of ATCOLD are eager to contribute to ICOLD, supporting the Congress in Vienna. Together our aim is a productive coming together for our community based on hospitality and friendship.

We look forward to welcoming you in Vienna.

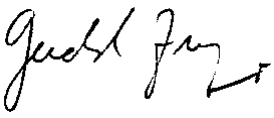

Gerald Zenz, President
Austrian National Committee on Large Dams

The questions for the Congress are the following:

- Q100 - Reservoir sedimentation and sustainable development
- Q101 - Safety and risk analysis
- Q102 - Geology and dams
- Q103 - Small dams and levees

Hydro Engineering Symposium

Symposium Topics

1. **Climate Changes Reservoir Operation**
   (Catchment, permafrost, glacier melting, erosion and sedimentation)

2. **Permission and safety assessment**
   (Construction and operation of hydraulic structures, inspection & assessment of operating devices)

3. **Dam and foundation sealing**
   (Long term behaviour and assessment of uplift distribution)

4. **Caverns and power water ways**
   (Design, construction and monitoring, power water way and lining with high strength steel)

5. **Stability of reservoir slopes**
   (Reservoir operation, avalanches, impulse waves, dam breach)

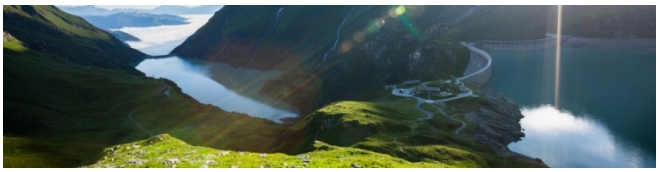

Contact

Renate Androsch-Holzer
organization@icoldaustria2018.com
Tel: +41 1 489 64 09 12

Claudia Lojer
registration@icoldaustria2018.com
Tel: + 43 1 489 64 09 16

GeoChine 2018 - 5th GeoChina International Conference Civil Infrastructures Confronting Severe Weathers and Climate Changes: From Failure to Sustainability, July 23-25, , HangZhou, China, http://geochina2018.geoconf.org

UNSAT2018 The 7th International Conference on Unsaturated Soils, 3 - 5 August 2018, Hong Kong, China, www.unsat2018.org

6th International Conference on
Industrial & Hazardous Waste Management
4-7 September 2018, Chania, Crete, Greece
www.hwm-conferences.tuc.gr

Dear Colleagues,

It's a great honour and pleasure for me to announce the conduction of the 6th International Conference of the CRETE series on Industrial and Hazardous Waste Management on 4th - 7th of September 2018 at Chania.

CRETE 2018 will be special, as it marks the 10th anniversary of the conduction of this unique IWWG conference, that is co – organized by the Technical University of Crete, the University of Padua and the Technical University of Hamburg.

CRETE 2018 conference topics have been enriched, in order to allow broader study of the numerous industrial and hazardous waste management aspects, but also more special focus on hot issues.

More interesting and new ideas are being explored by our Organizing Committee, promising an even more remarkable and sucessfull Conference, always under the condition of your valuable contribution and presence.

Attached you may find our 1st flyer, with relevant information, that can be printed and placed on your desks, in the form of a three-fold triangle, as a kind reminder of CRETE 2018.

Our official website (www.hwm-conferences.tuc.gr) is under preparation and will be soon ready to provide more information.

I am looking forward to co-operate with you all, for this special upcoming conference and welcome you once again at our beautiful island.

Best regards,

Prof. Evangelos GIDARAKOS
Conference Chairman

CRETE 2018 Conference Secretariat
Technical University of Crete
School of Environmental Engineering
University Campus, 73100, Chania
Crete, GREECE
Tel. +30 28210 37736 (or +30 28210 37790)
Fax. + 30 28210 37850
E-mail: hwm.conferences@enveng.tuc.gr

SAHC 2018 11th International Conference on Structural Analysis of Historical Constructions "An interdisciplinary approach", 11-13 September 2018, Cusco, Perύ http://sahc2018.com

11th International Conference on Geosynthetics (11ICG), 16 - 20 Sep 2018, Seoul, South Korea, www.11icg-seoul.org

CHALK 2018 Engineering in Chalk 2018, 17-18 September 2018, London, U.K., www.chalk2018.org

ARMS10 - 10th Asian Rock Mechanics Symposium, ISRM Regional Symposium, 29 October - 3 November 2018, Singapore, www.arms10.org

16th World Conference of Associated research Centers for the Urban Underground Space
"Integrated Underground Solutions for Compact Metropolitan Cities"
5 – 7 November 2018, Hong Kong, China
www.acuus2018.hk

The conference will invite globally recognized speakers and world authorities in Urban Underground Space to share their experiences and knowledge with planners, architects and engineers in the region. It is intended to hold keynote presentations to showcase latest thinking and approach in integrated compact city urban design.

Parallel sessions to suit various interests will be organized to further present the state of the art in those related and key underground space disciplines. Discussion and debate will be sought to analyse and assess topical key issues related to urban underground design and implementation.

The conference will seek high quality papers that can provide insight, rigour and useful practical examples of integrated underground solutions for compact metropolitan cities.

Topics

- Integrated Planning
- Architecture and Design
- Underground Infrastructure
- Sustainability and Environment
- Safety and Human Factors
- Economics and Legal
- Technical Approach and Innovation

Contact

ACUUS 2018 Secretariat
c/o International Conference Consultants Limited
Office address: Unit C-D, 17/F, Max Share Centre, 373 King's Road, North Point, Hong Kong
Tel: (852) 2559 9973
Fax: (852) 2547 9528
General enquiry: enquiry@acuus2018.hk
Registration: reg@acuus2018.hk
Abstracts: abstract@acuus2018.hk
Sponsorship and exhibition: sponsor@acuus2018.hk

WTC2019 Tunnels and Underground Cities: Engineering and Innovation meet Archaeology, Architecture and Art and ITA - AITES General Assembly and World Tunnel Congress, 3-9 May 2019, Naples, Italy, www.wtc2019.com

7 ICEGE 2019

International Conference on Earthquake Geotechnical Engineering
17 - 20 June 2019, Rome, Italy

Organizer: TC203 and AGI (Italian Geotechnical Society)
Contact person: Susanna Antonielli
Address: AGI - Viale dell' Università 11, 00185, Roma, Italy
Phone: +39 06 4465569
Fax: +39 06 44361035
E-mail: agi@associazionegeotecnica.it

ISDCG 2019

7th International Symposium on Deformation Characteristics of Geomaterials
26 - 28 June 2019, Glasgow, Scotland, UK,

The Technical Committee 101 of the ISSMEG is pleased to announce the organisation of the 7th International Symposium on Deformation Characteristics of Geomaterials (ISDCG) in 2019, in Glasgow, UK. The symposium is co-organised by the University of Strathclyde in Glasgow, the University of Bristol, and the Imperial College in London.

Building on the success of the previous Symposia organised in Sapporo (Japan) Japan in 1994, Torino (Italy) in 1999, Lyon (France) in 2003, Atlanta (US) in 2008, Seoul (Korea) in 2011 and Buenos Aires (Argentina) in 2015, the 7th ISDCG will equally follow both its traditions and active promotion of new technical elements to maintain it as one of the most popular and vibrant events within the geotechnical community. The technical core themes will focus on: (i) advanced laboratory geotechnical testing; (ii) application of advanced laboratory testing in research, site characterisation, and ground modelling; (iii) application of advanced testing to practical geotechnical engineering. In addition to these traditional topics, sub-themes will include cutting-edge techniques and approaches, for example experimental micro-mechanics, non-invasive monitoring systems, nano and micro-sensors, new sensing technologies. A key goal is to engage with the full spectrum of geotechnical specialists, from early career engineers and researchers through to world leading experts.

The 17th European Conference on Soil Mechanics and Geotechnical Engineering
1st - 6th September 2019, Reykjavik Iceland
www.ecsmge-2019.com

The theme of the conference embraces all aspects of geotechnical engineering. Geotechnical engineering is the foundation of current as well as future societies, which both rely on complex civil engineering infrastructures, and call for mitigation of potential geodangers posing threat to these. Geotechnical means and solutions are required to ensure infrastructure safety and sustainable development. Those means are rooted in past experiences enhanced by research and technology of today.

At great events such as the European Geotechnical Conference we should: Spread our knowledge and experience to our colleagues; Introduce innovations, research and development of techniques and equipment; Report on successful geotechnical constructions and application of geotechnical design methods, as well as, on mitigation and assessment of geohazards and more.

Such events also provide an opportunity to draw the attention of others outside the field of geotechnical engineering to the importance of what we are doing, particularly to those who, directly or indirectly, rely on our services, knowledge and experience. Investment in quality geotechnical work is required for successful and safe design, construction and operation of any infrastructure. Geotechnical engineering is the key to a safe and sustainable infrastructure and of importance for the society, economy and the environment. This must be emphasized and reported upon.

14th ISRM International Congress
13-18 September 2019, Iguassu Falls, Brazil
www.isrm2019.com

Dear fellow rock engineer

2019 will be a special year for the ISRM South America National Groups when the region welcomes the ISRM family for its 14th Congress. Brazil, Argentina and Paraguay will be the host countries for the event that is to be held in Foz do Iguassu, city that marks the common border amongst these countries. It is an honor to organize such a venue but it is also a great responsibility to maintain the tradition of memorable ISRM congresses.

The central theme of the Congress is Rock Mechanics for Natural Resources and Infrastructure Development, a theme much relevant and needed for the current stage of most of the countries. All ISRM regions are invited to share their experience in the theme. The technical programme is being established by an International Scientific Committee in order to attract different categories of geotechnical professionals as academics, consultants, contractors, public companies and should incorporate issues of ISRM Technical Commissions.

On behalf of the Brazilian Rock Mechanics Committee, Argentinian Society of Geotechnical Engineering and Paraguayan Society of Geotechnics it is a great pleasure to announce the preparation for the 2019 ISRM International Congress and also to invite you to start getting ready to come and join us in Foz do Iguassu.

Sergio Fontoura (General Chair)
Ricardo Jose Rocca (Co-chair)
José Pavón Mendoza (Co-Chair)

Preliminary Scientific Topics

- Blasting and rockbursts
- Case histories in rock engineering
- Characterization of faults and other geological features
- Characterization of intact rocks and rock masses
- CO2 sequestration
- Constitutive models in prediction of rock behavior
- Containment and support structures
- Coupled processes in rock mechanics
- Crustal stress and earthquakes
- Dams and foundations in rocks
- Design of underground and open pit mines
- Dynamic phenomena in rock mechanics
- Education in rock engineering
- Exploration and production of geothermal energy
- Fluid flow and pore pressure in rocks
- Fracture and damage of rocks
- Geophysics and geology related to rock mechanics
- Hazard and risk assessment in rock engineering
- Hydraulic fracturing
- In situ stress measurements and estimation
- Instrumentation and monitoring
- Laboratory and field testing and measurements
- Mechanics of hard rocks
- Mechanics of soft rocks
- Natural and ancient stones preservation
- Numerical and analytical modeling of rock phenomena
- Ornamental rocks
- Petroleum reservoir and well geomechanics
- Rock heterogeneity and multiscale approaches
- Rock mechanics data
- Rock tunneling
- Seismic behavior of rock masses
- Slope stability and landslides
- Underground Nuclear Power Plants
- Underground Research Laboratories URL
- Underground storage and radioactive waste disposal

Contact us

Organization and Sale
MCI São Paulo
Rua George Ohm, 230 – Torre A, 19º Andar
04576-020 - São Paulo - SP
Phone / Fax: 55 11 3056-6000
atendimento@mci-group.com

General Chair
isrm.2019@puc-rio.br

XVI Asian Regional Conference on Soil Mechanics and Geotechnical Engineering
21 - 25 October 2019, Taipei, China
www.16arc.org

Dear Colleagues,

It is my great happiness to inform you that ***The 16th Asian Regional Conference on Soil Mechanics and Geotechnical Engineering (16ARC)*** will be held on ***October 14-18 in 2019*** in ***Taipei International Convention Center (TICC)***, Taipei, Taiwan. The main theme of the 16ARC is **Geotechnique for Sustainable Development and Emerging Market Regions**. A number of subjects on modern geotechnical technologies and activities will be covered up to match up the main theme. In a roll of 60 years, we sincerely hope that the 16ARC will continue to bring great success following the glories of past ARCs (New Delhi 1960, Tokyo 1963, Haifa 1967, Bangkok 1971, Banglore 1975, Singapore 1979, Haifa 1983, Kyoto 1987, Bangkok 1991, Beijing 1995, Seoul 1999, Singapore 2003, Kolkata 2007, Hong Kong 2011, Fukuoka 2015).

As the President of Chinese Taipei Geotechnical Society (CTGS), the host of 16ARC and the Chairman of the Organizing Committee, I cordially welcome your participations and kind supports at this coming event in 2019. To provide you with more information of 16ARC, besides the conference's website (www.16arc.org), two Bulletin will be disseminated before the collections of technical papers. The 1st Bulletin will be issued in December 2016 with general information of the conference. The 2nd Bulletin will be issued in July 2017 with the announcements of call-for-paper mainly through Asian member societies of ISSMGE and invitations on ATC/TC Sessions. As to the technical programs, social events, and other available information of the conference, please visit conference website, we will keep it updated as the time to come.

Taiwan, the hosting country, locates in the geographical center of East Asia. With frequent flights, it is conveniently reached from most of the Asian cities. During the conference, all the guests can experience some of the finest Chinese cuisine, bustling nightlife (24-hour convenient stores, Internet cafes, restaurants, bars and night markets), efficient transportation that brings visitors exploring the beauty of nature within a short time. Taiwan is one of the safest country to visit. Taiwanese are friendly, kind-hearted and helpful. Taiwanese are always ready to welcome you with great hospitality. In the end, with our open arms and warmest regards, it would be our pleasure to welcome you to experience this great event and enjoy the dynamics of Taiwan.

Chang-Yu Ou, Ph.D.
Chairman, Organizing Committee of 16ARC
President of Chinese Taipei Geotechnical Society

Topics

1. Soil characteristics and properties
2. Underground and deep excavations
3. Tunneling
4. Slope, debris flow and embankment
5. Dam
6. Shallow and deep foundation
7. Soil dynamics and geotechnica earthquake engineering
8. Soil improvement
9. Geoenvironmental engineering
10. Geotechnical reliability, risk assessment and management
11. Geosynthetics and geo-products
12. Engineering geology and rock engineering
13. Forensic engineering
14. Offshore and harbor geotechnics
15. Geotechnical training and education
16. In-situ testing and monitoring
17. GeoEnergy
18. Case history

Key Contacts

16ARC Congress Secretariat c/o Elite Professional Conference Organizer
General Issue
Email: secretariat@16arc.org

XVI Panamerican Conference on Soil Mechanics and Geotechnical Engineering
18-22 November 2019, Cancun, Quintana Roo, Mexico
http://panamerican2019mexico.com/panamerican

The first Pan-American Congress of Soil Mechanics and Geotechnical Engineering was held in Mexico in 1959. In November 2019 it will return to our country; with the Mexican Caribbean as its headquarters. Cancun is recognized worldwide for its natural beauty, first class tourist infrastructure and important and attractive archaeological sites.

On this occasion, the 5th International Deep Foundations Symposium will be held in parallel with the joint collaboration of the Geo Institute (ASCE) and the Deep Foundations Institute (DFI). It is worth mentioning that, within the activities, more than 10 technical sessions are planned with the participation of specialists from all over America and the rest of the world, as well as pre-congress courses of great interest to professional practice and the Arthur Casagrande Conference.

On the part of the Organizers, we extend a friendly invitation to the international engineering community, in order to establish the problems, challenges and solutions facing this engineering sector.

Technical program

- Topic1. Laboratory and in situ testing
- Topic 2. Analytical and physical modelling in geotechnics
- Topic 3. Numerical modelling in geotechnics
- Topic 4. Unsaturated soils
- Topic 5 Soft soils.
- Topic 6. Foundations and retaining structures
- Topic 7. Excavations and tunnels

- Topic 8. Offshore Geotechnics
- Topic 9. Transportation in geotechnics
- Topic 10. Natural hazards
- Topic 11. Embankments and tailings dams
- Topic 12. Soils dynamics and earthquake engineering
- Topic 13. Ground improvement
- Topic 14. Sustainability, energy and geoenvironment.
- Topic 15. Preservation of historic sites
- Topic 16. Forensics engineering
- Topic 17. Rock mechanics
- Topic 18. Education

Contact Info

IBEROSTAR Cancún
Blvd. Kukulkan Km 17, Zona Hotelera,
77500 Cancún, QROO
Tel (+(52) 1 55 5677-3730, +(52) 1 55 5679-3676
Iberostar: 01 800 849 1047
info@panamerican2019mexico.com
chat@panamerican2019mexico.com

Nordic Geotechnical Meeting
27-29 May 2020, Helsinki, Finland

Contact person: Prof. Leena Korkiala-Tanttu
Address: SGY-Finnish Geotechnical Society,
Phone: +358-(0)50 312 4775
Email: leena.korkiala-tanttu@aalto.fi

ΕΝΔΙΑΦΕΡΟΝΤΑ ΓΕΩΤΕΧΝΙΚΑ ΝΕΑ

Brexit 1.0: Scientists find evidence of Britain's separation from Europe

Researchers have found evidence of how ancient Britain separated from Europe, which happened in two stages, they report in Nature Communications.

Nearly 450,000 years ago, when Earth was in the grip of an ice age, ice stretched right across the North Sea, from Britain to Scandinavia. The low sea levels meant that the entire English Channel was dry land, a frozen tundra landscape, crisscrossed by small rivers.

Based on the evidence that we've seen, we believe the Dover Strait 450,000 years ago would have been a huge rock ridge made of chalk joining Britain to France, looking more like the frozen tundra in Siberia than the green environment we know today.

Dr Jenny Collier
Department of Earth Science and Engineering
Imperial College

This illustration captures what the land bridge between France and Britain may have looked like.

Britain's separation from mainland Europe is believed to be the result of spill over from a proglacial lake - a type of lake formed in front of an ice sheet - in the North Sea, but this has remained unproven. Now, researchers from Imperial College London and their colleagues from institutes in Europe show that the opening of the Dover Strait in the English Channel occurred in two episodes, where an initial lake spill over was followed by catastrophic flooding.

Ten years ago, the researchers from Imperial College London revealed geophysical evidence of giant valleys on the seafloor in the central part of English Channel. They believed these valley networks were evidence of a megaflood gouging out the land, which they speculated may have been caused by a catastrophic breach in a chalk rock ridge joining Britain to France.

The new study by the team, working with their colleagues in Europe, now shows for the first time the details of how this chalk ridge in the Dover Strait, between Dover and Calais, was breached. New geophysical data collected by colleagues from Belgium and France has been combined with seafloor data from the UK showing evidence of huge holes and a valley system located on the seafloor.

Without this dramatic breaching Britain would still be a part of Europe. This is Brexit 1.0 – the Brexit nobody voted for

Professor Sanjeev Gupta
Department of Earth Science and Engineering
Imperial College

The team show that the chalk ridge acted like a huge dam and behind it was a proglacial lake. This lake was first hypothesised by scientists more than 100 years ago and the authors of today's study show how the lake overflowed in giant waterfalls, eroding the rock escarpment, weakening it and eventually causing it to fail and release huge volumes of water onto the valley floor below.

The team believe that the huge holes that they analysed on the seafloor are plunge pools, created when water cascading over an escarpment hit the ground and eroded rock. The plunge pools in the Dover Strait are huge – up to several kilometres in diameter and around 100 metres deep and were drilled into solid rock. Around seven plunge pools run in a line from the ports of Calais to Dover. The researchers suggest these plunge pools are evidence of an overflow of water from the lake in the southern North Sea.

The straight line of the plunge pools suggests they were cascading off one single rock ridge perhaps 32 kilometres long and 100 metres high– the land bridge between Europe and the UK.

The researchers have also found evidence that a second event fully opened the Dover Strait. Later on, perhaps hundreds of thousands of years later, a new valley system, the Lobourg Channel, was carved by megaflood processes that crossed the Dover Strait. The researchers demonstrate that this valley system is connected to the giant valley network in the central English Channel. They suggest that a spill over of other, smaller lakes in front of the ice sheets in the North Sea may have been responsible for the later episode of flood erosion.

Putting the puzzle together

It has taken ten years, but by pulling all the pieces of the geological jigsaw puzzle together the team say they are more confident about what may have caused the megaflood in the English Channel thousands of years ago.

Dr Collier

Dr Jenny Collier, a co-author of the study from the Department of Earth Science and Engineering at Imperial College London, said: "Based on the evidence that we've seen, we believe the Dover Strait 450,000 years ago would have been a huge rock ridge made of chalk joining Britain to France, looking more like the frozen tundra in Siberia than the green environment we know today. It would have been a cold world dotted with waterfalls plunging over the iconic

white chalk escarpment that we see today in the White Cliffs of Dover.

"We still don't know for sure why the proglacial lake spilt over. Perhaps part of the ice sheet broke off, collapsing into the lake, causing a surge that carved a path for the water to cascade off the chalk ridge. In terms of the catastrophic failure of the ridge, maybe an earth tremor, which is still characteristic of this region today, further weakened the ridge. This may have caused the chalk ridge to collapse, releasing the megaflood that we have found evidence for in our studies."

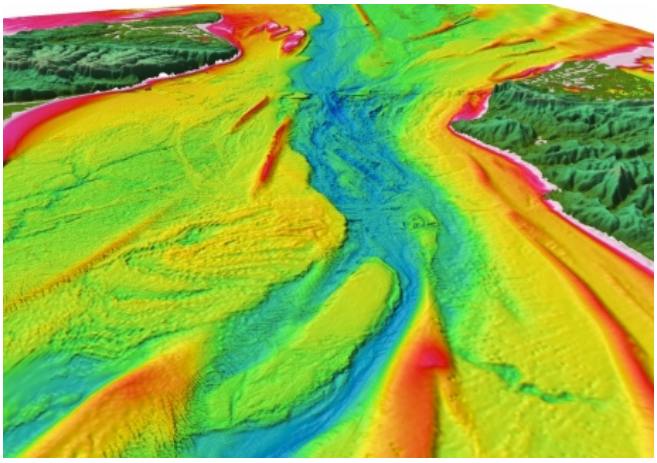

The Dover Strait seafloor image shows signs of huge megafloods (blue), which scoured the Ice Age environment

Engineers first found evidence of the plunge pools when they were carrying out geological surveys of the Dover Strait seafloor back in the 1960s. No one knew what caused them, but they were called the Fosse Dangeard. The loose gravel and sand infilling these plunge pools meant that the engineers had to move the route of the Channel Tunnel to avoid them. In 1985 a marine geologist named Professor Alec Smith, from Bedford College in London, first proposed that the holes were created by ancient waterfalls, but the lack of hard evidence meant that the assertions were largely forgotten. Now, the authors of today's study say Smith's original assertions were right.

The scientists say if it wasn't for a set of chance geological circumstances, Britain may have still remained connected to mainland Europe, jutting out into the sea similarly to Denmark.

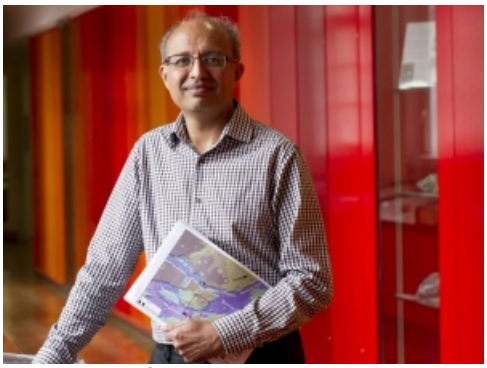

Professor Sanjeev Gupta

Professor Sanjeev Gupta, a co-author from the Department of Earth Science and Engineering at Imperial, added: "The breaching of this land bridge between Dover and Calais was undeniably one of the most important events in British history, helping to shape our island nation's identity even today. When the ice age ended and sea levels rose, flooding the valley floor for good, Britain lost its physical connection to the mainland. Without this dramatic breaching Britain would still be a part of Europe. This is Brexit 1.0 – the Brexit nobody voted for."

The team still do not have an exact timeline of events. In the next step, the researchers would like to take core samples of the in-filled sediments in the plunge pools, which they will analyse to determine the timing of erosion and infill of the plunge pools, the environments represented by these sediments, and the source of the sediments. Developing a timeline of events would enable them to learn more about the distinctive evolution of Britain, compared to mainland Europe. However, this will be a real challenge for the team as getting sediment core samples in the Dover Strait means dealing with huge tidal changes and traversing the world's busiest shipping lane.

The study was carried out in conjunction with researchers from Royal Observatory Belgium; Ghent University, Belgium; CNRS, the University of Lille, and the University of Western Britanny in France; and Top-Hole Studies Ltd, UK.

(Colin Smith / Imperial College News, 04 April 2017, http://www3.imperial.ac.uk/newsandeventspggrp/imperialcollege/newssummary/news_31-3-2017-12-15-59?utm_source=alumni-bulletin&utm_medium=email&utm_campaign=alumniebulletin)

Το πρώτο Brexit: Όταν η Βρετανία έγινε νησί Σαρωτική πλημμύρα

Ένας γιγάντιος καταρράκτης φαίνεται πως γκρέμισε τη γέφυρα ξηράς και έσκαψε το βυθό της Μάγχης (Πηγή: Chase Stone / Imperial College London)

Μέχρι πριν από μισό εκατομμύριο χρόνια, η Βρετανία ήταν ενωμένη με την ηπειρωτική Ευρώπη με μια λωρίδα ξηράς που εκτεινόταν μέχρι τη Γαλλία. Όταν άλλαξε όταν μια γιγάντια λίμνη ξεχείλισε, δημιούργησε έναν τεράστιο καταρράκτη και έσκαψε το κανάλι της Μάγχης. Ήταν η πρώτη φορά που η Βρετανία έγινε νησί.

Τα απομεινάρια αυτής της λωρίδας ξηράς διακρίνονται ακόμα και σήμερα στους εντυπωσιακούς άσπρους γκρεμούς του Ντόβερ στις ακτές της Βρετανίας και του Καλέ απέναντι στη Γαλλία. Το ίδιο ασβεστολιθικό πέτρωμα ένωνε κάποτε τις δύο χώρες.

Η εξαφάνιση αυτής της λωρίδας «η Βρετανία θα ήταν ακόμα μέρος της Ευρώπης. Ήταν το Brexit 1.0, το Brexit για το οποίο δεν ψήφισε κανείς» σχολιάζει Sanjeev Gupta του Imperial College στο Λονδίνο, πρώτος συγγραφέας της δη-

μοσίευσης στο Nature Communications (http://www.nature.com/articles/ncomms15101).

Οι περίφημοι λευκοί βράχοι του Ντόβερ είναι απομεινάρι μιας γέφυρας ξηράς που ένωνε τη Βρετανία με τη Γαλλία μέχρι πριν από 450.000 χρόνια (Πηγή: Immanuel Giel / CC BY-SA 3.0)

Η αρχή του διαζυγίου ήρθε πριν από 450.000 χρόνια, όταν η Γη βρισκόταν στη μέση μιας εποχής των παγετώνων, και μια γιγάντια πλάκα πάγου κάλυπτε την Ευρώπη από τη Σκανδιναβία μέχρι τη Βρετανία. Οι πάγοι στην ξηρά διατηρούσαν αποθηκευμένες τόσο μεγάλες ποσότητες νερού ώστε η στάθμη της θάλασσας βρισκόταν 120 μέτρα πιο χαμηλά από ό,τι σήμερα.

Με τη στάθμη τόσο χαμηλά, η περιοχή στην οποία βρίσκεται σήμερα η θάλασσα της Μάγχης ήταν ξηρά -μια τούνδρα που πρέπει να θύμιζε τη σημερινή Σιβηρία. Μαμούθ, ιπποπόταμοι και Νεάντερταλ μπορούσαν να μετακινούνται ελεύθερα προς βορρά και νότο.

Η κατάσταση άλλαξε δραματικά και απότομα λόγω μιας τεράστιας λίμνης που είχε σχηματιστεί στη μέση του πάγου στην περιοχή της Βόρειας Θάλασσας. Τροφοδοτούμενη από ποτάμια, η λίμνη φούσκωνε και φούσκωνε μέχρι που υπερχείλισε και άρχισε να αδειάζει το νερό της πάνω από τη λωρίδα ξηράς που ένωνε το Ντόβερ και το Καλέ.

Οι καταρράκτες που σχηματίστηκαν πρέπει να ήταν ασύλληπτο θέαμα, καθώς είχαν πλάτος γύρω στα 30 χιλιόμετρα και ύψος 50 με 100 μέτρα. Η ροή του νερού ήταν τόσο μεγάλη που κατεδάφισε τη λωρίδα ξηράς και έσκαψε βαθιά την κοιλάδα όπου βρίσκεται σήμερα η Μάγχη.

Όταν η στάθμη της θάλασσας ανέβηκε με το τέλος της εποχής των παγετώνων, το κανάλι της Μάγχης πλημμύρισε και η Βρετανία έμεινε απομονωμένη ως νησί.

Η θεωρία της μεγάλης πλημμύρας είχε διατυπωθεί για πρώτη φορά το 1985 από τον γεωλόγο Άλεκ Σμιθ, ο οποίος απεβίωσε το 2015 χωρίς να έχει πείσει τους συναδέλφους του.

Η νέα μελέτη βασίστηκε σε γεωλογικές μετρήσεις γιγάντιων λάκκων που βρέθηκαν στο βυθό της Μάγχης τις δεκαετίες του 1960 και 1970, όταν ξεκίνησαν οι μελέτες για την κατασκευή της Σήραγγας της Μάγχης.

Οι λάκκοι αυτοί, γεμάτοι με βράχια και ιζήματα, βρίσκονται ακριβώς δίπλα στην εξαφανισμένη λωρίδα ξηράς, και σύμφωνα με τους ερευνητές σχηματίστηκαν από τα νερά του καταρράκτη που έσκαψαν το βυθό.

Η Βρετανία παρέμεινε νησί για δεκάδες χιλιάδες χρόνια, ξαναενώθηκε όμως με την Ευρώπη σε μεταγενέστερες φάσεις, όταν η Γη πέρασε σε νέες παγετώδεις περιόδους που έκαναν το βυθό της Μάγχης να αναδυθεί.

Η τελευταία φορά που η Βρετανία ξανάγινε νησί ήταν πριν από 9.000 χρόνια.

Και τώρα που η Βρετανία ετοιμάζεται να οριστικοποιήσει το διαζύγιο με την Ευρωπαϊκή Ένωση, η γεωλογική απομόνωση γίνεται και πολιτική.

(Βαγγέλης Πρατικάκης / Newsroom ΔΟΛ, 05 Απρ. 2017, http://news.in.gr/science-technology/article/?aid=1500137808)

Technology to improve rockfall analysis on cliffs could save money, lives

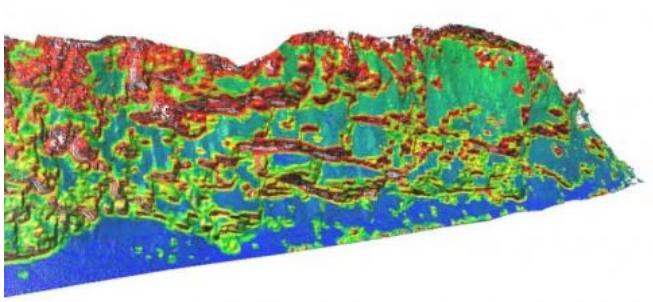

This LiDAR image of a rock slope on Alaska's Glenn Highway show the "kinetic energy" of the slope, with red indicating a higher hazard from rockfalls. *Credit: Image by Matt O'Banion, courtesy of Oregon State University*

Researchers in the Pacific Northwest have developed a new, automated technology to analyze the potential for rockfalls from cliffs onto roads and areas below, which should speed and improve this type of risk evaluation, help protect public safety and ultimately save money and lives.

Called a "rockfall activity index," the system is based on the powerful abilities of light detection and ranging, or LIDAR technology. It should expedite and add precision to what's now a somewhat subjective, time-consuming process to determine just how dangerous a cliff is to the people, vehicles, roads or structures below it.

This is a multi-million dollar global problem, experts say, of significant concern to transportation planners.

It's a particular concern in the Pacific Northwest with its many mountain ranges, heavy precipitation, erosion of steep cliffs and unstable slopes, and thousands of roads that thread their way through that terrain. The evaluation system now most widely used around the world, in fact, was developed by the Oregon Department of Transportation more than 25 years ago.

The new technology should improve on that approach, according to scientists who developed it from the University of Washington, Oregon State University and the University of Alaska Fairbanks. Findings on it were just published in *Engineering Geology*.

"Rockfalls are a huge road maintenance issue," said Michael Olsen, an associate professor of geomatics in the College of Engineering at Oregon State University, and co-author of the report.

"Pacific Northwest and Alaskan highways, in particular, are facing serious concerns for these hazards. A lot of our highways in mountainous regions were built in the 1950s and 60s, and the cliffs above them have been facing decades of

erosion that in many places cause at least small rockfalls almost daily. At the same time traffic is getting heavier, along with increasing danger to the public and even people who monitor the problem."

The new approach could replace the need to personally analyze small portions of a cliff at a time, looking for cracks and hazards, with analysts sometimes even rappelling down it to assess risks. LIDAR analysis can map large areas in a short period, and allow data to be analyzed by a computer.

"Transportation agencies and infrastructure providers are increasingly seeking ways to improve the reliability and safety of their systems, while at the same time reducing costs," said Joe Wartman, associate professor of civil and environmental engineering at the University of Washington, and corresponding author of the study.

"As a low-cost, high-resolution landslide hazard assessment system, our rockfall activity index methodology makes a significant step toward improving both protection and efficiency."

The study, based on some examples in southern Alaska, showed the new system could evaluate rockfalls in ways that very closely matched the dangers actually experienced. It produces data on the "energy release" to be expected from a given cliff, per year, that can be used to identify the cliffs and roads at highest risk and prioritize available mitigation budgets to most cost-effectively protect public safety.

"This should improve and speed assessments, reduce the risks to people doing them, and hopefully identify the most serious problems before we have a catastrophic failure," Olsen said.

The technology is now complete and ready for use, researchers said, although they are continuing to develop its potential, possibly with the use of flying drones to expand the data that can be obtained.

Tens of millions of dollars are spent each year in the U.S. on rock slope maintenance and mitigation.

Journal Reference:

Lisa Dunham, Joseph Wartman, Michael J. Olsen, Matthew O'Banion, Keith Cunningham. **Rockfall Activity Index (RAI): A lidar-derived, morphology-based method for hazard assessment**. *Engineering Geology*, 2017; 221: 184 DOI: 10.1016/j.enggeo.2017.03.009

(ScienceDaily, April 12, 2017, https://www.sciencedaily.com/releases/2017/04/170412105904.htm)

Rockfall Activity Index (RAI): A lidar-derived, morphology-based method for hazard assessment

Abstract

In this paper, we introduce the Rockfall Activity Index (RAI), a point cloud-derived, high-resolution, morphology-based approach for assessing rockfall hazards. With the RAI methodology, rockfall hazards are evaluated in a two-step procedure. First, morphological indices (local slope and roughness) are used to classify mass wasting processes acting on a rock-slope. These classifications are then used with estimated instability rates to map rockfall activity across an entire slope face. The rockfall hazard is quantified as the estimated annual kinetic energy produced by rockfall along 1-m length segments of a slope face. Field assessment of the RAI method at multiple study sites indicates that the morphology-derived classification and hazard assessment routines provide results that closely match the observed behavior and performance of rock slopes.

http://doi.org/10.1016/j.enggeo.2017.03.009

http://www.sciencedirect.com/science/article/pii/S0013795216305671

NEC Successfully Trials Landslide Prediction System in Thailand

Japan-Thailand cooperation project on disaster prevention ICT

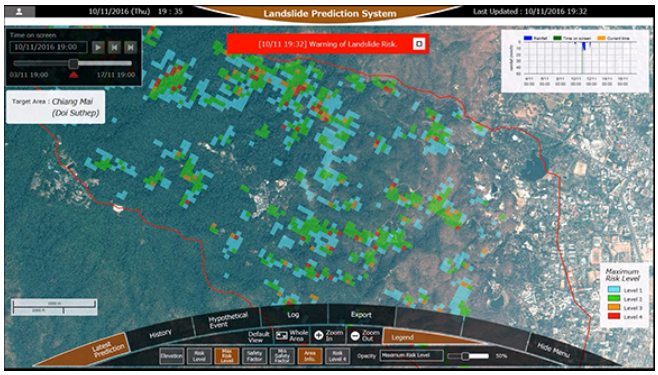

NEC Landslide Simulation System

NEC Corporation (NEC; TSE: 6701), in collaboration with Thailand's National Disaster Warning Center (NDWC), announced today the completion of a trial for a system that identifies areas where there is danger of a landslide occurring. The effectiveness of the system was confirmed as the trial was conducted in Chiang Mai Province in Northern Thailand during the period from November 2016 to March 2017.

Landslides caused by heavy rainfall are frequent in Thailand, and they result in personal injury and damage to property as well as affecting transportation by destruction of roads. For those reasons, measures for reducing such damage are urgently needed.

In April 2015, Japan's Ministry of Internal Affairs and Communications and Thailand's Ministry of Information and Communication Technology (*1) issued a joint statement announcing that the two countries would cooperate in a wide range of areas, including the development of more sophisticated disaster prevention ICT and the use and application of the technologies. As a country that experiences frequent natural disasters, Japan is expected to contribute to disaster prevention in Thailand through provision of its advanced technologies.

This trial supports the disaster prevention cooperation project between Thailand and Japan. NEC conducted this trial in collaboration with the Embassy of Japan in Thailand as part of the "Research and study for the development of a landslide simulator in Thailand" project commissioned by Japan's Ministry of Internal Affairs and Communications.

NEC joined NDWC (*2) in conducting verification experiments with a flooding simulation system in Uttaradit Province in Northern Thailand between November 2015 and March 2016 (*3). The trial reported here is a follow-up to that work.

The landslide prediction system is one of the modules of NEC's "integrated risk management system." The integrated risk management system consists of a shared platform that has functions such as data integration, visualization, and early warning, and disaster modules specialized for particular disasters such as landslides, flooding, and earthquakes. The disaster modules or functions can be selected individually as required, or several disaster modules can be combined in order to predict multiple disasters simultaneously.

The landslide prediction system performs a simulation based on meteorological data (observed rainfall and forecast rainfall), topographical data (elevation values, land use purposes), and soil data (soil depth, hydraulic conductivity, porosity, cohesion force, internal friction angle, etc.), making it possible to predict the degree of landslide danger.

Further, the system can perform detailed simulations using a 50-m quadrilateral mesh and provide hourly-basis prediction for a period of up to seven days in advance. This allows NDWC to issue warnings to threatened areas before the landslides occur, helping to reduce potential damage. Moreover, even during periods when no disaster is forecast, areas at risk of landslides can be identified by performing simulations using previous rainfall data, which enables hazard maps to be prepared.

"We were able to construct the NEC landslide simulation system in cooperation with various Thai government organizations. The system is optimized for Thailand and is expected to have a role in the operations of the Department of Disaster Prevention and Mitigation and the NDWC," said RADM Thavorn Charoendee, Executive Expert, National Disaster Warning Center. "With the ongoing cooperation of Japan, the Thai government will continue to expand the simulation area."

"NEC will continue to contribute to the development of more sophisticated disaster prevention ICT and the use and application of the technology for preventing disasters in Thailand, such as landslides and flooding," said Minoru Hirata, General Manager, Smart Infrastructure Division, NEC Corporation. "Further, we will harness the experience and knowhow gained through this trial to actively promote the system to other countries in Asia that experience frequent damage from landslides."

***

- *1Currently, the Ministry of Digital Economy and Society, following reorganization.

- *2Affiliated with the Ministry of Information and Communication Technology up to September, 2016, and subsequently affiliated with the Department of Disaster Prevention and Mitigation of the Ministry of Interior.

- *3NEC Successfully Trials Flood Simulation System in Thailand http://www.nec.com/en/press/201605/global_20160523_01.html

About NEC Corporation

NEC Corporation is a leader in the integration of IT and network technologies that benefit businesses and people around the world. By providing a combination of products and solutions that cross utilize the company's experience and global resources, NEC's advanced technologies meet the complex and ever-changing needs of its customers. NEC brings more than 100 years of expertise in technological innovation to empower people, businesses and society. For more information, visit NEC at http://www.nec.com.

The NEC Group globally provides "Solutions for Society" that promote the safety, security, efficiency and equality of society. Under the company's corporate message of "Orchestrating a brighter world," NEC aims to help solve a wide range of challenging issues and to create new social value for the changing world of tomorrow. For more information, please visit http://www.nec.com/en/global/about/vision/message.html

(NEC Corporation, April 25, 2017, http://www.nec.com/en/press/201704/global_20170425_01.html)

On the Inside The Leaning Tower of Pisa

The Pisa Tower construction started in August 1173. The tower's tilt, began during construction, and was caused by an inadequate foundation on ground too soft to properly support the structure's weight.

Galileo Galilei, himself, is said to have dropped two spheres of different masses from the Leaning Tower of Pisa to demonstrate that their time of descent was independent of their mass.

Ignacio Zuloaga

Interesting video on the improvement works around this unique geotechnical problem.

https://www.youtube.com/watch?v=3qTq4WqqLp0&feature=share

ΕΝΔΙΑΦΕΡΟΝΤΑ - ΣΕΙΣΜΟΙ

Scientists search for Caribbean quake clues

By following the flow of seawater deep into the earth's crust, researchers hope to understand the region's instability

Geologically speaking the Caribbean is a lively place. Recent reminders include the 1995 volcanic eruption on Montserrat, and the devastating magnitude 7 earthquake that struck Haiti in January 2010. Occasionally the Caribbean produces even more powerful outbursts.

Back in February 1843 the region was shaken by an estimated magnitude 8.3 quake, reducing Pointe-a-Pitre in Guadeloupe to ruins and killing one third (1,500) of its inhabitants. Meanwhile, 2,000 people are thought to have perished in a quake of unspecified magnitude which shook Jamaica in 1692.

So when will the Caribbean's next major rumble be? This month scientists aboard a research ship – the RRS James Cook – will be taking measurements to try to gain some early warning clues. Led by Jenny Collier of Imperial College London, they will be following the seawater that is drawn down into the Earth east of the Caribbean islands, where the oceanic plate dives underground.

Using seismic reflections and sensitive recording devices on the seafloor, the scientists will see if they can spot where water comes into the system and how this affects the surrounding geology.

"Water is a key component in causing the mantle to melt, which eventually forms magma at shallower depths, causing potentially hazardous volcanoes," explains Stephen Hicks from the University of Southampton. "It may also lubricate or increase the pressure along titanic faults that have the potential to cause huge earthquakes."

By tracking the movement of water, down to hundreds of miles depth, they hope to better understand what causes the build-up of magma in some places, and why some parts of the plate boundary produce more earthquakes than others.

(Kate Ravilious / The Guardian, Sunday 30 April 2017, https://www.theguardian.com/world/2017/apr/30/scientists-search-caribbean-quake-clues-terrawatch)

ΕΝΔΙΑΦΕΡΟΝΤΑ - ΓΕΩΛΟΓΙΑ

Τα ηφαίστεια ως φυσικός πόρος
Η Ισλανδία θέλει να ηλεκτροδοτήσει τη Βρετανία με ενέργεια από μάγμα

Συμβατική γεωθερμική εγκατάσταση στο ηφαίστειο Κράφλα. Η παραγωγή θα μπορούσε ακόμα και να δεκαπλασιαστεί.

Διεθνής κοινοπραξία ετοιμάζεται να δημιουργήσει στην Ισλανδία την πρώτη γεωθερμική εγκατάσταση που αξιοποιεί τη θερμότητα από το μάγμα ενός ηφαιστείου. Και εφόσον το εγχείρημα πετύχει, η Ισλανδία θα μπορούσε να κατασκευάσει ένα υποθαλάσσιο καλώδιο που θα εξάγει ηλεκτρική ενέργεια στη Βρετανία.

Η Ισλανδία ήδη καλύπτει το σύνολο των αναγκών της σε ηλεκτρική ενέργεια με γεωθερμικές και υδροηλεκτρικές εγκαταστάσεις.

Οι πρώτες ενδείξεις για τη δυνατότητα αύξησης της παραγωγής ήρθαν το 2009, όταν ερευνητές που πραγματοποιούσαν ερευνητική γεώτρηση χτύπησαν κατά λάθος το θάλαμο μάγματος κάτω από το ηφαίστειο Κράφλα της Ισλανδίας. Κατάφεραν τελικά να αξιοποιήσουν τη σπάνια ευκαιρία , δείχνοντας ότι η γεώτρηση μπορούσε να προσφέρει μεγάλες ποσότητες ατμού, που θα μπορούσε να διοχετευτεί σε ηλεκτρογεννήτριες.

Το νέο σχέδιο για την εμπορική αξιοποίηση αυτής της ενέργειας αφορά μια νέα γεώτρηση βάθους 2,1 χιλιομέτρων μέσα στον ίδιο θάλαμο μάγματος.

Όπως αναφέρει το Reuters, το πρόγραμμα των 100 εκατομμυρίων δολαρίων συντονίζεται από την ισλανδική Ομάδα Γεωθερμικής Έρευνας (GEORG) και τη βρετανική γεωλογική υπηρεσία BGS, με τη συμμετοχή 38 εταιρειών και ινστιτούτων από 11 χώρες.

Σύμφωνα με το GEORG, μια γεώτρηση που αντλεί θερμότητα απευθείας από το μάγμα μπορεί να δώσει 5 με 10 φορές περισσότερη ενέργεια από μια συμβατική γεωθερμική γεώτρηση.

Η εμπορική αξιοποίηση της ενέργειας του μάγματος θα μπορούσε να δώσει ώθηση στο σχέδιο που συμφώνησαν πέρυσι η Ισλανδία με τη Βρετανία για την κατασκευή υποθαλάσσιου αγωγού ηλεκτρικού ρεύματος.

Το προτεινόμενο καλώδιο IceLink, που θα ήταν το μεγαλύτερο του κόσμου με μήκος 1.000 χιλιόμετρα, θα αρκούσε για την ηλεκτροδότηση 1,6 εκατομμυρίων νοικοκυριών στη Βρετανία.

Το σχέδιο όμως καθυστέρησε έπειτα από το δημοψήφισμα υπέρ του Brexit και την ανησυχία ότι οι εξαγωγές ενέργειας θα οδηγούσαν σε αύξηση των τιμών του ηλεκτρικού ρεύματος για τους ισλανδούς καταναλωτές.

Το ηφαίστειο Κράφλα, όμως, θα μπορούσε να αυξήσει θεαματικά την ηλεκτροπαραγωγή. Αυτό «σχεδόν σίγουρα θα έδινε ώθηση στο προτεινόμενο σχέδιο [του IceLink]» εκτίμησε μιλώντας στο Reuters ο Γουέιν Μπράιαν, αναλυτής της British Alpha Energy.

Η πρώτη φάση του προγράμματος στο Κράφλα προγραμματίζεται να αρχίσει το 2020 με προϋπολογισμό 30 εκατομμυρίων δολαρίων, ανακοίνωσε την Παρασκευή η βρετανική γεωλογική υπηρεσία.

Στη φάση αυτή προβλέπονται επίσης μελέτες για την προστασία από ηφαιστειακές εκρήξεις. Οι ερευνητές του GEORG, πάντως, διαβεβαιώνουν ότι οι γεωθερμικές γεωτρήσεις είναι εντελώς απίθανο να οδηγήσουν σε έκρηξη.

(Επιμέλεια: Βαγγέλης Πρατικάκης / Newsroom ΔΟΛ, 11 Απρ. 2017, http://news.in.gr/science-technology/article/?aid=1500138902)

Λιμνούλα ο θησαυρός
Μοναδική συλλογή πυρήνων πάγου έλιωσε λόγω βλάβης

Ερευνητές βγάζουν έναν φρέσκο πυρήνα πάγου στην Αρκτική. Η αντικατάσταση των χαμένων δειγμάτων είναι δύσκολη ως αδύνατη.

Χιλιάδες χρόνια κλιματικής ιστορίας έλιωσαν και έγιναν λιμνούλα στο πάτωμα: ένας χαλασμένος καταψύκτης έγινε αιτία να χαθεί ένα σημαντικό μέρος από το Καναδικό Αρχείο Πυρήνων Πάγου, το οποίο προσφέρει πολύτιμα στοιχεία για τις μεταβολές του κλίματος στην Αρκτική.

Το δωμάτιο κρυοσυντήρησης «έμοιαζε με αποδυτήρια στο κολυμβητήριο» αναφέρει στο δικτυακό τόπο του Science ο Martin Sharp, ερευνητής του Πανεπιστημίου της Αλμπέρτα στο Έντμοντον (http://www.sciencemag.org/news/2017/04/unique-canadian-ice-core-collection-suffers-catastrophic-meltdown), το οποίο έχει αναλάβει τη διαχείριση του αρχείου.

Οι πυρήνες πάγου -κυλινδρικά δείγματα που εξάγονται με γεωτρύπανα- περιέχουν αρχαίους κόκκους γύρης, φυσαλίδες αέρα και άλλα στοιχεία που μπορούν να δείξουν ποιες ήταν οι κλιματικές συνθήκες όταν σχηματίστηκε ο πάγος, ακόμα και δεκάδες χιλιάδες χρόνια στο παρελθόν.

Λόγω της βλάβης η θερμοκρασία στο χώρο εκτοξεύτηκε από τους -37 στους 40 βαθμούς Κελσίου, με αποτέλεσμα να χαθούν 180 κύλινδροι πάγου μήκους ενός μέτρου ο καθένας.

Η απώλεια αντιστοιχεί στο 12,8% της συλλογής των 1408 δειγμάτων από όλη την καναδική Αρκτική. Δυστυχώς, όμως, ορισμένοι από τους λιωμένους πυρήνες ήταν από τους αρχαιότερους του αρχείου.

Και η αντικατάστασή τους είναι μάλλον απίθανη, δεδομένου ότι ο Μάρτιν Σαρπ εκτιμά ότι το κόστος θα κυμαινόταν από μισό έως ένα εκατομμύριο δολάρια ανά πυρήνα.

(Επιμέλεια: Βαγγέλης Πρατικάκης / Newsroom ΔΟΛ, 11 Απρ. 2017, http://news.in.gr/science-technology/article/?aid=1500138887)

University of Alberta geologist Martin Sharp examines an ice core (University of Alberta/Ian Jackson for Alberta)

A Massive Lake Of Molten Carbon The Size Of Mexico Was Just Discovered Under The US

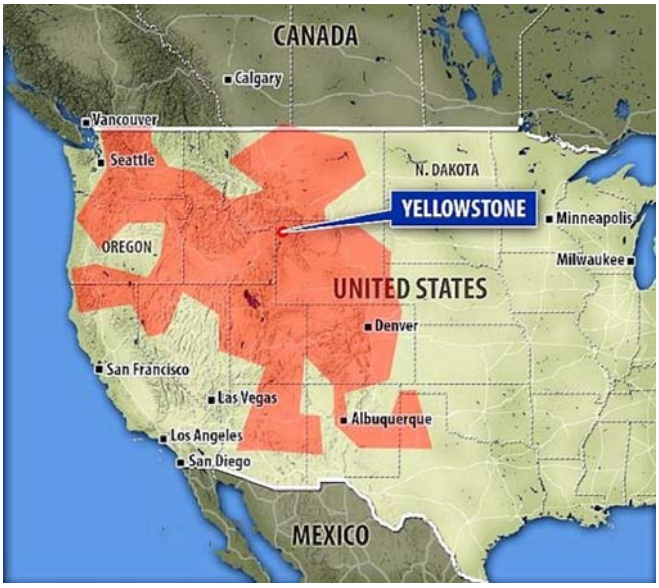

Extent of molten carbon lake beneath the western US

A recent scientific discovery (Pervasive upper mantle melting beneath the western US http://www.sciencedirect.com/science/article/pii/S0012821X16307543/) has drastically changed our view of the global carbon cycle and identified a new significant risk. Researchers have discovered a giant lake or reservoir made up of molten carbon sitting below the western US.

The molten carbon (primarily in the form of carbonate) reservoir could drastically and immediately change the global climate for over a decade if it were to be released. Thankfully there is little risk in the near future of this happening. The carbon sits 217 miles beneath the surface of the Earth in the upper mantle and has no immediate pathway to the surface. In total the lake covers approximately 700,000 square miles, approximately the size of Mexico. This has redefined how much carbon scientists believe sits locked away in the Earth's mantle and its interaction with surface and atmospheric carbon.

Geologists at Royal Holloway University of London were able to use the largest array of seismic sensors in the world to detect what exists below the surface of the western US. In total 538 sensors were used to create a three-dimensional view of the regions subsurface. They do this by measuring the time it takes for sound waves to travel into the Earth and bounce back. Depending on the structure of rock in the subsurface, different waves will bounce back at different times and at different angles. Complex algorithms integrate the data to reveal a picture of what exists below the surface of the Earth. Scientists are limited to viewing the molten lake through seismic imagery as it is far too deep to reach via a drill bit.

You may be asking why and how this lake of molten carbonate exists in the first place. It is a result of the Pacific Plate subducting underneath the North American Plate. As the Pacific Plate subducts, it experiences increasingly high pressures and temperatures. This, combined with the presence of gasses such as CO_2 and water locked away in the rock, allows for partial melting of the plate. This is a similar process by which the Rockies Mountains formed in the western US. For a more in depth review, this is a great explanation.

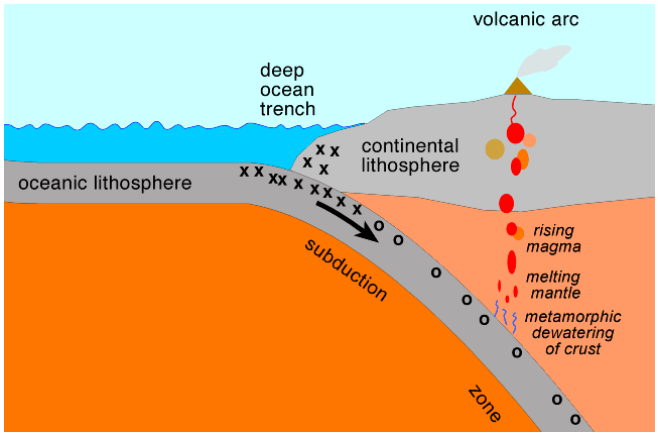

Schematic of a subduction zone whereby the subducting plate melts, causing volcanism at the surface.

The molten carbonate sits beneath Yellowstone National Park, which in and of itself is a super volcano with the power of a massive eruption. The last major eruption was 640,000 years ago at Yellowstone, however if the super volcano did erupt it could cause the US to go into a volcanic winter. The eruption, when it does occur, would be on the order of 1,000 times more powerful than the 1980's Mount St. Helens eruption.

In part due to this research, scientists now believe the Earth's upper mantle may hold up to 100 trillion metric tons

of carbon. To put this into perspective, the US EPA estimated that in total 10 billion metric tons of carbon was emitted in 2011, or approximately 0.01% of the carbon sitting in Earth's mantle. Thankfully the release of the mantle's carbon happens very slowly over time primarily through volcanic eruptions. However, paleoclimatic fluctuations in CO_2, creating ice ages and greenhouse global conditions are partially linked to dynamic changes in volcanism.

The molten carbonate through thermal decomposition would release carbon dioxide and calcium oxide, however it would need a viable pathway to Earth's surface to inject the CO_2 into the atmosphere

Release of just 1 percent of the mantle's carbon would equate to burning 2.3 trillion barrels of oil. This gives some perspective on just how important it is to understand this deep carbon system and how it interacts with and drives the atmospheric carbon system driving climate change.

(Trevor Nace / Forbes, APR 30, 2017, https://www.forbes.com/sites/trevornace/2017/04/30/a-massive-lake-of-molten-carbon-the-size-of-mexico-was-just-discovered-under-the-us/#665fc5ae420b)

ΕΝΔΙΑΦΕΡΟΝΤΑ - ΠΕΡΙΒΑΛΛΟΝ

Geothermal heat: an episodic heat source in oceans

Plate climatology (www.plateclimatology.com) is a theory introduced in 2014 by James Kamis. Unlike the Sun which is the first order driver of earth's climate, it is an underestimated second order driver which can contribute significantly to regional natural variations. The overall theory contends that periods of active earth tectonics and volcanism can be correlated to periods of active climate change and/or climate related events.

According to the National Atmospheric and Oceanographic Administration (NOAA), 2015 was the hottest year since record began in 1880 from globally averaged temperatures over land and ocean surfaces following the 17year pause since 1998. A popular explanation is an immense amount of heat released from the Pacific Ocean caused by the strongest and longest El Niño year this century during 2015 but what triggered such a condition is unresolved. Proponents of anthropogenic global warming including the United Nations have used the temperature rise as signaling a return to global warming.

In this article, two initially submarine volcanic eruptions and one subaerial volcanic eruption all contributing to the regional warming of the Pacific Ocean are investigated using available information including satellite records of sea-surface temperature anomalies and ocean surface topography. In conclusion, geothermal heat is a reminder of a dynamic earth in spite of overpopulation and resource usage on planet earth.

The Pacific Ocean and the Atlantic Ocean are the two oceans with connections to the two poles. Because an estimated three quarters of the world's active volcanoes are located within the Ring of Fire, the release of geothermal heat through volcanism in the Pacific Ocean is the highest and may provide a heat source additional to the sun for triggering El Niño years. This is supported by 'Explanation for the northern Pacific Blob' featured in the Autumn 2016 issue of Imperial ENGINEER. Currently such geological forcing by plate tectonics on climate is not well appreciated by climate scientists probably because of their atmospheric bias.

Three volcanic eruptions generating positive sea-surface water anomalies in different parts of the Pacific Ocean from before November 2013 until November 2015 based on reported information are analysed. Two of the eruptions were initially submarine followed by subaerial eruptions after new islands were created while the third eruption is entirely subaerial with basaltic lava flows at ~1000°C entering the ocean. All three eruptions contributed geothermal heat to the longest-lasting El Niño this century in 2015 perhaps even stronger than the 1997 to 1998 event. Important environmental impacts included the suppression of heat loss from the ocean during winter, record high summer temperatures over parts of land in the Pacific northwest, record sea-surface temperatures in the Pacific Geothermal heat: an episodic heat source in oceans northeast for February since the 1980s, record high sea-surface pressure for the years 1949 to 2014, acceleration in the contraction of Arctic sea ice during the summers of 2014 and 2015, catastrophic ecological damage such as coastal algal blooms and coral bleaching, and, the return to La Niña conditions after sea-surface temperature returned to equilibrium during 2016.

Events related to the three volcanic eruptions which contributed to the development of the abnormally strong El Niño conditions in 2015 are shown in the summary table below.

Date	Event(s)	Observation(s)
Mar 2013	Submarine eruption of Nishino-shima	Warming first detectable in sea-surface temperature anomalies maps (start of submarine eruption).
Nov 2013	Submarine and subaerial eruption of Nishino-shima	Source: en.wikipedia.org/wiki/Nishinoshima_(Ogasawara); during northern hemisphere winter.
Feb 2014	Temperature measurement	Sea-surface temperature ~2.5°C above normal was reported.
Jun 2014	Island ~2.3 km in diameter; ~110 m above sea level	Name Blob was coined by Nicholas Bond; size reached 1600 km by 1600 km and 91 m deep; spread to the coast of North America with patches off Alaska, Victoria/California and Mexico.
Jul-Sep 2014	Mass coral bleaching in Hawaii	Reported by the University of Queensland; area of warm water exceeded 9 million km^2 during peak stage; rapid contraction of Arctic sea ice during summer and early autumn.
Jan-Aug 2014	Episodic eruption of Nishino-shima with lava flows	Japanese Coast Guard reported increase in area of the island through lava flows; onset of El Niño conditions; abnormally hot summer in Pacific northeast.
Dec 2014	Submarine and subaerial eruption of Hunga, Tonga	Source: en.wikipedia.org/wiki/Hunga_Tonga; occurred during southern hemisphere summer; year without winter in Pacific northeast.
Jan 2015	Eruption of Hunga ended	Strong El Niño conditions forecast; coral bleaching in the northern parts of the Great Barrier Reef.
Mar 2015	Severe tropical cyclone Pam	Most intense tropical cyclone of the South Pacific in terms of sustained wind; Vanuatu's worst natural disaster.
May-Jun 2015	Eruption of Wolf, Galapagos	Lava flows entered the ocean exacerbating the already strong El Niño conditions; rapid contraction of Arctic sea ice during summer and early autumn.
Early 2016	Blob dissipation	Change to La Niña conditions.

Summary table of events attributable to three volcanic eruptions releasing geothermal heat in different parts of the Pacific Ocean, contributing to the development of the strongest and longest lasting El Niño this century. For further details on the environmental and ecological damage see 'The Heat Wave' featured in the September 2016 issue of *National Geographic*.

Out of the three eruptions, the longest lasting and the most powerful in terms of the quantity of geothermal heat released was from the Nishino-shima volcano located 940 km south of Tokyo. The Volcanic Explosivity Index (VEI) based on the volume of subaerially erupted materials from November 20, 2013 to November 17, 2015 was rated 2 but this is not reflective of the severity of the submarine eruption because such a measurement scale is not currently available. On November 20, 2013, the beginning of the northern hemisphere winter, the appearance of a new island adjacent to Nishino-shima was reported. An examination of NOAA satellite sea-surface anomalies map archives has revealed that hot sea-surface water was already in existence at the site during the end of March 2013 six months earlier when the submarine eruption started. In late 2013, the patch of warm surficial water spread into the Gulf of Alaska to form the northern Pacific blob. The interaction between the warm ocean's surfaces with the atmosphere generated a long-lasting high-pressure condition referred to as the 'Ridiculously Resilient Ridge' which resulted in weird weather conditions in the Pacific northeast. Surveys by the Japan Coast Guard show the new land area of the volcanic island increased from a total area of 0.01 km^2 on November 20, 2013 to an area of 1.08 km^2 on July 7, 2014, and, to a maximum area of 2.71 km^2 on August 18, 2015. The continuous expansion of the volcanic island through episodic lava flows means geothermal heat was available to sustain blob through ocean circulation changes until early 2016 since seawater is a poor conductor of heat. During the peak stage, the warm water covered a total area exceeding 9M km^2 from Mexico to Alaska, an area larger than the contiguous US.

The existence of the north Pacific blob in the Gulf of Alaska which is connected to the Arctic Ocean through the Bering Strait is consistent with the record of sea ice contraction observed during the summers of 2014 and 2015. Based on monthly maps of the National Snow and Ice Data Centre during the northern hemisphere summer and early autumn, Arctic sea ice contraction was much more rapid and extensive in the Arctic Ocean portion adjacent to the northern Pacific Ocean compared to the northern Atlantic Ocean.

The second eruption, Hunga volcano, from November 2014 to January 23, 2015 during the peak of the southern hemisphere summer is also the second long lasting. The VEI based on the volume of erupted materials with a reported plume height ranging from 7-10 km was rated 2. There is again an underestimation of the severity of the submarine eruption because of the absence of a measurement scale.

On December 19, 2014, local fishermen reported a tall white steam plume rising from the ocean over the submarine volcano. On December 29, satellite images taken showed the eruption continuing, with discoloured seawater possibly caused by smoke and ash released below the surface, or by disturbance of the seabed. The eruption entered a new stage on January 11, 2015, when the volcano began sending ash plumes as high as 9 km. On January 13, the large amounts of nitrogen and phosphorous released underwater caused an explosion in the growth of algae and causing a red tide. At the end of the eruption, a new island 1 km wide, 2 km long and 120 m high was created. Subsequent environmental impacts of the warm sea-surface water included coral bleaching of the Great Barrier Reef from January 2015 and the development of severe tropical cyclone Pam which devastated Vanuatu in mid-March 2015.

The third eruption, the Wolf volcano from May 25 to June 2, 2015 is the shortest in duration. The high VEI 4 rating is in response to the much larger volume of subaerially erupted materials. Lava flows were reported to first reach the sea on May 28 (see satellite image) exacerbating the already strong El Niño conditions.

Thermal infrared image of the Wolf volcano, Galapagos acquired on June 11, 2015 after the May 25 to July 2, 2015 eruption, showing lava flows reaching the sea to the east.

The NOAA sea-surface temperature anomalies map of August 31, 2015 (next page) highlights the pattern characterised by the longest-lasting event this century is distinctly different from El Niño events in the past covered by satellite observation records. The causation factors for each event must therefore differ.

A comparison of ocean surface topography during the two strongest and longest El Niño years this century, 1997 to 1999 and 2015 to 2017, is shown (below). The hot seasurface water generated by the three volcanic eruptions during 2013 to 2015 described in this study provides the best explanation to both the pattern and the timing of the ocean surface topographical changes observed.

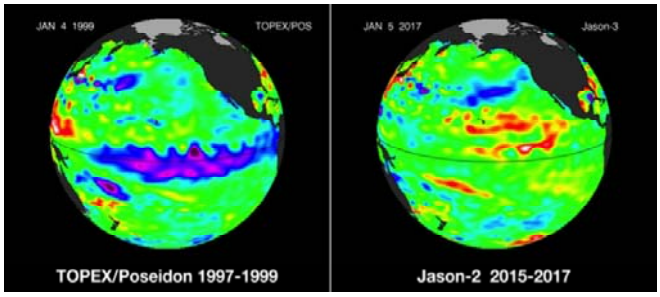

Satellite-based ocean surface topography still image comparison of the two strongest El Nipo years this century

The three volcanic eruptions causing regional warming in different parts of the Pacific Ocean over the three-year period from 2013 to 2015 is supported by the satellite sea-surface temperature anomalies records and ocean surface topography records. The warm sea-surface water was responsible for oceanic and atmospheric circulation changes regionally which cannot be accounted for by carbon dioxide variations.

For future work, Smithsonian's Global Volcanism Program (GVP) should be extended to include coverage of submarine volcanic eruptions. A severity scale based on the amount of geothermal heat released from such eruptions taking into account the eruption history should be devised assisted by an expanded ARGO monitoring data buoy network.

Thanks are due to Wikipedia, NOAA, NASA, GVP and miscellaneous media reports for providing information to assist this article.

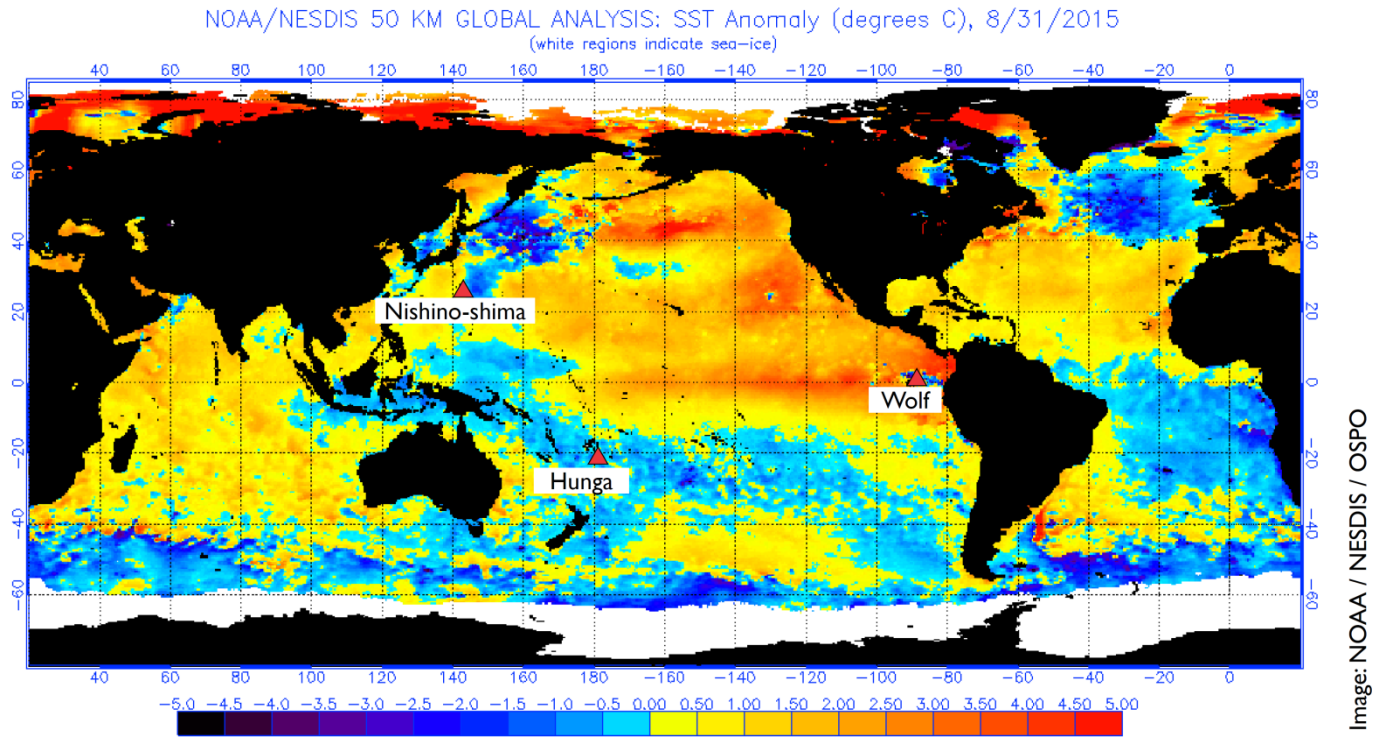

Global map of sea-surface temperature anomalies showing the El Nipo conditions on August 31, 2015 under the influence of the northern Pacific blob and further exacerbated by the May 25, 2015 Wolf eruption with lava flows into the sea. The locations of the Nishino-shima, Hunga and Wolf volcanoes are also shown. The severe contraction of Arctic sea ice in the north Pacific compared to the north Atlantic and the cold water upwelling in the northwest Pacific can also be explained by the seasurface temperature distribution.

Professor Wyss Yim DSc PhD DIC FGS was at Imperial College in the Department of Geology from 1971-1974. After that he spent 35 years until retirement at the University of Hong Kong where he taught civil engineering, geosciences and environmental management students, and, helped found the Department of Earth Sciences. He was awarded the DSc by the University of London in 1997. Wyss erved as the Deputy Chairman of the Climate Change Science Implementation Team of UNESCO's International Year of Planet Earth 2007-2009.

Imperial ENGINEER Issue 26 Spring 2017, pp. 14-15, https://www.imperial.ac.uk/media/imperial-college/faculty-of-engineering/public/imperial-engineer/Imperial-Engineer-26.pdf.

ΕΝΔΙΑΦΕΡΟΝΤΑ - ΛΟΙΠΑ

The Amazing Engineering Feats of the Lost City of Petra

Historically speaking, the lost city of Petra, in the Arabic country of Jordan, is one of the most enigmatic civilizations that have ever existed. With their successful and prolific business trading spices and silks with China, India, Rome and Egypt, the people of ancient Petra, the Nabateans, have managed to endow their city with extravagant structures and infrastructures. The lost city of Petra has been the centerpiece of legends and fictional stories since its rediscovery in 1812 by the Swiss explorer Johann Ludwig Burckhardt. The incredible fact about Petra's structures is that they were not constructed, but were carved out of giant sandstone canyons surrounding the lost city.

With that said, allow me to take you back in time and discover for ourselves the engineering wonders and riches that made Petra one of the new seven wonders of the world.

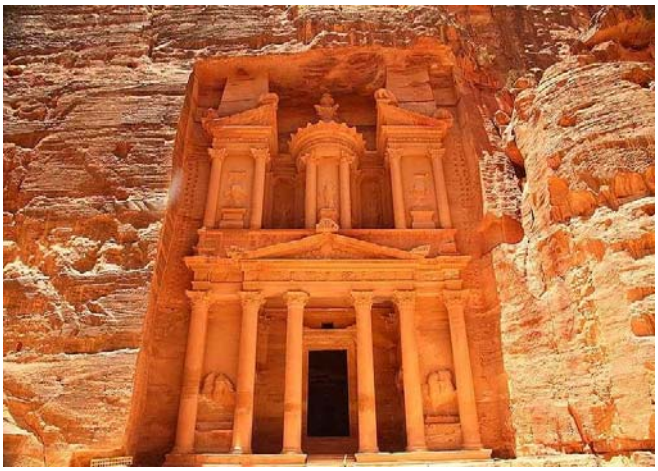

The Treasury

The Treasury

Quietly hidden between the canyons of Petra is this magnificent structure carved out of the sandstone rock face known as the Treasury or Al-Khazneh in Arabic. It was originally carved during the reign of Aretas IV Philopatris, a Nabatean King, at the start of the 1st century AD. The origin of the Treasury is attributed to a few legends – one of which is that it was used as a treasury of Egyptian Pharaohs during Moses' time.

The entrance of Al-Kazneh is guarded by the statues of the twin Castor and Pollux and the entire rock face is adorned with other mythological creatures and Greek-inspired designs. The strapping entrance doorway leads to three separate chambers and contrary to the building's facade, the interior of the Treasury is plain without any ornate designs. Its sheer dimension, 80 feet wide and127 feet tall, makes the Treasury a giant sandstone sculpture. Al-Kazneh was carved out starting from the top down using only simple iron chisels and hammers.

Many of the carved details have already eroded due to its old age, however, the Treasury still remains to be one of the most epic structures of the ancient world and can easily rival the grandeur of Egypt, Greece, and Rome.

The Monastery

Another carved out sculpture building from the sandstone mountains is called the Monastery. It stands at 45 meters high and 50 meters wide and echoes the typical Nabatean classical style. Inside this structure is a single chamber with double staircases heading up to a cultic niche. Historians think that the Monastery is possibly a temple devoted to the Nabatean king Obodas I in the first century BC.

The Tombs

Like the ancient civilization of Egypt, the lost city of Petra is also host to several tombs which serves as the resting place for royalties. The Royal tombs consist of the Urn tomb, Silk tomb, Corinthian tomb, and Palace tomb. All of which were carved out from the city's sandstone canyons too. Some suggest that the Urn tomb was made for the Nabataean King Malchus II who died in 70 AD. Others believe that it was built as the tomb of Aretas IV.

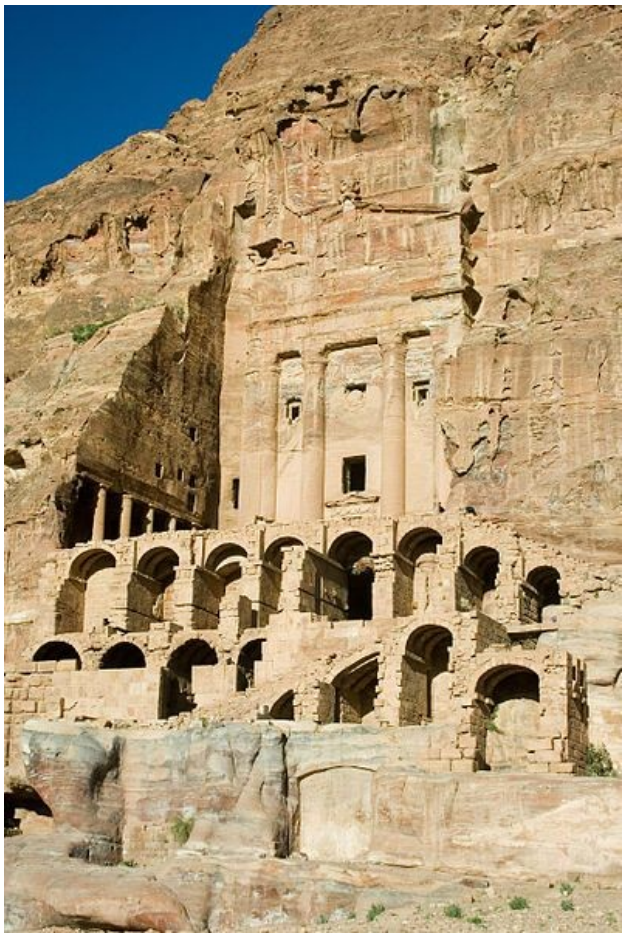

Urn Tomb

The amphitheater and the great temple

Petra's amphitheater was carved out, too, from the mountain rock and can seat a maximum of 8,500 people. The amphitheater was dated back to the 1st century AD and was designed with features from the Hellenistic period. The majority of the theater's features have eroded due to the flash floods and earthquake that occurred in the city around 300 AD.

At the heart of the lost city, the Great Temple sits as the major architectural feat with its towering columns and intricate subterranean canals. The perimeter of the temple measures at 35 meters wide and around 42.5 meters in length and is considered as the largest freestanding structure in Petra. This impressive temple was in use until the arrival of the Byzantine period around the fifth century CE.

Petra's impressive ancient hydrology system

All of the carved out structures above are just the cherry on top of the cake, the real engineering ingenuity of the Nabateans can be realized from their intelligent design of Petra's hydrology system. The carving of all of Petra's structure requires a bountiful supply of water and other facilities and the Nabateans were aware of this. They have engineered a vast series of ceramic pipeline segments to transport water from the source called Ain Musa or the spring of Moses to the urban city of ancient Petra. Modern day hydraulic engineers have discovered that the Nabateans have managed to effectively transport water five miles from the source to Petra by carving out pipe ridges along the mountains with a four-degree slope. The long-haul pipelines were perfectly engineered to provide a constant supply of water to the busy towns of the lost city.

As the Treasury sits between the canyons' gorges, the Nabateans had to come up with a way to control flash floods and sudden water surges that may potentially ruin the carved structure. They did this by constructing a series of dams made from stone blocks mortared together and anchored to carved out canyon groves. This design allows the dams to withstand extreme pressures from large volumes of water that are stored behind it.

Petra's Aqueduct

Overall, Petra's ancient urban hydrology network consists of 8 springs for fresh drinking water, 36 dams to protect the city from flash floods, over 125 miles of pipeline to manifold all of the water systems, and over 100 reservoirs and cisterns to store water supply. This complex hydrology system can provide a single person with 8 liters of water per day which is thought to be luxurious during that period.

It is believed that the entire infrastructure and carved out structures of Petra were all built at the same time with a grand master plan.

Petra is famously known as the 'Rose City' because of its sandstone's red color and the best time to visit these enigmatic carved out structures is during the height of the afternoon. The colors and features of the structures come alive under the heat and brightness of the desert sun.

(Kathleen Villaluz / National Geographic Channel, April 13, 2017, http://interestingengineering.com/amazing-engineering-feats-lost-city-of-petra/)

ΗΛΕΚΤΡΟΝΙΚΑ ΠΕΡΙΟΔΙΚΑ

https://www.issmge.org/filemanager/article/434/ISSMGE_BULLETIN_2017_APR-FINAL.pdf

Κυκλοφόρησε το Τεύχος # 2 του Τόμου 11 **του ISSMGE Bulletin** (Απριλίου 2017) με τα ακόλουθα περιεχόμενα:

- Research highlights – HKUST Geotechnical Group

- Project highlight

Pilot the way to Hong Kong's urban underground space development

- Conference reports

The 3rd EUROFUGE 2016

- **Hot news**

New book: Ground Engineering

Indian Geotechnical Journal: Call for papers

- Obituary

Professor T. W. Lambe

Professor Dr. Ir. Djoko Soelarnosidji

- Event Diary

- Corporate Associates

- Foundation Donors

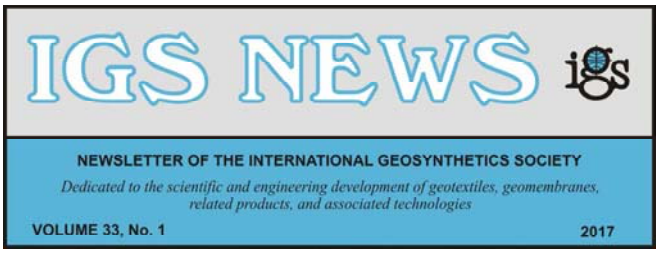

http://www.geosyntheticssociety.org/wp-content/uploads/2017/04/IGS-News-Vol.-33-Issue-1.pdf

Κυκλοφόρησε το Τεύχος #1 του Τόμου 33 των **IGS NEWS** με τα ακόλουθα περιεχόμενα:

General Information for IGS Members

IGS Awards: Call for Nominations 2014 – 2017

Request for Proposals to Host 12 ICG 12th International Conference on Geosynthetics

Young Members Committee meet at Geotechnical Frontiers Orlando Conference

New Translations Available for Geosynthetics for Sustainable Development

Announcement of the International Conference of IGS

11th ICG International Conference on Geosynthetics

Announcements of Regional Conferences of IGS

GeoAfrica 2017 – 3rd African Regional Conference on Geosynthetics

Announcements of Conferences under the Auspices of IGS

Transportation Geotechnics and Geoecology – TGG 2017

EurAsian Geotextiles Symposium (EAGS)

GeoMEast 2017 International Congress and Exhibition "Sustainable Civil Infrastructures: Innovative Infrastructure Geotechnology"

News from the IGS Chapters and the Membership

IGS-North America Photo Contest Winners

XXVIII Italian National Conference on Geosynthetics

One-day Workshop "Geosynthetics for Slope Stabilization"

French Geosynthetics Committee

6th Upper Austrian Geotechnical Day - Geosynthetics

List of IGS Chapters

Official Journals of the IGS

Geosynthetics International

Geotextiles & Geomembranes

Corporate Membership

Case Studies – Use the Chance!

Securing Hazardous Waste in Uganda

A Reinforced Earth Embankment for a New Sanitary Landfill – Italy

Winston Salem State University, NCSlope Stability Solution

Corporate Members of the IGS

IGS News Publisher, Editor and Chapter Correspondents

IGS Council

IGS Officers

Calendar of Events

Geosynthetics International

Content of Volume: 24, Issue: 1 (February 2017)

Analytical method for calculating natural frequencies of geosynthetic-reinforced wall with full-height concrete facing, M. S. Ramezani, A. Ghanbari, S. A. A. Hosseini

Deterministic and probabilistic failure analysis of simple geosynthetic reinforced soil slopes, S. Javankhoshdel, R. J. Bathurst

Investigation of the micro-mechanics of sand–rubber mixtures at very small strains, J. C. Lopera Perez, C. Y. Kwok,

K. Senetakis

Three-dimensional analysis of geosynthetic-encased granular columns for liquefaction mitigation, L. Geng, L. Tang, S. Y. Cong, X. Z. Ling, J. Lu

Time-dependent behaviour of fully and partially penetrated geosynthetic encased stone columns, S. Rajesh

Experimental study on the combined application of vacuum preloading – variable-spacing electro-osmosis to soft ground improvement, H. Fu, Y. Cai, J. Wang, P. Wang

Physical and hydraulic response of geomembrane wrinkles underlying saturated fine tailings, P. Joshi, R. K. Rowe, R. W. I. Brachman

Tensile behaviour of an HDPE geogrid under cyclic loading: experimental results and empirical modelling, G. Cardile, N. Moraci, M. Pisano

Book review, R.J. Bathurst

Please find the download of the articles at:
http://www.icevirtuallibrary.com/content/issue/gein/24/1
For the IGS members to have FREE access to the papers they MUST log in through the IGS website.

Geotextiles & Geomembranes

Content of Volume 45, issue 2 (April 2017)

Load transfer mechanism and deformation of reinforced piled embankments, Diego F. Fagundes, Márcio S.S. Almeida, Luc Thorel, Matthieu Blanc

Efficiency of cellular geosynthetics for foundation reinforcement, Mohammad Oliaei, Saeed Kouzegaran

Laboratory and field investigation of the effect of geogrid-reinforced ballast on railway track lateral resistance, Morteza Esmaeili, Jabbar Ali Zakeri, Mohammad Babaei

Performance monitoring of Geosynthetic Reinforced Soil Integrated Bridge System (GRS-IBS) in Louisiana, Milad Saghebfar, Murad Abu-Farsakh, Allam Ardah, Qiming Chen, Benjamin A. Fernandez

The effect of thickness reduction on the hydraulic transmissivity of geonet drains using rigid and non-rigid flow bound-aries, N. Yarahmadi, I. Gratchev, D.-S. Jeng

Groups of encased stone columns: Influence of column length and arrangement, Jorge Castro

Micromechanical analyses of the effect of rubber size and content on sand-rubber mixtures at the critical state, J.C. Lopera Perez, C.Y. Kwok, K. Senetakis

Please find the download of the articles at:
http://www.sciencedirect.com/science/journal/02661144
For IGS members to have FREE access to the G&G journal articles they MUST log in through the IGS website.

ΕΚΤΕΛΕΣΤΙΚΗ ΕΠΙΤΡΟΠΗ ΕΕΕΕΓΜ (2015 – 2018)

Πρόεδρος	:	Γεώργιος ΓΚΑΖΕΤΑΣ, Δρ. Πολιτικός Μηχανικός, Καθηγητής Ε.Μ.Π. president@hssmge.gr, gazetas@ath.forthnet.gr
Α' Αντιπρόεδρος	:	Παναγιώτης ΒΕΤΤΑΣ, Πολιτικός Μηχανικός, ΟΜΙΛΟΣ ΤΕΧΝΙΚΩΝ ΜΕΛΕΤΩΝ Α.Ε. otmate@otenet.gr
Β' Αντιπρόεδρος	:	Μιχάλης ΠΑΧΑΚΗΣ, Πολιτικός Μηχανικός mpax46@otenet.gr
Γενικός Γραμματέας	:	Μιχάλης ΜΠΑΡΔΑΝΗΣ, Πολιτικός Μηχανικός, ΕΔΑΦΟΣ ΣΥΜΒΟΥΛΟΙ ΜΗΧΑΝΙΚΟΙ Α.Ε. mbardanis@edafos.gr, lab@edafos.gr
Ταμίας	:	Γιώργος ΝΤΟΥΛΗΣ, Πολιτικός Μηχανικός, ΕΔΑΦΟΜΗΧΑΝΙΚΗ Α.Ε.- ΓΕΩΤΕΧΝΙΚΕΣ ΜΕΛΕΤΕΣ Α.Ε. gdoulis@edafomichaniki.gr
Έφορος	:	Γιώργος ΜΠΕΛΟΚΑΣ, Δρ. Πολιτικός Μηχανικός, Επίκουρος Καθηγητής ΤΕΙ Αθήνας gbelokas@teiath.gr, gbelokas@gmail.com
Μέλη	:	Ανδρέας ΑΝΑΓΝΩΣΤΟΠΟΥΛΟΣ, Δρ. Πολιτικός Μηχανικός, Ομότιμος Καθηγητής ΕΜΠ aanagn@central.ntua.grn
		Βάλια ΞΕΝΑΚΗ, Δρ. Πολιτικός Μηχανικός, ΕΔΑΦΟΜΗΧΑΝΙΚΗ Α.Ε. vxenaki@edafomichaniki.gr
		Μαρίνα ΠΑΝΤΑΖΙΔΟΥ, Δρ. Πολιτικός Μηχανικός, Αναπληρώτρια Καθηγήτρια Ε.Μ.Π. mpanta@central.ntua.gr
Αναπληρωματικό Μέλος	:	Κωνσταντίνος ΙΩΑΝΝΙΔΗΣ, Πολιτικός Μηχανικός, ΕΔΑΦΟΜΗΧΑΝΙΚΗ Α.Ε. kioannidis@edafomichaniki.gr
Εκδότης	:	Χρήστος ΤΣΑΤΣΑΝΙΦΟΣ, Δρ. Πολιτικός Μηχανικός, ΠΑΝΓΑΙΑ ΣΥΜΒΟΥΛΟΙ ΜΗΧΑΝΙΚΟΙ Ε.Π.Ε. editor@hssmge.gr, ctsatsanifos@pangaea.gr

ΕΕΕΕΓΜ

Τομέας Γεωτεχνικής
ΣΧΟΛΗ ΠΟΛΙΤΙΚΩΝ ΜΗΧΑΝΙΚΩΝ
ΕΘΝΙΚΟΥ ΜΕΤΣΟΒΙΟΥ ΠΟΛΥΤΕΧΝΕΙΟΥ
Πολυτεχνειούπολη Ζωγράφου
15780 ΖΩΓΡΑΦΟΥ

Τηλ. 210.7723434
Τοτ. 210.7723428
Ηλ-Δι. secretariat@hssmge.gr ,
geotech@central.ntua.gr
Ιστοσελίδα www.hssmge.org (υπό κατασκευή)

«ΤΑ ΝΕΑ ΤΗΣ ΕΕΕΕΓΜ» Εκδότης: Χρήστος Τσατσανίφος, τηλ. 210.6929484, τοτ. 210.6928137, ηλ-δι. ctsatsanifos@pangaea.gr, editor@hssmge.gr, info@pangaea.gr

«ΤΑ ΝΕΑ ΤΗΣ ΕΕΕΕΓΜ» «αναρτώνται» και στην ιστοσελίδα www.hssmge.gr